

PARAMETRIC STUDY OF HEAT DIFFUSION IN VIBROTHERMOGRAPHY
USING ANALYTICAL AND NUMERICAL METHODS

by

Anthony James Trudnowski

A thesis submitted in partial fulfillment
of the requirements for the degree

of

Master of Science

in

Mechanical Engineering

MONTANA STATE UNIVERSITY
Bozeman, Montana

January 2012

©COPYRIGHT

by

Anthony James Trudnowski

2012

All Rights Reserved

APPROVAL

of a thesis submitted by

Anthony James Trudnowski

This thesis has been read by each member of the thesis committee and has been found to be satisfactory regarding content, English usage, format, citation, bibliographic style, and consistency and is ready for submission to The Graduate School.

Dr. Ahsan Mian

Approved for the Department of Mechanical and Industrial Engineering

Dr. Chris Jenkins

Approved for The Graduate School

Dr. Carl A. Fox

STATEMENT OF PERMISSION TO USE

In presenting this thesis in partial fulfillment of the requirements for a master's degree at Montana State University, I agree that the Library shall make it available to borrowers under rules of the Library.

If I have indicated my intention to copyright this thesis by including a copyright notice page, copying is allowable only for scholarly purposes, consistent with "fair use" as prescribed in the U.S. Copyright Law. Requests for permission for extended quotation from or reproduction of this thesis in whole or in parts may be granted only by the copyright holder.

Anthony James Trudnowski

January 2012

TABLE OF CONTENTS

1. BACKGROUND	1
Motivation.....	1
Fracture Mechanics.....	2
History of Fracture Mechanics.....	3
Theory of Fracture Mechanics.....	4
Overview of NDE Techniques.....	7
Radiography.....	7
Ultrasonic Testing.....	9
Liquid Penetrant Inspection.....	9
Magnetic Particle Inspection.....	10
Shearography.....	11
Resonance Testing.....	11
Vibrothermography.....	12
Project Overview	14
Parameters.....	16
2. MATHEMATICAL SET-UP	17
Heat Transfer Fundamentals.....	17
Modeling Set-up	20
One-Dimensional Heat Transfer Model.....	21
Two-Dimensional Heat Transfer Model:.....	23
Three-Dimensional Model:.....	24
Modeling Set-up Overview.....	26
3. FINITE DIFFERENCE APPROACH	27
Finite Difference Approximation of Derivatives.....	27
Finite Difference Approximations of Partial Derivatives.....	29
One-Dimensional Application of Finite Difference Model.....	30
Discretization of Internal Nodes	31
Top Boundary Condition	32
Bottom Boundary Condition:.....	34
Finite Difference Solution Method	35
4. FINITE ELEMENT APPROACH.....	38
Finite Element Overview	38
One-dimensional Finite Element Model.....	39
Two-Dimensional Finite Element Model.....	41

TABLE OF CONTENTS – CONTINUED

Three-Dimensional Finite Element Model	44
5. ANALYTICAL APPROACH	48
Overview of Separation of Variables Technique.....	48
Overview of Green’s Function	49
Overview of Point Load Generation.....	52
Procedure for Determining Analytical Solution.....	53
One-Dimensional Analytical Solution.....	54
Step 1. Perform Transformation of Variables.....	54
Step 2. Solve auxiliary problem.....	55
Step 3. Determine Green’s function from the auxiliary solution:.....	60
Step 4: Determine Transformed Variable Solution:	61
Step 5. Determine Overall Solution:.....	62
Two-Dimensional Analytical Solution	63
Step 1. Perform Transformation of Variables:.....	64
Step 2. Solve Auxiliary Problem	65
Step 3. Determine Green’s Function from the Auxiliary Solution.....	68
Step 4: Determine Transformed Variable Solution	69
Step 5. Determine Overall Solution	70
Three-Dimensional Analytical Solution	71
Step 1. Perform Transformation of Variables.....	72
Step 2. Solve Auxiliary Problem	73
Step 3. Determine Green’s Function from Auxiliary Solution.....	77
Step 4. Determine Transformed Variable Solution.....	78
Step 5. Determine Overall Solution.....	79
6. MODEL RESULTS	81
One-Dimensional Model Results.....	81
Time Dependent Solutions for the One-Dimensional Model	81
Generation Amount Dependent Solutions for the One-Dimensional Model.....	83
Specimen Thickness Dependent Solutions for the One-Dimensional Model.....	84
Discussion of One-Dimensional Model Results	85
Two-Dimensional Model Results	86
Time Dependent Solutions for the Two-Dimensional Model.....	87
Generation Amount Dependent Solutions for the Two-Dimensional Model	89
Specimen Thickness Dependent Solutions for the Two-Dimensional Model.....	90
Flaw Orientation Dependent Solutions for the Two-Dimensional Model.....	91
Flaw Size Dependent Solution for the Two-Dimensional Model.....	92
Discussion of Two-Dimensional Model Results	93

TABLE OF CONTENTS - CONTINUED

Three-Dimensional Model Results	94
Time Dependent Solutions for the Three-Dimensional Model.....	95
Generation Amount Dependent Solutions for the Three-Dimensional Model	97
Specimen Thickness Dependent Solutions for the Three-Dimensional Model	98
Flaw Orientation Dependent Solutions for the Three-Dimensional Model	99
Flaw Size Dependent Solution for the Three-Dimensional Model.....	100
Discussion of Three-Dimensional Model Results	101
Two-Dimensional Combined Analysis.....	102
Two-Dimensional Combined Analysis Parameters:	103
Two-Dimensional Combined Analysis Results	103
Discussion of Two-Dimensional Model Results:	106
Three-Dimensional Combined Analysis.....	106
Three-Dimensional Combined Analysis Parameters	106
Three-Dimensional Combined Analysis Results	107
Discussion of Three-Dimensional Model Results:	110
 7. CONCLUSION.....	 111
Results Summary	111
Future Work	112
 REFERENCES	 113
 APPENDICES	 114
APPENDIX A: Finite Difference Method MATLAB Files	117
APPENDIX B: Analytical Method MATLAB Files	121
APPENDIX C: Finite Element Method ANSYS Files	129
APPENDIX D: Simulation Data.....	151

LIST OF TABLES

Table	Page
1. Test plan for one-dimensional model	81
2. Test plan for two-dimensional model	87
3. Test plan for three-dimensional model	95

LIST OF FIGURES

Figure	Page
1. Liberty Ship failure	4
2. Crack growth exponential curve	6
3. X-Ray example (from NT3 digital X-Ray imaging Inc.)	8
4. Magnetic particle inspection phenomenon	10
5. One-dimensional heat transfer model	22
6. Two-dimensional heat transfer model	23
7. Three-dimensional heat transfer model	25
8. Node discretization for the finite difference method	31
9. Top surface finite difference energy balance.....	33
10. Bottom surface finite difference energy balance	34
11. Finite Difference MATLAB screenshot	37
12. ANSYS one-dimensional finite element model screenshots	41
13. ANSYS PLANE55 element.....	42
14. Two-dimensional finite element mesh.....	43
15. Two-dimensional model screenshots.....	44
16. SOLID70 geometry.....	45
17. Three-dimensional mesh.....	46
18. Three-dimensional model screenshots.....	47
19. Transient surface temperature results for the one-dimensional model	82

LIST OF FIGURES – CONTINUED

Figure	Page
20. Time delay between generation stopping and maximum recorded surface temperature in the one-dimensional model.....	81
21. Maximum surface temperature results as a function of generation amount in the one-dimensional model.....	84
22. Maximum surface temperature results as a function of specimen thickness for the one-dimensional model	85
23. Transient surface temperature results for the two-dimensional model.....	88
24. Time delay between generation stopping and maximum recorded surface temperature in the two-dimensional model	89
25. Maximum surface temperature results as a function of generation amount in the two-dimensional model.....	90
26. Maximum surface temperature results as a function of specimen thickness for the two-dimensional model	91
27. Maximum surface temperature results as a function of flaw orientation in the two-dimensional model	92
28. Maximum surface temperature results as a function of flaw orientation in the two-dimensional model	93
29. Transient surface temperature results for the three-dimensional model.....	96
30. Time delay between generation stopping and maximum recorded surface temperature in the three-dimensional model	97
31. Maximum surface temperature results as a function of generation amount in the three-dimensional model.....	98
32. Maximum surface temperature results as a function of specimen thickness for the two-dimensional model	99
33. Maximum surface temperature results as a function of flaw orientation in the three-dimensional model	100

LIST OF FIGURES – CONTINUED

Figure	Page
34. Maximum surface temperature results as a function of flaw orientation in the two-dimensional model	101

LIST OF EQUATIONS

Equation	Page
1. Fourier's Law	18
2. Convective Boundary Condition.....	18
3. Heat diffusion equation.....	19
4. One-dimensional mathematical model with boundary conditions.....	22
5. Two-dimensional mathematical model with boundary conditions	23
6. Three-dimensional mathematical model with boundary conditions	25
7. Derivative definition	27
8. Finite difference estimation of a first order derivative	27
9. Taylor series.....	28
10. Finite difference estimation of a second order derivative.....	29
11. Crank-Nicolson estimation of second order partial derivative	30
12. Discretization of second order partial derivative term.....	31
13. First order partial derivative term	32
14. Finite difference approximation of the on-dimensional HDE	32
15. Energy balance equation	33
16. Energy balance for boundary nodes.....	33
17. Finite difference energy balance on boundary nodes	34
18. Finite difference top boundary equation	34
19. Finite difference bottom boundary equation.....	35

LIST OF EQUATIONS – CONTINUED

Equation	Page
20. Finite difference discretized equations in matrix form	35
21. Finite difference coefficient matrix	36
22. Finite difference temperature vector	36
23. Finite difference solution vector	36
24. Solution form for separation of variables analytical technique	48
25. Relationship between temperature distribution and green's function.....	50
26. Relationship between temperature distribution and Green's function with no generation and homogeneous boundary conditions.....	51
27. Dirac delta function definition.....	52
28. Point-source generation term	52
29. Dirac delta function integral	53
30. Integration property functions with Dirac delta function	53
31. One-dimensional mathematical model with boundary conditions.....	54
32. Defined transformation variable	54
33. One dimensional transformed partial differential equation with boundary conditions.....	55
34. One-dimensional homogeneous auxiliary partial differential equation with boundary conditions.....	56
35. One-dimensional separation of variables assumed solution	56
36. One-dimensional separation of variables re-arrangement	56
37. One-dimensional x dependent ordinary differential equation with conditions.....	57

LIST OF EQUATIONS – CONTINUED

Equation	Page
38. Time dependent ordinary differential equation for one-dimensional model	57
39. Time dependent ordinary differential equation solution for one-dimensional model.....	58
40. X dependent ordinary differential equation solution for one-dimensional model	58
41. One-dimensional eigenvalue equation.....	58
42. Re-arranged eigenvalue equation.....	59
43. General solution of auxiliary one-dimensional problem	59
44. Orthogonality principal	59
45. One-dimensional constant.....	59
46. Definition of the Norm.....	60
47. Norm solution for one-dimensional model	60
48. Solution to auxiliary problem	60
49. Green's function expression for one-dimensional model.....	61
50. Green's function at $\tau=0$ for the one-dimensional model.....	61
51. Green's function for one-dimensional model.....	61
52. Solution to transformed one-dimensional problem.....	62
53. Reduced solution to transformed one-dimensional problem	62
54. Final temperature solution form for one-dimensional model	62
55. Final temperature solution for one-dimensional model	62
56. Two-dimensional mathematical model with boundary conditions	63

LIST OF EQUATIONS – CONTINUED

Equation	Page
57. Defined transformation variable	64
58. Two-dimensional transformed partial differential equation with boundary conditions.....	64
59. Two-dimensional homogeneous auxiliary partial differential equation with boundary conditions.....	65
60. Two-dimensional separation of variables assumed solution	66
61. X-direction ordinary differential equation for two-dimensional model	66
62. Y-direction ordinary differential equation for two-dimensional model	66
63. Time dependent ordinary differential equation for two-dimensional model	66
64. Time dependent ordinary differential equation solution for two-dimensional model.....	67
65. X-dependent ordinary differential equation solution for two-dimensional model	67
66. Y-dependent ordinary differential equation solution for two-dimensional model	67
67. Eigenvalue expressions for two-dimensional model	67
68. Auxiliary solution for two-dimensional model.....	68
69. Norm solutions for the two-dimensional model	68
70. Green's function relationship for two-dimensional model.....	68
71. Green's function at $\tau=0$ for the two-dimensional model.....	69
72. Green's function for the two-dimensional model.....	69
73. Solution to transformed two-dimensional problem	69
74. Reduced solution to transformed two-dimensional problem.....	70

LIST OF EQUATIONS – CONTINUED

Equation	Page
75. Final temperature solution form for the two-dimensional model	70
76. Final temperature solution for two-dimensional model.....	70
77. Three-dimensional mathematical model with boundary conditions	71
78. Defined transformation variable	72
79. Three-dimensional transformed partial differential equation with boundary conditions.....	72
80. Three-dimensional homogeneous auxiliary partial differential equation with boundary conditions	73
81. Three-dimensional separation of variables assumed solution	74
82. X-direction ordinary differential equation for three-dimensional model	74
83. Y-direction ordinary differential equation for three-dimensional model	74
84. Z-direction ordinary differential equation for three-dimensional model.....	75
85. Time dependent ordinary differential equation for three-dimensional model.....	75
86. Time dependent ordinary differential equation solution for two-dimensional model.....	75
87. x dependent ordinary differential equation solution for three-dimensional model....	75
88. y dependent ordinary differential equation solution for three-dimensional model....	75
89. z dependent ordinary differential equation solution for three-dimensional model....	76
90. Eigenvalue expressions for the three-dimensional model	76
91. Auxiliary solution for three-dimensional model.....	76
92. Norm solutions for three-dimensional model	77
93. Green's function relationship for three-dimensional model.....	77

LIST OF EQUATIONS – CONTINUED

Equation	Page
94. Green's function at $\tau=0$ for the three-dimensional model.....	78
95. Green's function for the three-dimensional model.....	78
96. Solution to transformed three-dimensional model.....	78
97. Reduced solution to transformed three-dimensional model	79
98. Final temperature solution form for the three-dimensional model	79
99. Final temperature solution for three-dimensional model.....	79

ABSTRACT

The development of precise and accurate non-destructive examination (NDE) techniques is an essential element in preventing failures and increasing reliability in engineering materials. In particular, few present day composite material NDE techniques give the desired precision and cost-effectiveness required for many high-reliability applications such as on airplane wings or wind turbine blades. This study contributes to the development of a NDE technique known as vibrothermography. Vibrothermography is performed by measuring frictional heating of internal flaws that occur as a result of inducing specimen vibrations via an ultrasonic transducer. This frictional heat conducts itself to the surface, where it can be detected by an infrared camera. Vibrothermography is a potential cost-effective alternative to detecting a wide variety of flaws in composite materials.

This study models the heat generation that occurs during a vibrothermography test; and it simulates the manner at which this heat would conduct to the specimen's surface. Once the models were developed, they were used to simulate the influence of the following potential test parameters: specimen thickness, flaw generation amount, flaw size, flaw depth, and flaw orientation. The results provide an initial insight of which of these parameters could most greatly influence a vibrothermography test, and which ones may or may not be able to be detectable from a vibrothermography test.

Lastly, in conjunction with Kyle Spaulding, an initial thermal-mechanical combined analysis was developed that includes specimen vibration, heat generation, and heat conduction to create a start to finish vibrothermography simulation. This model is soon to be compared with experimental data. If the model results match experimental data, then the models will be implemented as a useful tool in determining the overall feasibility, accuracy, reliability, and optimal test procedures for vibrothermography.

CHAPTER 1 – BACKGROUND

Motivation

A composite material is any material which is made up of a combination of two or more constituent materials. Engineering interests in composites began with observations of the advantageous properties of naturally occurring composites such as wood or bone. Composites are often stronger and more durable than any of their individual constituent materials. These observations began an ongoing revelation, as engineers and material scientists continue to study and develop composites designed with specific engineering applications in mind. These studies continue to produce cheap, lightweight, effective composites which are becoming more and more prevalent in commercial, industrial, aerospace, marine, and recreational structures. As examples, man-made composites are used to build aircraft components, boat and ship frames, fishing rods, golf clubs and even replacement body parts in orthopedic surgeries.

Many composite structures require reliable, high-precision, cost-effective non-destructive examination (NDE) techniques to be associated with the fabrication process and/or in-use maintenance. Because of the multiple materials and material boundaries that exist within composites, many traditional NDE methods are either unable to detect material flaws, or require undesired amounts of money, time, and/or input energy. As an example, one of the most common NDE technique for detecting flaws in wind turbine blade and airplane wing composites is the Computed Tomography (CT) scan. The CT scan, which involves hitting the specimen with a series of X-rays, is expensive, time intensive, and requires large power inputs. Despite the invention of many NDE

techniques (many of which are discussed later in this chapter), there still remains a high demand for the development of more precise, cost-effective NDE techniques for many composite material applications.

One NDE method that has shown potential to detect flaws and delaminations in composite materials in an efficient and cost-effective manner is vibrothermography (also known as vibrothermographic imaging). Vibrothermography--which is the focus of this study-- is a technique in which applied vibrations cause frictional heating at cracks or delaminations. Typically, the heating is measured by observing the specimen surface temperatures with an infrared camera. Despite showing potential, more research is required to determine the overall precision, feasibility, and reliability of vibrothermography. This study is focused on modeling the heat transfer occurring within a vibrothermography specimen, which will be useful in correlating flaw type, size, and location with measured surface temperature distributions.

Fracture Mechanics

In order to fully understand the importance of non-destructive examination in fatigue loaded structures (such as an aircraft component or wind turbine blade), a brief introduction of fracture mechanics is required. Fracture Mechanics is the study of the propagation of cracks in materials. When a crack, flaw, or delamination grows in size, it reduces the amount of undamaged material available to distribute internal stresses. Fatigue failure occurs when an initial material discontinuity--such as a crack or delamination--is propagated to a critical size at which the amount of undamaged material becomes too small to withstand local internal stresses, resulting in a fatigue failure.

Fatigue failures are typically brittle, sudden, and can be extremely dangerous. The next section gives a few examples of the catastrophic effect fatigue failures can have.

History of Fracture Mechanics

From the early 1800s through the mid-1900s, unexplainable structural failures and engineering disasters occurred despite a sufficient understanding of instantaneous failure and stress relationships (Anderson, 1969). A few of these examples are listed below:

- On December 13, 1898 a large gas tank unexplainably failed in New York City, killing three people and injuring several (Huge Gas Tank Collapses, 1898).
- The February 1866 journal of Engineering from Great Britain announced that between 50 and 60 boiler explosions were occurring annually. Many of the explosions were catastrophic.
- In the 1880s, failures associated with the sudden increase in railway production and implementation were so frequent that the New York Times began including “the most serious railroad accident of the week” (Anderson, 1969).
- Another increase in material failures occurred during World War II (WWII) when all-welded designs for military ships were developed. As an example, out of 2500 Liberty Ships built, 145 broke in two and almost 700 experienced serious non-combat related failures (Broek, 1986). The photograph in Figure 1 is taken from weldreality.com and is an example of a failed Liberty Ship.

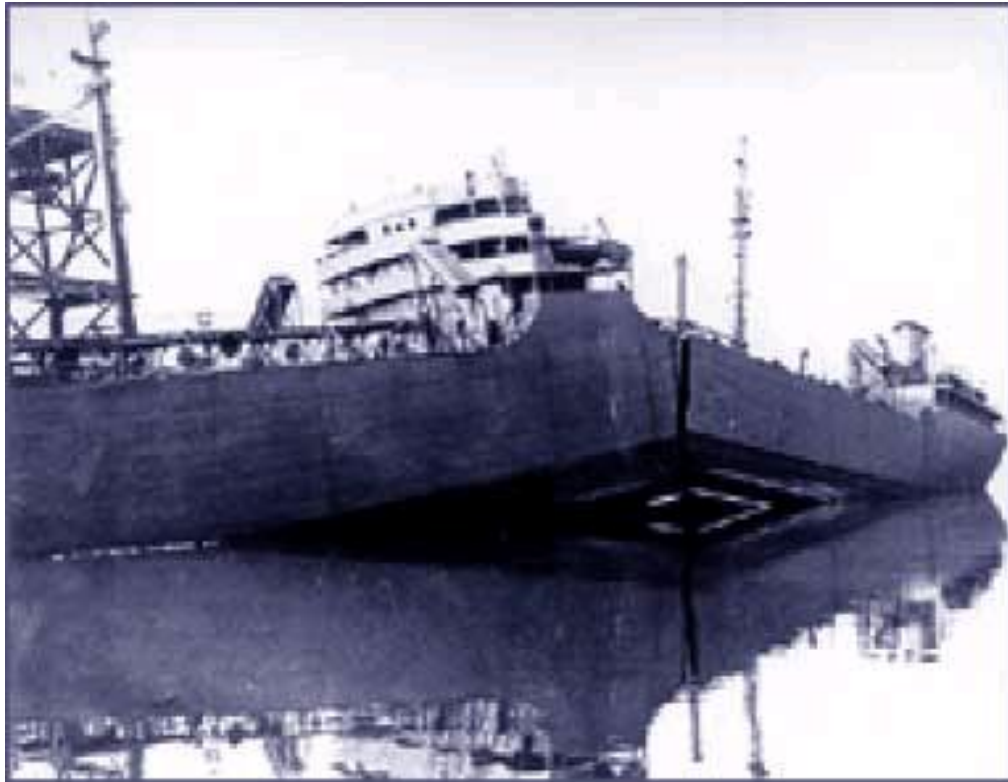


Figure 1. Liberty Ship failure

Theory of Fracture Mechanics

Material scientists and engineers alike studied many of these catastrophes, which often involved low stresses, strong materials, and brittle failures. The fundamentals of understanding these failures were actually already published with A.A Griffith and the Griffith criteria (Griffith, 1920); but the knowledge of Griffith's criteria and fracture mechanics remained, for the most part, unknown among most structural engineers. The Griffith criteria laid the fundamental foundation of understanding how initial material flaws propagate until failure is achieved by using a conservation of energy approach. (Similar fracture mechanics principals were also developed shortly after Griffith with a "fracture toughness" approach rather than a conservation of energy approach). Griffith's

criteria states “crack propagation will occur if the energy released upon crack growth is sufficient to provide all the energy that is required for crack growth.” (Griffith, 1920).

Beginning with the high demand to eliminate catastrophic failures, along with Griffith’s criteria, material scientists and engineers were able to develop--and continue to develop--relationships between material flaws, crack propagation, and fracture failures that catastrophically affected so many designs in the past. The study of these relationships is what is now what is known as Fracture Mechanics.

The most important concept in Fracture Mechanics is the relationship between crack length and the number of cycles in a fatigue loading situation. Through studies--many of which are experimental--engineers are able to accurately estimate a critical crack length (the crack length at which the material fails) for particular loading conditions. Once a failure criterion has been established, understanding the rate at which a crack grows is imperative in order to predict when failure will occur for a given loading condition. For fatigue loading cases, this relationship is characteristically exponential as shown in Figure 2. Because of this relationship, an engineer must not only be able to know how large a crack within a specimen is, but also where along this exponential relationship this crack falls. A very small crack can quickly propagate to a point of failure as a result of this exponential nature.

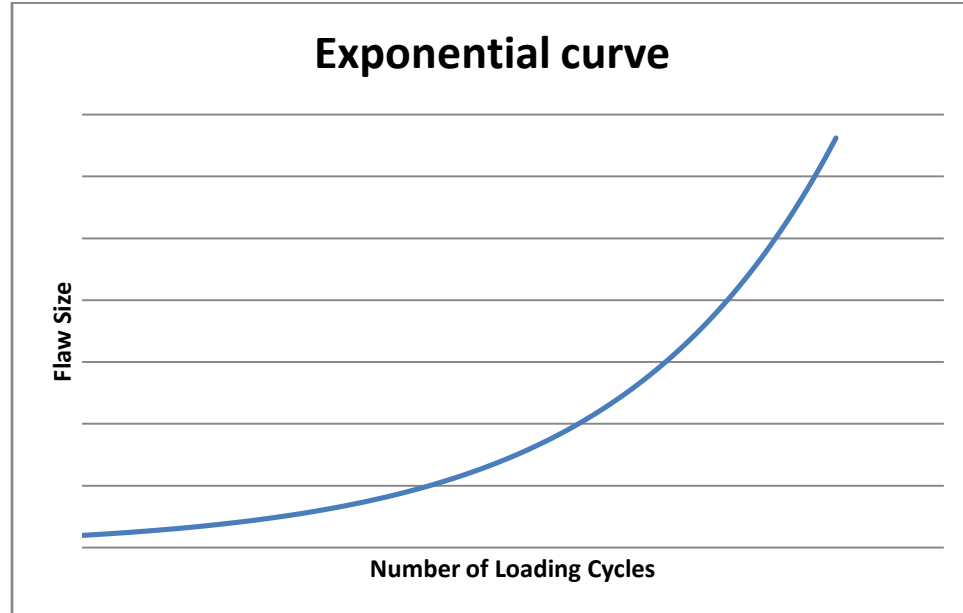


Figure 2. Crack growth exponential curve

As can be deduced from the catastrophes listed in the history of Fracture Mechanics section, the need to prevent material flaws from propagating to a critical size is imperative in all engineering industries. All materials have initial flaws, due to how they were formed in nature and/or any previous temperature, pressure, and physical loads they've undergone. Therefore, producing materials that will not fail due to fatigue is currently impossible, no matter how small the loading may be. The challenges are to maximize fatigue life and to predict, and therefore take action to prevent, fatigue failures before they catastrophically occur. Furthermore, the fatigue life of nearly all materials has a very large standard deviation, meaning the actual life varies significantly from individual specimen to individual specimen. This is because the initial flaws vary from specimen to specimen. Unlike time-independent characteristics such as compressive or tensile strength, accurate fatigue life predictions can't be deduced strictly from

experiments performed on multiple specimens of the same material. The spread in the data is too great.

Therefore, further information about the flaws in each individual specimen must be known. The actual material flaws themselves must be observed in order to accurately predict a specimen's fatigue life. Lastly, especially in cases in which loading has a random component, these flaws must also be monitored and checked many times throughout the material's life. This is why NDE is required both in the material fabrication process as well as an in-use maintenance check.

Overview of NDE Techniques

Some of the most common NDE methods applied today are: radiography, ultrasonic testing, liquid penetrant inspection, and magnetic particle inspection. Other newer NDE methods which are less common but of particular interest in this study for their potential to detect flaws in composite materials are shearography, resonance testing, and vibrothermography.

Radiography

Radiography is the technique of obtaining a shadow image of a solid using penetrating radiation such as x-rays or gamma rays. The contrast in a radiograph is due to different degrees of absorption of the radiation within the specimen. The amount of absorption depends on specimen thickness, different chemical constituents, non-uniform densities, flaws, discontinuities, or to scattering processes within the specimen (Cortz, 1995). Choosing the proper radiation frequency can allow an operator to isolate and

“bring out” material flaws and cracks on an image produced by the radiation waves. An example of an X-ray image is shown in Figure 3.

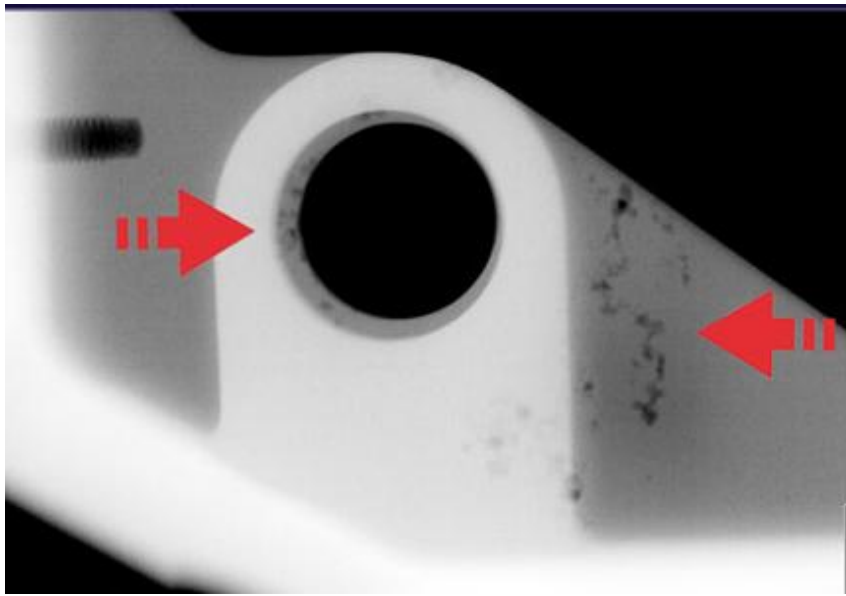


Figure 3. X-Ray example (from NT3 digital X-Ray imaging Inc.)

As previously mentioned, one radiography NDE technique that is commonly applied to composite materials is CT scanning or CT imaging. A CT scan is simply a series of X-ray photographs taken while the scanner is rotated 360° around the specimen. Together, the images can be input into a computer, which produces a three-dimensional image of the scanned specimen. CT scans can be applied, and effectively detect flaws in composite materials. However, a CT scan requires large power inputs, is difficult to apply to large specimens, and must inspect the composite in a time-intensive layer by layer fashion.

Ultrasonic Testing

Ultrasonic Testing (UT) is a method of NDE in which cracks, flaws, and material discontinuities are detected by monitoring how the waves scatter, reflect, or change in any way when traveling through the specimen. Most commonly, an ultrasonic test is performed by applying a pulse sound wave to the specimen via an ultrasonic transducer. The reflected wave amplitudes and frequencies are monitored through sensors attached to the transducer can. Also, when applying ultrasonic pulses from the transducer, the time delay between the applied wave and the reflected wave can be measured to estimate the depth of the crack, flaw, material boundary, or material discontinuity that reflected the initial wave.

Ultrasonic imaging is a specific type of ultrasonic testing which involves a larger transducer which sends out multiple waves at slightly different angles through the test specimen. Gathering the data from each of the waves can provide enough information to determine two-dimensional surfaces which are reflecting the waves. From these surfaces, computers can be used to create images which use color contrasts (the lighter the color the less waves are being reflected back) as a representative image of what lies beneath the material surface. Most people are familiar with medical industry ultrasounds, which provide doctors a means to inspect unborn babies.

Liquid Penetrant Inspection

Liquid Penetrant Inspection (LPI) is a method of NDE which is specific to finding surface flaws (Cortz, 1995). LPI is executed by applying a liquid penetrant by a spraying or submersion process over the surfaces under inspection. After the penetrant has been

given enough time to allow it to penetrate into any surface flaws, the excess surface penetrant is removed. After removal, a second substance, known as a developer, is applied to the surface of the specimen to draw out and absorb the penetrant which is in the specimen's surface flaws. Judging from the penetrant locations on the developer, one can now more clearly see the shape and size of the material's surface flaws.

Magnetic Particle Inspection

Magnetic Particle Inspection (MPI) is a NDE method which evolved from an observation in 1917 by Hoke (Cortz, 1995). He noticed that iron grindings formed when machining a piece of steel would migrate to cracks along the steel surface to form distinct patterns. When subject to magnetic potential, many flaws will have magnetic flux lines which are naturally distorted in and around material discontinuities. In the case of flaws near or at the surface, this distortion of the magnetic field can actually cause the field lines to leak onto or even outside the specimen, therefore causing magnetic particles to be attracted to these locations as shown in Figure 4.

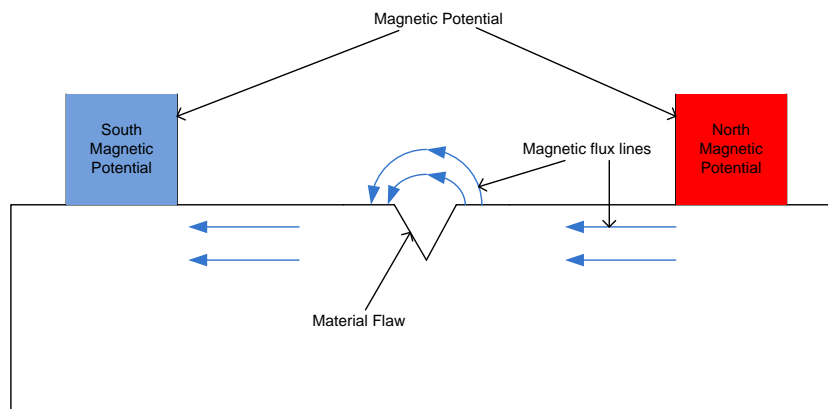


Figure 4. Magnetic particle inspection phenomenon

MPI is cheap and very effective at detecting surface flaws in metallic materials. However, MPI is unreliable when detecting sub-surface cracks, as well as inapplicable to non-metallic materials.

Shearography

Shearography is a NDE technique which takes advantage of the fact that flaws will induce strain concentrations around them (Huang, 1982). The test is performed by comparing images of un-deformed (with no applied load) and deformed images of the same location on the specimen. Shearography has been shown to be able to detect a wide variety of composite material flaws but requires substantial image manipulation, expensive light sources, and unique test set-ups in order to apply the load to large specimens. Also, the precision for shearography remains in question as this method continues to be one of the most extensively researched NDE techniques (Hung, 1996).

Resonance Testing

Resonance testing refers to any NDE method in which the specimen of interested is vibrated, and material flaws are located by identifying locations that display a sudden change in natural frequency. The most common resonance testing method is called tap testing. Tap testing was actually initially applied to glassware and fine chinaware before being introduced into the aerospace industry during World War I. During this time period, tap tests were performed manually by an experienced worker who would tap a quarter up and down each of the surfaces of an aircraft wing. Many workers were able to identify material flaws because locations near a material flaw would produce a noticeably different sound (i.e. frequency response) after the quarter struck the specimen.

Today, a wide variety of resonance test methods can be applied. One example includes robotic tap testers which simply take the place of the worker, and tap all surfaces of the specimen while measuring the sound waves coming back. Other resonance methods exist in which the entire specimen is vibrated at different modes while multiple accelerometers take measurements at many locations along all of the specimen's surfaces. Resonance tests are almost never implemented as a stand-alone NDE technique, and are usually performed as a quick check for any obvious flaws. NDE in the aerospace and wind industries require much more detailed results and higher dependability than can be offered by present day resonance testing technology (Cortz, 1995).

Vibrothermography

Vibrothermography, which is the focus of this study, measures surface temperature distribution of an object in response to induced energy. The induced energy in vibrothermography most commonly comes from a mechanical excitation device on the surface of the specimen. This excitation can be applied with devices such as piezoelectric shakers, electromagnetic shakers, piezoceramic actuators, air-coupled and water-coupled ultrasonic transducers or ultrasonic welders. Upon the correct excitation parameters, cracks of interest will rub together and begin generating frictional heat.

Vibrothermography first appeared in literature in 1979 (Henneke II, Reifsnider, & Stinchcomb, 1979), but was rarely applied in industry until Favro et al. (Favro, Han, Ouyang, Sun, Sui, & Thomas, 2000) showed that it had potential with high-precision detection in large specimens when the excitation parameters were correctly chosen. Also, Favro believed that vibrothermography had potential in detecting a wide variety of flaws

in a wide variety of materials, including delaminations in composites. The most common vibrothermography procedures use an ultrasonic welder as a vibration source which typically applies between 1-3 kW of power to the specimen.

One potential advantage of vibrothermography over other modern-day NDE techniques is in-plane (IP) and out-of-plane (OP) laminate waviness may possibly be detectable with vibrothermography. This is believed to be possible because the constitutive materials in many composite materials (especially glass-epoxy and carbon-fiber composites) have substantially different thermal conductivities. Detection of waviness is significant because waviness does affect composite strength, and is undetectable with currently implemented NDE techniques.

Despite its appealing potential, vibrothermography is rarely implemented because there are many challenges that must be overcome. First, excitation parameters and procedures must be able to dependably produce heat from all flaws of interest regardless of location and orientation. This is a unique challenge because different excitation parameters cause different modes of vibration to be induced, and flaws near node locations (locations within the specimen that have little to no displacement when the specimen is excited) may not produce heat. Therefore frequency, input power, and transducer location(s) must all be optimized and well planned in order to insure a reliable overall test. Also, there exist some limitations of excitation parameters because the specimen must never have any displacements large enough to cause further damage. Inputting too much energy could cause localized stress at flaw tips to actually cause existing flaws to propagate and prematurely fail the material. Furthermore, applied

excitation can cause localized damage on the specimen, and, in some experiments, has even caused composite materials to have localized melting. This melting looks similar to a cigarette burn.

Another challenge is developing mathematical models to simulate the heat generation and heat transfer that occur during vibrothermography. Accurate models will significantly reduce experimental costs and aid in the understanding of the effect that parameters such as flaw location, flaw size, flaw orientation, specimen size, and specimen shape could have on the recorded surface temperature distributions.

Project Overview

The purpose of this study is to model and determine the thermal effects of vibrothermography on composite materials. It is a component of a larger overall project funded by the Department of Energy (DOE) to determine the overall feasibility, precision, efficiency, and cost-effectiveness of incorporating vibrothermography as a NDE method to detect cracks and delaminations within composite materials. The overall project is shared between Montana State University in Bozeman, MT and Resodyn Corporation from Butte, MT, and will specifically address all the challenges described in the previous section.

Resodyn is in the process of completing a series of experimental tests with a carbon-fiber ply drop composite specimen. The specimen is over 8 in. wide, is 0.5 in. thick before the ply drop and 0.75 in. thick after the ply drop. The specimen has two known flaws that are known to exist, with the largest flaw located just downstream of the ply drop. The experiments are being performed with clamped-free boundary conditions

with excitation frequencies ranging from 18.0 kHz to 20.0 kHz. The tests are being completed with a pre-load ranging from 35 lbf to 39 lbf (156 to 173 N). The top surface temperature and side surface temperature are measured with a high-precision infrared camera.

At Montana State, two sets of models have been developed in order to simulate experiments such as the one currently being performed at Resodyn. The first set of models -- developed by another group at Montana State -- determines the amount of heat generated at a flaw during a vibrothermography experiment. The other Montana State group has produced one-dimensional, two-dimensional, and three-dimensional models with the finite element software ANSYS which are capable of simulating the mechanical vibrothermography effects for a wide variety of specimen sizes, excitation parameters, flaw types, and flaw sizes.

The second set of models -- which are developed in this study -- are designed to simulate the heat transfer as a result of the heat generation determined in the other group's mechanical models. These thermal models, which have been developed with the finite element, finite difference, and analytical methods, serve to provide a relationship between a known heat generation source and the resulting surface temperature result.

Individually, the models can be applied to determine the effect a parameter of interest, such as flaw depth for example, can have on the amount of heat generated and/or the resulting temperature distribution during a vibrothermography test. Together, the models can be used to simulate vibrothermography experiments, and compare simulated results to experimental results.

In this study, a parametric study showing the effects of the parameters given in the next section is also included.

Parameters

The parametric study found in this paper was performed by investigating the change in surface temperature of a specimen as a result of heat generation occurring from a point source, line source, or surface area source used to represent a flaw during a vibrothermography experiment. The study investigated the following parameters:

- Heat generation amount ($100 - 500 \frac{W}{m^2}$ which corresponds to $0.06 - 0.32 \frac{W}{in^2}$)
- Flaw depth (10 – 90% of the specimen thickness)
- Flaw size (measured in in. or in.²)
- Flaw orientation (0 – 90 degrees with respect to the top surface)
- Specimen thickness (0.1 – 2 inches corresponds to 0.254 – 5.08 cm)

The ranges applied for each of the listed parameters were designed to replicate possible values likely to occur during Resodyn's future experiments.

CHAPTER 2 – MATHEMATICAL SET-UP

Heat Transfer Fundamentals

Heat transfer is defined as the study of how thermal energy transfers from hotter regions of a body to cooler regions. Heat transfer is broken into three mechanisms, heat conduction, heat convection, and radiation.

From a micro scale, conduction is defined as “the direct microscopic exchange of kinetic energy of particles through the boundary between two systems” (Ozisik, 1993). On a macro-scale heat conduction is defined by the flow of thermal energy in fluids or solids at rest.

Heat convection is defined as the phenomenon of bulk flow of a fluid carries heat along with the flow of matter in the fluid (Ozisik, 1993). Heat convection can't occur within solids where no mass exchange is taking place.

Thermal radiation is defined as the transfer of thermal energy through electromagnetic radiation. Radiation is unique in that it is not linearly related to the temperature difference between two mediums and that it does not need the presence of physical molecules in order to transfer the energy (i.e. thermal radiation can occur in a vacuum).

The heat transfer problem observed in this system involves a solid medium initially assumed to be at thermal equilibrium until heat is generated at a particular crack location as a result of vibrothermography. This heat then conducts away from its source and ultimately reaches a surface, where it is then convected to the ambient air.

Heat can't be measured directly, but the concept of heat flow is related to the measurable scalar quantity of temperature. Therefore, heat transfer problems are solved by first determining a temperature distribution within the volume or mass of interest, and then basic laws relating temperature to heat flow are applied to determine heat transfer.

For heat conduction, Fourier's Law describes the relationship between heat flow and temperature distribution. Fourier's Law is given in Cartesian form in Equation 1.

Equation 1. Fourier's Law

$$\vec{q}(x, y, z, t) = -\vec{i} * k * \frac{\partial T}{\partial x} - \vec{j} * k * \frac{\partial T}{\partial y} - \vec{k} * k * \frac{\partial T}{\partial z}$$

Where:

$\vec{q}(x, y, z, t)$ = the heat flux vector ($\frac{W}{m^2}$)

k = thermal conductivity ($\frac{W}{m * K}$)

T = temperature (K or C)

x, y, z = orthogonal directions in a Cartesian coordinate system

$\vec{i}, \vec{j}, \vec{k}$ = unit vectors in the $x, y,$ and z directions respectively

For heat convection, the boundary condition equation used to describe the solid/fluid interface is shown in Equation 2.

Equation 2. Convective Boundary Condition

$$k * \frac{\partial T}{\partial n} + h * T = h * T_{amb}$$

Where:

h = convective heat transfer coefficient ($\frac{W}{m^2 * K}$)

n = outward normal vector to the material surface

The overall temperature distribution in a solid body is described by the Heat Diffusion Equation (HDE). The HDE is given in the Cartesian coordinate system in Equation 3.

Equation 3. Heat diffusion equation

$$\frac{\partial^2 T}{\partial x^2} + \frac{\partial^2 T}{\partial y^2} + \frac{\partial^2 T}{\partial z^2} + \frac{g(x, y, z, t)}{k} = \frac{1}{\alpha} * \frac{\partial T}{\partial t}$$

Where:

$g(x, y, z, t)$ = heat generation ($\frac{W}{m^3}$)

α = thermal diffusivity = $\frac{k}{\rho * C_p}$

ρ = mass density ($\frac{kg}{m^3}$)

C_p = specific heat capacity ($\frac{J}{kg * K}$)

The HDE is a second order linear non-homogeneous partial differential equation (PDE). The closed form solution is dependent upon the boundary conditions and initial condition associated with each individual problem. Many times, closed form solutions for the HDE are difficult or impossible to directly obtain due to singularities that may arise from some types of boundary conditions and/or non-continuous terms (such as a non-continuous heat generation term). Methods for solving the HDE discussed in this study (see Chapters 3-5) are:

- The Separation of Variables Technique

- Green's Function
- Finite Difference Method
- Finite Element Method

Modeling Set-up

The specimen modeled was a 5 inch (12.7 cm) wide in x direction by 1 in. (2.54 cm) long in z direction fiberglass composite. In the models, the thickness of the specimen was varied from 0.1 inches (0.254 cm) to 2 inches (5.08 cm) in y direction. All of the material properties that were applied to the models were determined experimentally at Resodyn from one of their fiberglass composite materials as shown below. The convective coefficient was determined from (Ozisik, 1993) as a typical coefficient in ambient air.

- Mass density = 1850 kg/m^3
- Specific heat = $800 \text{ J/(kg}\cdot\text{K)}$
- Thermal conductivity = $1.34 \text{ W/(m}\cdot\text{K)}$
- Convective heat transfer coefficient = $10 \text{ W/(m}^2\cdot\text{K)}$

The parameters that were varied in the heat transfer models of this study were:

- Heat generation value
- Flaw depth
- Flaw orientation
- Specimen thickness

The mathematical models produced in this study determined surface temperature distributions vs. time as a result of a localized flaw generation. The HDE conditions that were applied to model the one-dimensional, two-dimensional, and three-dimensional vibrothermography effects are given in the following three sections, respectively.

One-Dimensional Heat Transfer Model

The one-dimensional heat transfer problem modeled to simulate the heat transfer effects of vibrothermography is shown in Figure 5. In the figure, the x direction represents the direction of the specimen depth, and L represents the value of the specimen thickness.

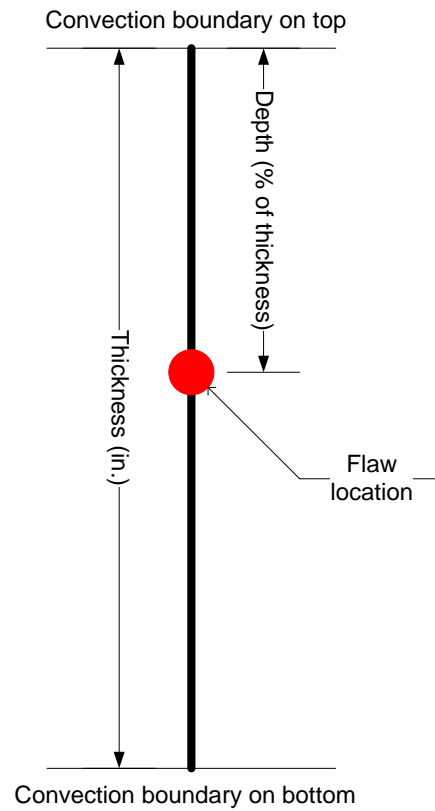


Figure 5. One-dimensional heat transfer model

For the one-dimension situation shown in Figure 5, the HDE can be reduced to the expression given in Equation 4.

Equation 4. One-dimensional mathematical model with boundary conditions

$$\frac{\partial^2 T}{\partial x^2} + \frac{g(x, t)}{k} = \frac{1}{\alpha} * \frac{\partial T}{\partial t}$$

Boundary conditions (B.C.)

$$-\frac{\partial T}{\partial x} + \frac{h}{k} * T = T_{amb} \quad @ \ x = 0$$

$$\frac{\partial T}{\partial x} + \frac{h}{k} * T = T_{amb} \quad @ \ x = L$$

Initial condition (I.C)

$$T = f(x)$$

@ t=0

Two-Dimensional Heat Transfer Model:

The two-dimensional heat transfer problem modeled to simulate the heat transfer effects of vibrothermography is shown in Figure 6. H represents the specimen thickness and W represents the specimen width.

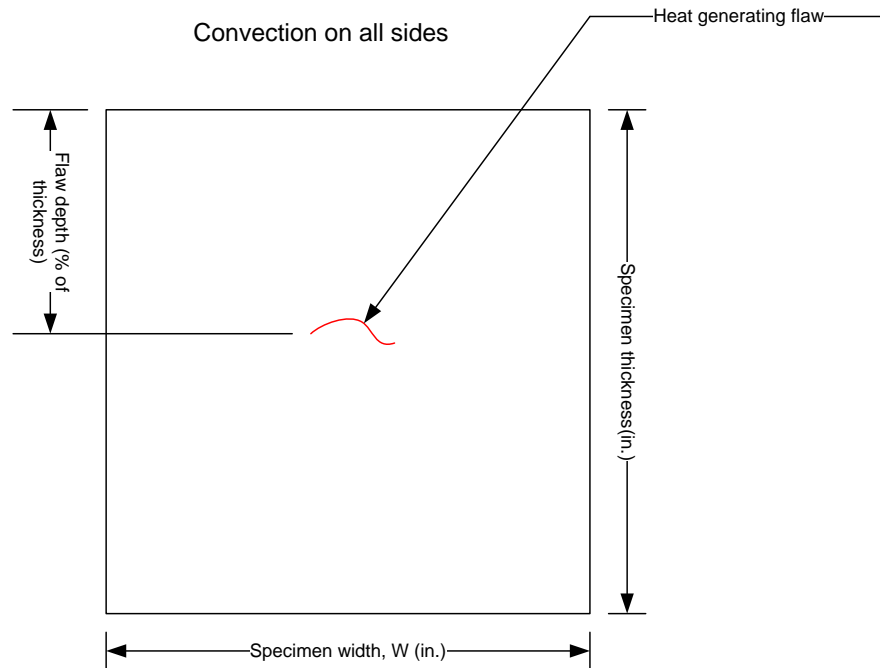


Figure 6. Two-dimensional heat transfer model

For the two-dimensional situation shown in Figure 6, the HDE reduces to the expression given in Equation 5.

Equation 5. Two-dimensional mathematical model with boundary conditions

$$\frac{\partial^2 T}{\partial x^2} + \frac{\partial^2 T}{\partial y^2} + \frac{g(x, y, t)}{k} = \frac{1}{\alpha} * \frac{\partial T}{\partial t}$$

Boundary conditions (B.C.)

$$-\frac{\partial T}{\partial x} + \frac{h}{k} * T = T_{amb} \quad @ \ x = 0$$

$$\frac{\partial T}{\partial x} + \frac{h}{k} * T = T_{amb} \quad @ \ x = W$$

$$-\frac{\partial T}{\partial x} + \frac{h}{k} * T = T_{amb} \quad @ \ y = 0$$

$$\frac{\partial T}{\partial x} + \frac{h}{k} * T = T_{amb} \quad @ \ y = -H$$

Initial condition (I.C)

$$T = f(x, y) \quad @ \ t=0$$

Three-Dimensional Model:

The three-dimensional heat transfer problem modeled to simulate the heat transfer effects of vibrothermography is shown in Figure 7. W represents the specimen width in the x-direction, L represents the specimen length in the z-direction, and H represents the specimen thickness in the y-direction.

Convection on all outer surfaces

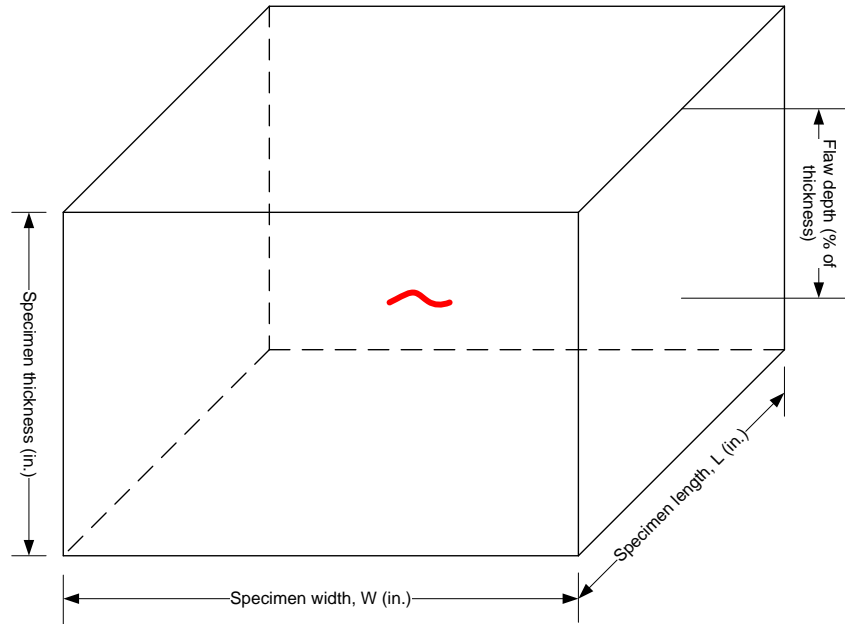


Figure 7. Three-dimensional heat transfer model

The HDE for the three-dimensional model shown in Figure 7 can be reduced to the expression given in Equation 6.

Equation 6. Three-dimensional mathematical model with boundary conditions

$$\frac{\partial^2 T}{\partial x^2} + \frac{\partial^2 T}{\partial y^2} + \frac{\partial^2 T}{\partial z^2} + \frac{g(x, y, z, t)}{k} = \frac{1}{\alpha} * \frac{\partial T}{\partial t}$$

Boundary conditions

$$-\frac{\partial T}{\partial x} + \frac{h}{k} * T = T_{amb} \quad @ \ x = 0$$

$$\frac{\partial T}{\partial x} + \frac{h}{k} * T = T_{amb} \quad @ \ x = W$$

$$-\frac{\partial T}{\partial y} + \frac{h}{k} * T = T_{amb} \quad @ \ y = 0$$

$$\frac{\partial T}{\partial y} + \frac{h}{k} * T = T_{amb} \quad @ \ y = H$$

$$-\frac{\partial T}{\partial x} + \frac{h}{k} * T = T_{amb} \quad @ z = 0$$

$$\frac{\partial T}{\partial x} + \frac{h}{k} * T = T_{amb} \quad @ z = L$$

Initial condition (I.C)

$$T = f(x, y, z) \quad @ t=0$$

Modeling Set-up Overview

As stated earlier, there were three solution methods investigated to solve the models given in Equations 4, 5, and 6.

1. Finite difference method
2. Finite element method
3. Analytical method

These three methods all produce surface temperature distributions as a function of time. Only a one-dimensional model was created with the finite difference method, while one, two, and three-dimensional models were developed with the analytical and finite element methods. The different models serve as a means to check solutions for consistency.

CHAPTER 3 – FINITE DIFFERENCE APPROACH

Finite Difference Approximation of Derivatives

The finite difference method is a method which discretizes all derivative terms in a differential equation (Chapra, 2008). The derivation simply discretizes the definition of a derivative, which is shown in Equation 7.

Equation 7. Derivative definition

$$\frac{df(x)}{dx} = \lim_{h \rightarrow 0} \frac{f(x+h) - f(x)}{h}$$

In the finite difference method, this derivative is estimated simply by replacing the limit value of h with a very small numeric value. The smaller h is, then the more accurately the derivative is estimated. However, if the value of h is too small, round-off errors and computational times can negatively influence results.

Equation 8. Finite difference estimation of a first order derivative

$$\frac{df(x)}{dx} \approx \frac{f(a+h) - f(a)}{h}$$

To solve a thermal problem with the finite difference method, the line, area, or volume of interest must be discretized into nodes. Nodes represent discrete locations within the line, area, or volume of interest in which you are solving for the temperature. The temperature at each node is solved for one by one, by applying the finite difference approximations of the HDE at each node. In the following paragraphs note that x_i denotes the node of interest along the x -axis.

The most common method to determine the finite difference estimations of higher order derivatives is to apply the Taylor Series (Chapra, 2008), which is given below in Equation 9.

Equation 9. Taylor series

$$f(x_{i+1}) = f(x_i) + h \frac{df(x_i)}{dx} + \frac{h^2}{2!} \frac{d^2f(x_i)}{dx^2} + \frac{h^3}{3!} \frac{d^3f(x_i)}{dx^3} + \dots + \frac{h^n}{n!} \frac{d^n f(x_i)}{dx^n}$$

Where:

h = step size between nodes

x_i = the current x location in a Cartesian coordinate system

x_{i+1} = the next x location in a Cartesian coordinate system

$f(x_i)$ = value of the function at location x_i

$f(x_{i+1})$ = the value of the function at location x_{i+1}

There exist three methods to estimate a first derivative term: (1) Backward difference approximation, (2) Forward difference approximation, and (3) Central difference approximation. The Backward difference approximation estimates the value of the function in terms of the value at the previous location, the forward solves for the function value in terms of the next value, and the central difference solves for the current value in terms of both the previous and next values. For this study, central difference approximations were applied because the central difference has the smaller error terms than the forward or backward difference methods (Chapra, 2008).

Higher order derivatives can be estimated by taking two Taylor series (one forward approximation and one backward approximation for example), and subtracting

them from each other to eliminate terms of higher order than the derivative you are solving for. The next step is to re-arrange the resulting equation to solve for the derivative term of interest.

The result of the central finite difference approximation for a second-order derivative is given in Equation 10.

Equation 10. Finite difference estimation of a second order derivative

$$\frac{d^2 f(x_i)}{dx^2} \approx \frac{f(x_{i+1}) - 2 * f(x_i) + f(x_{i-1}))}{h^2}$$

The last wrinkle in the finite difference method is to estimate partial derivatives, which is explained in the following section.

Finite Difference Approximations of Partial Derivatives

A second order partial derivative term, $\frac{\partial^2 T(x,t)}{\partial x^2}$, is estimated in a similar fashion to the second order full derivative term. However, there still remains some dependence on the time, t, which must be taken into account when determining the partial derivative finite difference approximation. There exist three common methods that are typically applied to deal with this time dependence.

1. Implicit method: use all the Temperature values from the current time step
2. Explicit Method: Use all the temperature values from the previous time step
3. Combination methods: use a combination of implicit method and explicit method results

Although it is the most computationally expensive, the combination methods have been shown to produce the most stable finite difference estimations for partial derivative

terms (Chapra, 2008). There exist many different ways to combine the current and previous time step nodal temperatures for these combination methods. The most popular of these is known as the Crank-Nicolson Method, which simply averages the implicit method and explicit method results as shown in Equation 11.

Equation 11. Crank-Nicolson estimation of second order partial derivative

$$\frac{\partial^2 T(x, t)}{\partial x^2} \approx \frac{T(x_{i+1}, t_j) - 2 * T(x_i, t_j) + T(x_{i-1}, t_j) + T(x_{i+1}, t_{j-1}) - 2 * T(x_i, t_{j-1}) + T(x_{i-1}, t_{j-1})}{2 * h^2}$$

Where:

$T(x_i, t_j)$ = Temperature at node i during the current time step j

$T(x_i, t_{j-1})$ = Temperature at node i during the previous time step j-1

One-Dimensional Application of Finite Difference Model

The finite difference model was applied to the one-dimensional model given in Equation 4. The one-dimensional finite difference model was discretized into nodes as shown in Figure 8.

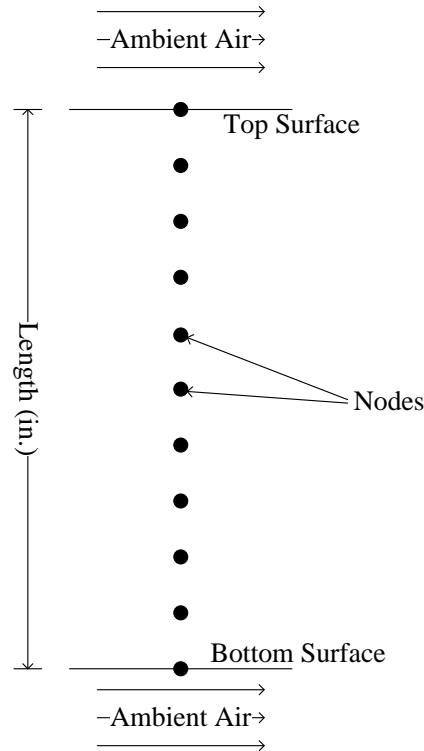


Figure 8. Node discretization for the finite difference method

Discretization of Internal Nodes

The first step in deriving the discretized equations associated with the one-dimensional model is to determine the finite difference estimations of the partial derivative terms. Applying the Crank-Nicolson method, those terms can be estimated as shown in Equations 12 and 13.

Equation 12. Discretization of second order partial derivative term

$$\frac{d^2T(x_i, t)}{dx^2} \approx \frac{1}{2} \left[\frac{T(x_{i+1}, t_j) - 2 * T(x_i, t_j) + T(x_{i-1}, t_j) + T(x_{i+1}, t_{j-1}) - 2 * T(x_i, t_{j-1}) + T(x_{i-1}, t_{j-1})}{\Delta x^2} \right]$$

Equation 13. First order partial derivative term

$$\frac{\partial T}{\partial t} = \frac{T(x_i, t_j) - T(x_i, t_{j-1})}{\Delta t}$$

These equations can be substituted into the HDE given back in Equation 4 and rearranged to yield Equation 14.

Equation 14. Finite difference approximation of the on-dimensional HDE

$$\begin{aligned} \left[\frac{1}{\alpha \Delta t} + \frac{1}{\Delta x^2} \right] T(x_i, t_j) - \frac{T(x_{i-1}, t_j)}{2\Delta x^2} - \frac{T(x_{i+1}, t_j)}{2\Delta x^2} \\ = \left[\frac{1}{\alpha \Delta t} - \frac{1}{\Delta x^2} \right] T(x_i, t_{j-1}) + \frac{T(x_{i-1}, t_{j-1})}{2\Delta x^2} + \frac{T(x_{i+1}, t_{j-1})}{2\Delta x^2} + \frac{g}{k} \end{aligned}$$

Notice that all the terms on the left-hand side of Equation 14 are from the current time step, t_j , and all the terms on the right hand side are from the previous time step, t_{j-1} . All the previous time step temperature values are known from the previous solution or, in the case of the initial time ($t=0$) the assumed equilibrium initial condition is applied to all the nodes.

Equation 14 is discretized into $n-2$ equations where n is the number of nodes. This is because this equation is valid for $i=1, i=2, \dots, i=n-1$. Equations for $i=1$ and $i=n$ must be determined from the boundary conditions.

Top Boundary Condition

The top boundary condition was determined by applying an energy balance to the discretized situation shown in Figure 9.

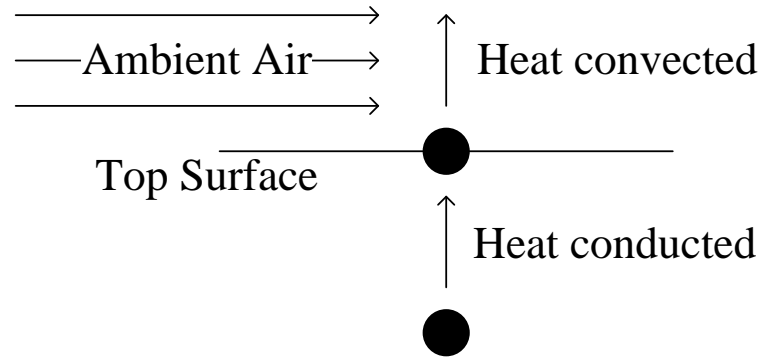


Figure 9. Top surface finite difference energy balance

The energy balance is based on Equation 15.

Equation 15. Energy balance equation

$$q'' = \rho V C \frac{dT}{dt}$$

Where:

q'' = total incoming heat flux $\left(\frac{W}{m^2}\right)$

ρ = mass density $\left(\frac{kg}{m^3}\right)$

V = volume of interest = $\Delta x \Delta y \Delta z (m^3)$

$\frac{dT}{dt}$ = rate of Temperature change $\left(\frac{K \text{ or } C}{sec}\right)$

The q value can be represented as the sum of the heat coming in through conduction from below and the heat coming in through convection from above as shown in Equation 16.

Equation 16. Energy balance for boundary nodes

$$q'' = k \frac{\partial T}{\partial x} + h(T_{amb} - T)$$

Substituting Equation 16 into Equation 15 yields the expression shown in

Equation 17:

Equation 17. Finite difference energy balance on boundary nodes

$$k \frac{\partial T}{\partial x} + h(T_{amb} - T) = \rho C \Delta x \Delta y \Delta z \frac{\partial T}{\partial t}$$

Next, a finite difference discretization of the derivative terms can be performed.

For the $\frac{\partial T}{\partial x}$ term, a forward difference Crank-Nicolson method must be applied since there is no node present above the top node. The discretized equation can be re-arranged to yield:

Equation 18. Finite difference top boundary equation

$$\begin{aligned} & \left[\frac{1}{\alpha \Delta t} + \frac{1}{2\Delta x^2} + \frac{1}{2k\Delta x} \right] T(x_1, t_j) - \frac{T(x_2, t_j)}{2\Delta x^2} \\ & = \left[\frac{1}{\alpha \Delta t} - \frac{1}{2\Delta x^2} - \frac{h}{2k\Delta x} \right] T(x_1, t_{j-1}) + \frac{T(x_2, t_j)}{2\Delta x^2} + \frac{hT_{amb}}{k\Delta x} \end{aligned}$$

Bottom Boundary Condition:

The energy balance method was repeated for the bottom boundary as shown in

Figure 10.

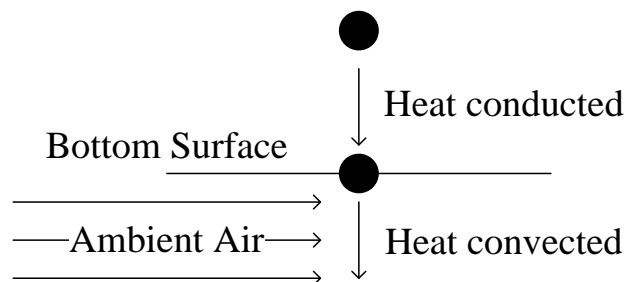


Figure 10. Bottom surface finite difference energy balance

The resulting finite difference bottom node equation is given in Equation 19.
Equation 19. Finite difference bottom boundary equation

$$\left[\frac{1}{\alpha t} + \frac{1}{2\Delta x^2} + \frac{1}{2k\Delta x} \right] T(x_n, t_j) - \frac{T(x_{n-1}, t_j)}{2\Delta x^2}$$

$$= \left[\frac{1}{\alpha\Delta t} - \frac{1}{2\Delta x^2} - \frac{h}{2k\Delta x} \right] T(x_n, t_{j-1}) + \frac{T(x_{n-1}, t_j)}{2\Delta x^2} + \frac{hT_{amb}}{k\Delta x}$$

Finite Difference Solution Method

The finite difference solution can now be obtained because the number of equations is equal to the number of unknown nodal temperatures. These equations can be used to develop a coefficient matrix and solution vector as shown in Equation 20.

Equation 20. Finite difference discretized equations in matrix form

$$[C]\{T\} = \{v\}$$

Or

$$\{T\} = [C]^{-1}\{v\}$$

Where C is the coefficient matrix, T is the temperature vector, and v is the solution vector. The formulation of each of these variables is given in Equation 21, 22, and 23.

The matrix equation produces the temperature distribution at the current time step. During the next time step, the current solution would be stored as the j-1 time step, and the solution process repeated. Because this study is interested in the transient temperature distribution, the results from every time step were saved. The programming to execute the one-dimensional finite difference method was written in MATLAB and is available in the appendix.

A sample of the MATLAB solution output, this time showing surface temperature vs time, from a one-inch thick specimen with a $500 \frac{W}{m^2}$ heat generation point source located at a depth of 0.5 in. is shown in Figure 11.

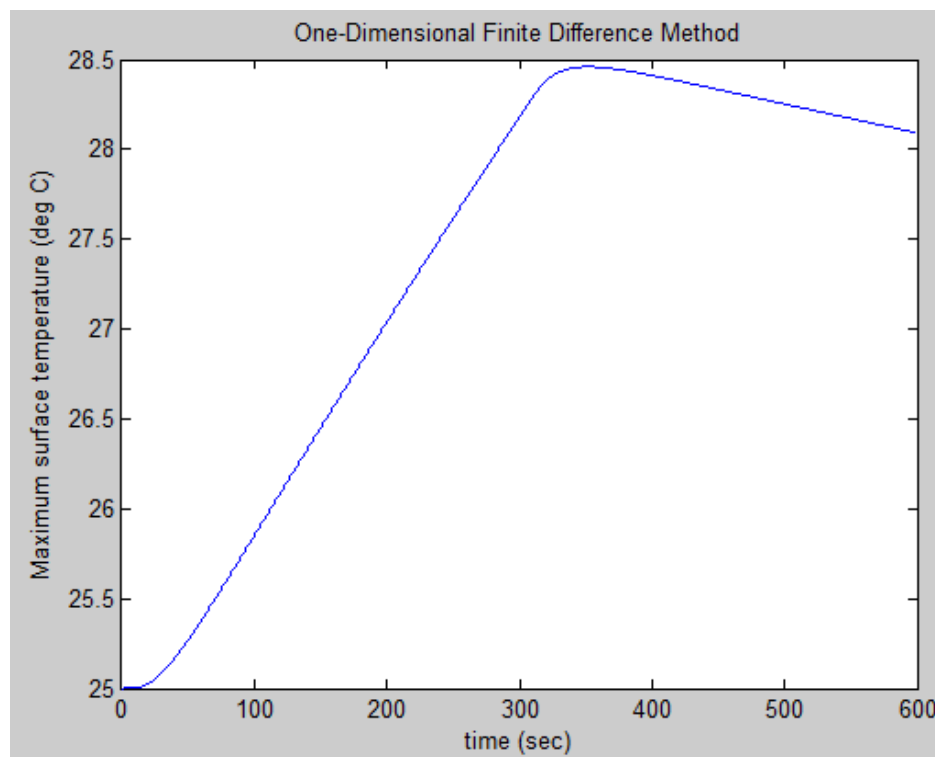


Figure 11. Finite Difference MATLAB screenshot

CHAPTER 4 – FINITE ELEMENT APPROACH

Finite Element Overview

The finite element method was developed with the software package ANSYS. For heat transfer models, the finite element is very similar to the finite difference method with a couple of exceptions. First, the two methods are discretized in a different manner. Finite difference methods are discretized strictly into individual nodes, which are representative of line, area, or volume that surrounds it. In the finite element method, the model is discretized into elements, which share nodes with adjacent elements. The temperature distribution within each element is determined by a curve-fit function known as a “shape function”. Secondly, the governing discretized equations are developed in a different manner. Recall that the finite difference discretized equations were developed simply by taking a Taylor series expansion of all derivative terms within the governing differential equation. The finite element discretized equations are developed from an energy flux balance on each individual element by applying Fourier’s Law, which was given back in chapter 2.

According to (Cook, Malkus, Plesha , & Witt, 2002), the finite difference has a smaller error term than a finite element model with the same number of nodes for a typical heat transfer problem. However, the finite element method is much more flexible in dealing with diverse geometry and meshing set-ups, as well as in cases where coupled structural-thermal analyses are required. Furthermore, with the aid of software packages such as ANSYS, the finite element method can be more easily implemented without as

great a risk of user coding errors, such is the case when developing a custom finite difference MATLAB program.

The results taken from the finite element method were extracted only after a grid independency study was conducted for each case. The grid independency study is designed to insure a convergent solution, and it was performed by increasing the number of elements that exist in the model until the surface temperature solution did not change (converged) even as the number of elements continued to increase. The criteria to check for convergence was to insure that doubling the number of elements produced a less than 0.1% change in surface temperature increase results.

One-Dimensional Finite Element Model

The one-dimensional finite element model was developed with the same material properties and boundary conditions as the finite difference model. The element applied to this model was ANSYS's LINK33 element, which is a one-dimensional conduction bar element with temperature as its only degree of freedom. At the ends, ANSYS's LINK34 element was applied to model convection. The models were meshed with 25-100 elements depending on the specimen thickness and flaw depth parameters. The generation was modeled as an input heat flow located at the flaw depth. The mesh was designed to be ten times finer at the location of the heat generation than in the surrounding line.

For both the finite element and finite difference model, the heat generation was assumed to occur for the first five minutes. Then, the heat generation is set to zero (to represent the stopping of the transducer application), at which point the heat continues to

conduct due to temperature gradients which exist within the medium. The one-dimensional finite element ANSYS batch files are available in Appendix C.

ANSYS screenshots obtained from a sample model run is shown in Figure 12. In this figure, a generation of $1 \frac{W}{m^2}$ located at a depth of 0.5 in. (1.27 cm) on a 1 in. (2.54 cm) thick specimen is shown at a time of 5 minutes after the onset of the generation.

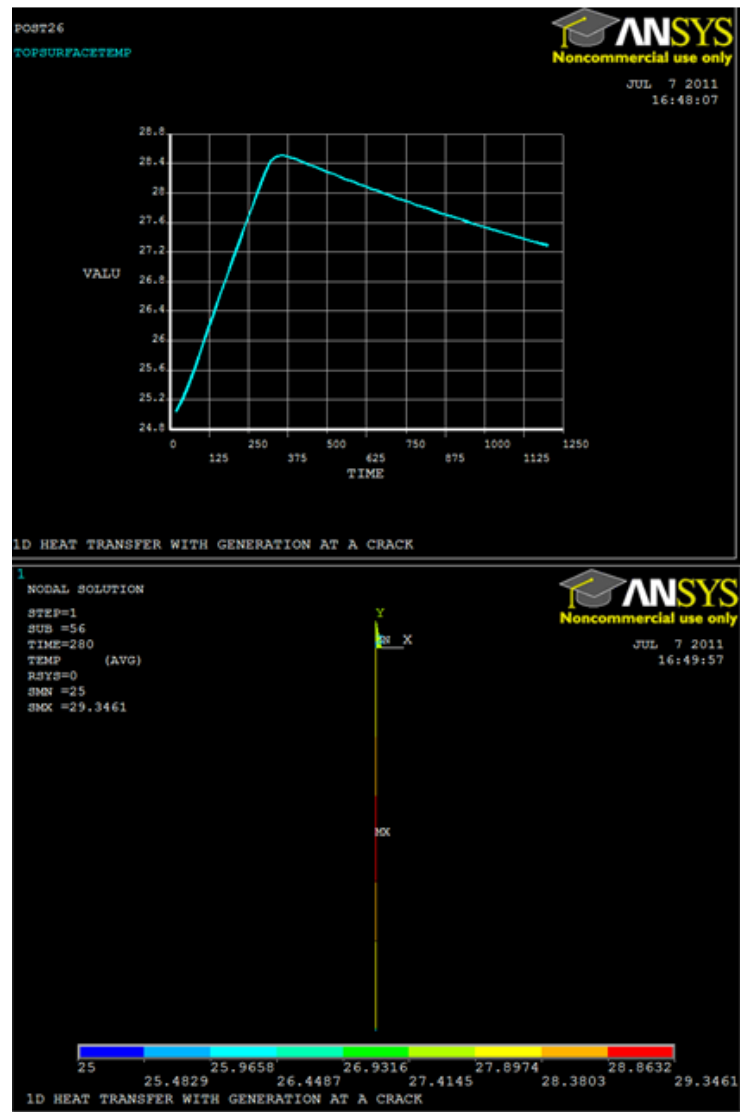


Figure 12. ANSYS one-dimensional finite element model screenshots

Two-Dimensional Finite Element Model

The two-dimensional model was constructed with ANSYS's PLANE55 element type. PLANE55--shown in Figure 13 --is a two-dimensional 4-node quad element with heat conduction capabilities and temperature as its only degree of freedom. The two-dimensional model is capable of representing the heat generation flaw as a linear line, a sinusoidal line, or a point load.

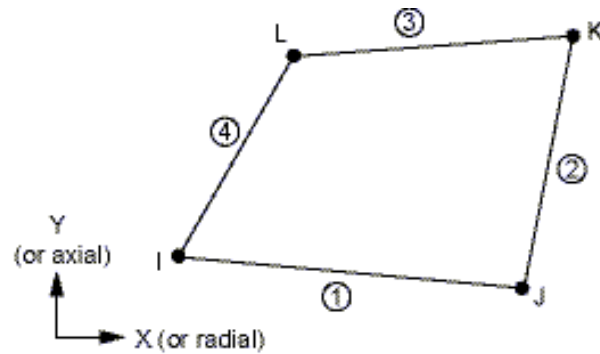


Figure 13. ANSYS PLANE55 element

The mesh around the crack region is meshed with 2-5 times finer mesh than the outside perimeter. A screenshot of a typical mesh in which the generation is modeled as a horizontal line in the center of the specimen for the two-dimensional heat transfer model is shown in Figure 14.

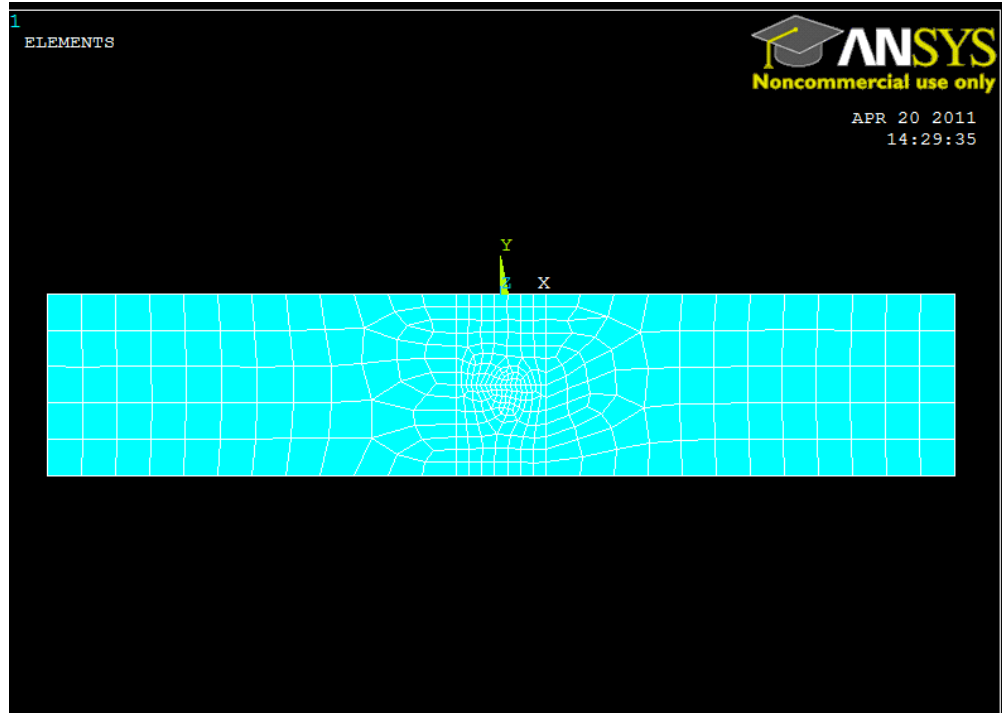


Figure 14. Two-dimensional finite element mesh

The model solution was given as a temperature distribution for every time step. The number of time steps reported, as well as the time between steps is easily specified by the user. For the cases executed thus far, a maximum time step size of 5 sec was applied. An example of the temperature distribution change as a result of a 0.5 in. (1.27 cm) horizontal flaw that is located in the center of the specimen and generating heat at a rate of $5 \frac{W}{m}$ is given in Figure 15. The two-dimensional finite element ANSYS batch input file is available in Appendix C.

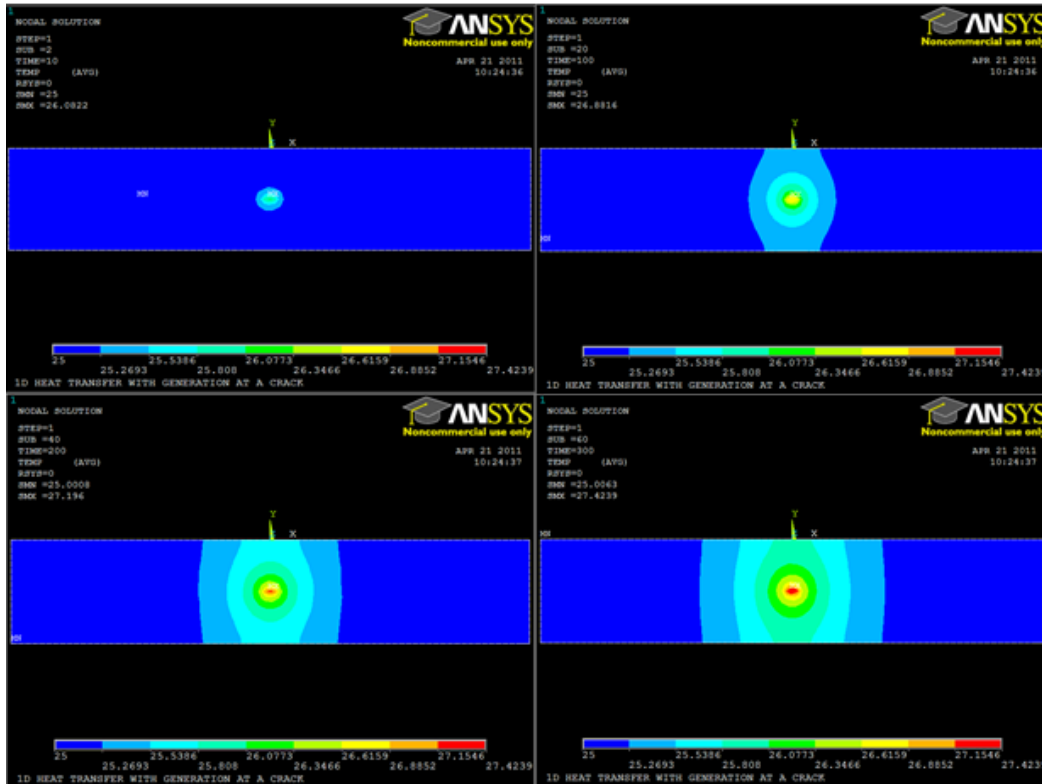


Figure 15. Two-dimensional model screenshots

Three-Dimensional Finite Element Model

The three-dimensional model was designed after the geometry shown back in Figure 7. The three-dimensional model was constructed with ANSYS's SOLID70 (shown in Figure 16) element type. SOLID70 is a three-dimensional quadratic heat conduction element with temperature as its only degree of freedom. The three-dimensional model is capable of representing the heat generation flow as a linear line, a sinusoidal line, a rectangular surface area, or a point load.

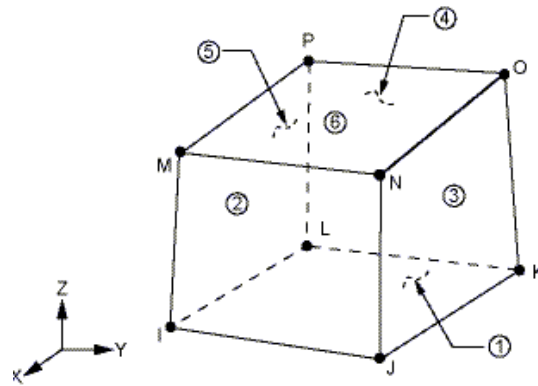


Figure 16. SOLID70 geometry

The geometry is meshed in one of two ways. The first is simply to apply a uniform mesh throughout the entire specimen. The second is to have a slightly finer mesh for on one or two sides of the heat generation flaw (typically the sides closest to an outer surface). This is because the solution converged better if there was a finer mesh in situations where not very much room existed between a surface and the flaw. Also, a third meshing option has been developed in which a mesh 1.5-4 times more fine is applied in a rectangular volume surrounding the generation area. Places within the specimen that are not close to the flaw are then meshed more coarsely. This type of mesh is believed to be useful in situations where convergence or computational time is an issue. However, up to this point, convergence and computational times have not been a problem, and therefore the more user-friendly meshes were applied to obtain the data presented. An example of the three-dimensional mesh is given in Figure 17.

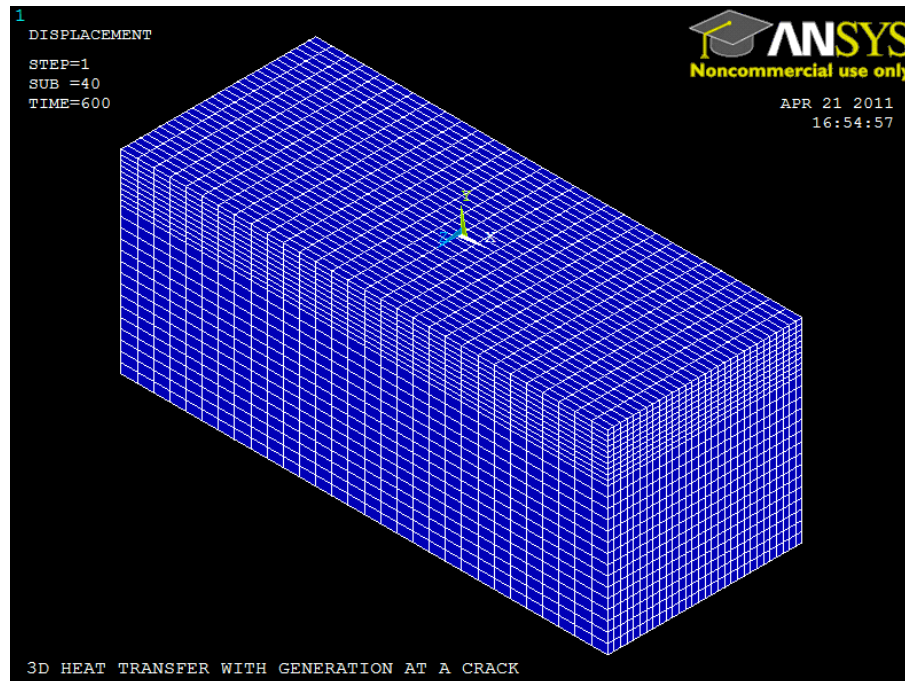


Figure 17. Three-dimensional mesh

The output solution for the three-dimensional model gives the temperature distribution throughout the rectangular specimen at any time or time-step the user desires. The result of the temperature change given by the three-dimensional model for the case in which a 0.03 in^2 (0.19 cm^2) surface area located 0.5 inches (1.27 cm) from the top surface in a 5 inch (12.7 cm) by 2 inch (5.08 cm) by 2 inch specimen is producing heat at a rate of 0.25 W is shown in Figure 18. The heat generation is assumed to occur for a period of 5 minutes, at which the transducer is removed, and the heat continues to conduct to the ambient air until the specimen reaches thermal equilibrium. The three-dimensional finite element ANSYS input batch files are available in Appendix C.

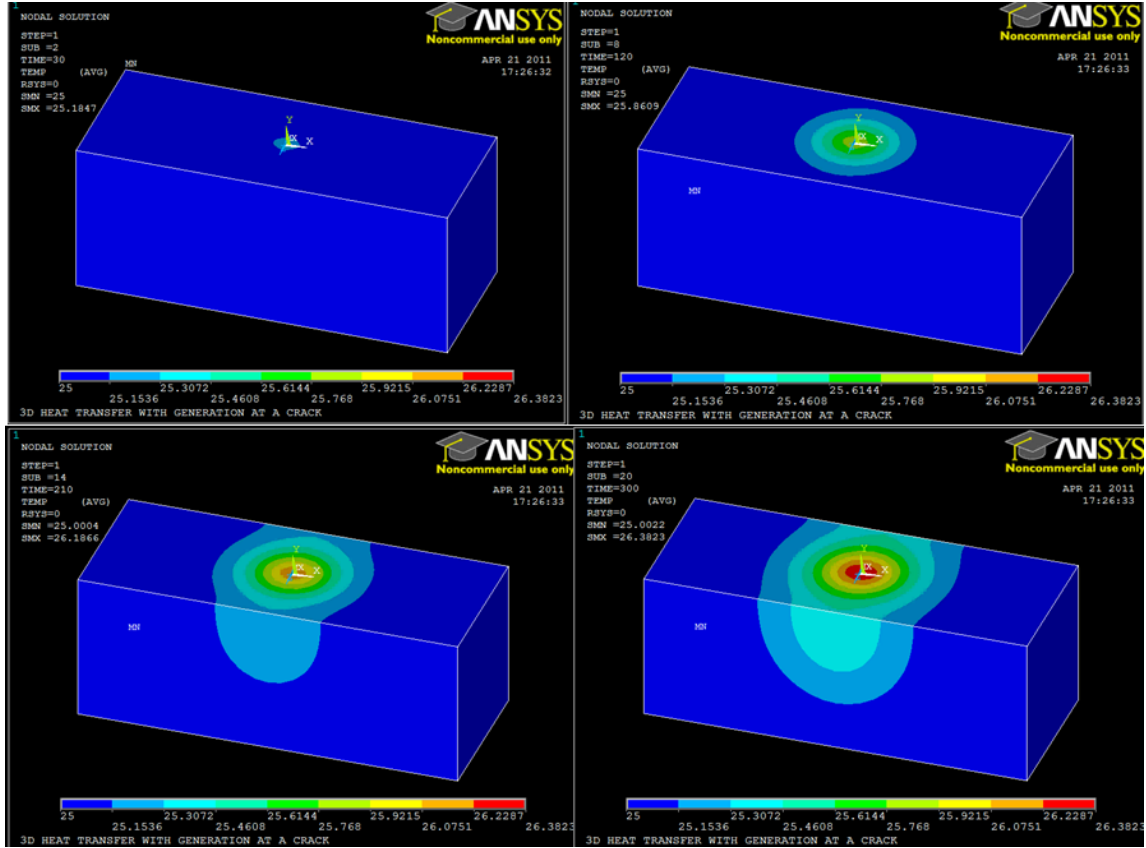


Figure 18. Three-dimensional model screenshots

CHAPTER 5 – ANALYTICAL APPROACH

Overview of Separation of Variables Technique

One of the most common methods for solving partial differential equations such as the HDE is the separation of variables technique and will serve as the starting method for solving the HDE in this study. The separation of variables technique breaks the HDE from Equation 3 into four independent ordinary differential equations which are functions of x , y , z , and time, t , respectively. The overall solution is assumed to be the product of each of the four ordinary differential equation solutions as shown in Equation 24. If a closed-form solution of this form does not exist, or if the initial partial differential equation is unable to be separated into independent ordinary differential equations, then the separation of variables technique will not produce a solution, and another method is required.

Equation 24. Solution form for separation of variables analytical technique

$$T(x, y, z, t) = X(x) * Y(y) * Z(z) * \Gamma(t)$$

Where:

$X(x)$ = solution to x direction ordinary differential equation

$Y(y)$ = solution to y direction ordinary differential equation

$Z(z)$ = solution to the z direction ordinary differential equation

$T(t)$ = solution to the time dependent ordinary differential equation

Another potential problem that may arise when applying this technique is too many non-homogeneous conditions (includes both boundary conditions and initial condition). If more than one non-homogeneous condition exists, the problem must be

broken into a set of smaller problems--which is not always possible. Lastly, as will be the case when modeling vibrothermography, if any of the terms within the partial differential equation are non-continuous--such as the generation term $g(x, y, z, t)$ --then a singularity arises that often prohibits a converging closed-form solution to be determined. More details about the separation of variables technique will be displayed when the actual solutions are determined in the following sections. Also, more information about common solution techniques, including the separation of variables technique, is available in (Haberman, 2004).

Overview of Green's Function

Green's function is a special solution method which can be applied to the HDE in cases where a point-load heat source is applied either on a surface or within the specimen. The application of Green's function for point-source heat transfer problems is most commonly found in heat transfer models associated with welding or laser-bonding (Ozisik, 1993). Although most of these publications involve surface generation loads, the method of applying Green's function is well described in Chapter 6 of (Ozisik, 1993) and Chapters 9 and 11 of (Haberman, 2004), and is applicable to internal point generation loads.

Green's function can be developed to describe the influence of each non-homogeneous and/or forcing term (in the HDE, the generation is a mathematical forcing term) that exist in many partial differential equations. The solution to a three-dimensional Cartesian coordinate system HDE with homogeneous boundary conditions, a

non-homogeneous initial condition, and a generation term written in terms of Green's function is given in Equation 25.

Equation 25. Relationship between temperature distribution and green's function

$$\begin{aligned}
 T(x, y, z, t) &= \int_{x'=0}^W \int_{y'=0}^H \int_{z'=0}^L G(x, y, z, t | x', y', z', \tau = 0) f(x', y', z') dx' dy' dz' \\
 &+ \frac{\alpha}{k} \int_{\tau=0}^t \int_{x'=0}^W \int_{y'=0}^H \int_{z'=0}^L G(x, y, z, t | x', y', z', \tau) g(x', y', z', \tau) dx' dy' dz' d\tau
 \end{aligned}$$

Where:

$G(x, y, z, t | x', y', z', \tau)$ = Green's function

$g(x', y', z', \tau)$ = generation term ($\frac{W}{m^2}$)

The physical representation of the notation of Green's function

$G(x, y, z, t | x', y', z', \tau)$ is the temperature at location x, y, z at time t due to an instantaneous point source of unit strength located at x', y', z' releasing its heat at time $t = \tau$ (Ozisik, 1993). The first term in Equation 25 represents the contribution of the initial condition $f(x', y', z')$ on the temperature distribution and the second term represents the contribution of the generation $g(x', y', z', \tau)$ on the temperature distribution. Additional terms can be included in Equation 25 if non-homogenous boundary conditions are present. The actual form of these terms would differ depending on the type of boundary condition that is applied (Haberman, 2004). For this study, non-homogeneous boundary condition terms do not need to be included because the boundary conditions in this study can be made homogeneous through a transformation of variables. More details on transformation of variables is available in the next section.

The next step is to determine Green's function. There are many methods of determining Green's function which are outlined in (Haberman, 2004). The simplest of these methods begins simply by looking back at Equation 25. Note that for a case where there is no generation, homogeneous boundary conditions, and a non-homogeneous initial condition, the second term disappears from Equation 25; and you are left with the expression given in Equation 26.

Equation 26. Relationship between temperature distribution and Green's function with no generation and homogeneous boundary conditions

$$T(x, y, z, t) = \int_{x'=0}^W \int_{y'=0}^H \int_{z'=0}^L G(x, y, z, t | x', y', z', \tau = 0) f(x', y', z') dx' dy' dz'$$

Also, the temperature distribution for this special case, $T(x, y, z, t)$, can also be solved with the separation of variables technique. The separation of variables solution can be substituted into the left-hand side of Equation 26, and Green's function can then be determined by observation. Once Green's function is determined, it can be applied to Equation 25 for situations in which different non-homogeneous conditions exist.

This method displays the biggest advantage of applying Green's function. The value of Green's function is not changing regardless of which conditions are homogeneous and which are non-homogeneous (as long as the conditions are the same type). The overall solution then takes into account the non-homogeneous conditions of interest once Green's function is substituted into Equation 25. Examples of this application are shown in the One-Dimensional Analytical Solution, Two-Dimensional Analytical Solution, and Three-Dimensional Analytical solution sections later in this chapter.

Overview of Point Load Generation

The last subject that must be discussed is the generation point load that will be placed to model the vibrothermography phenomenon. This will be done with the Dirac delta function given in Equation 27.

Equation 27. Dirac delta function definition

$$\delta(x) = \begin{cases} 1 & \text{when } x = 0 \\ 0 & \text{otherwise} \end{cases}$$

Therefore, in a three-dimensional model, a constant generation load located at the point (a,b,c) in a Cartesian coordinate system can be represented by the expression given in Equation 28.

Equation 28. Point-source generation term

$$g(x, y, z, t) = g_p^c \delta(x - a) \delta(y - b) \delta(z - c)$$

Where:

g_p^c = constant generation point load quantity

The notation g_p^c was taken from (Ozisik, 1993). The c represents constant generation (as opposed to an impulse heat release, which would be denoted with an “i”), and the p represents a point load (as opposed to an “a” for surface area load or a “v” for volume).

There is one property of the Dirac delta function that also must be applied to determine the temperature distribution as a result of a point heat source. This property of integration is displayed in Equation 29 (Ozisik, 1993).

Equation 29. Dirac delta function integral

$$\int \delta(x)dx = 1$$

And therefore, by the product rule, Equation 30 holds true.

Equation 30. Integration property functions with Dirac delta function

$$\int f(x)\delta(x)dx = f(x)$$

Where:

$f(x)$ = any continuous function of x

These properties will be taken advantage of when the analytical solutions are determined in the following sections.

Procedure for Determining Analytical Solution

The analytical solution for the HDE with a point load located at (a,b,c) within the specimen was determined by following steps:

1. Perform a transformation of variables to eliminate non-homogeneous boundary conditions
2. Determine solution to homogeneous (ignoring generation term) auxiliary problem
3. Determine Green's function from homogeneous auxiliary problem solution
4. Determine overall transformed variable solution from Equation 25
5. Perform the inverse transformation of variables to determine overall temperature solution

One-Dimensional Analytical Solution

Recall the one-dimensional heat transfer problem used to model vibrothermography from Equation 4 in Chapter 2 (shown again in Equation 31).

Equation 31. One-dimensional mathematical model with boundary conditions

$$\frac{\partial^2 T}{\partial x^2} + \frac{g(x, t)}{k} = \frac{1}{\alpha} * \frac{\partial T}{\partial t}$$

Boundary conditions (B.C.)

$$\text{(B.C. \#1)} \quad -\frac{\partial T}{\partial x} + \frac{h}{k} * T = T_{amb} \quad @ \ x = 0$$

$$\text{(B.C. \#2)} \quad \frac{\partial T}{\partial x} + \frac{h}{k} * T = T_{amb} \quad @ \ x = L$$

Initial condition (I.C)

$$\text{(I.C)} \quad T = f(x) \quad @ \ t=0$$

The temperature distribution for this one-dimensional model was determined by following the steps outlined in the “Procedure for Determining Analytical Solution” section as follows:

Step 1. Perform Transformation of Variables

First, a transformation of variables is performed to eliminate the non-homogeneous boundary conditions at $x=0$ and $x=L$. This is done by defining a new variable, $\theta(x,t)$, with the relationship given in Equation 32.

Equation 32. Defined transformation variable

$$\theta(x, t) = T(x, t) - T_{amb}$$

Where:

$\theta(x, t)$ = Transformed temperature variable (deg C or K)

$T(x, t)$ = Temperature variable (deg C or K)

T_{amb} = Ambient temperature constant (deg C or K)

The variable transformation is executed by re-arranging this defined relationship and substituting for $T(x, t)$ in the one-dimensional HDE from Equation 31. The transformed variable partial differential equation can now be written in terms of $\theta(x,t)$ as shown in Equation 33.

Equation 33. One dimensional transformed partial differential equation with boundary conditions

$$\frac{\partial^2 \theta}{\partial x^2} + \frac{g(x, t)}{k} = \frac{1}{\alpha} * \frac{\partial \theta}{\partial t}$$

Boundary conditions (B.C.)

$$\text{(B.C. \#1)} \quad -\frac{\partial \theta}{\partial x} + \frac{h}{k} * \theta = 0 \quad @ \ x = 0$$

$$\text{(B.C. \#2)} \quad \frac{\partial \theta}{\partial x} + \frac{h}{k} * \theta = 0 \quad @ \ x = L$$

Initial condition (I.C)

$$\text{(I.C)} \quad \theta = f(x) - T_{amb} = f_2(x) \quad @ \ t=0$$

Note that by performing this transformation of variables, both the boundary condition at $x=0$ (B.C. #1) and the boundary condition at $x=L$ (B.C. #2) are now homogeneous.

Step 2. Solve Auxiliary Problem

Green's function for the partial differential equation given in Equation 26 can now be determined by solving the homogenous boundary condition with no generation

auxiliary problem shown in Equation 34. The solution to this auxiliary problem is different than the final temperature distribution so a new variable, $\psi(x, t)$, is introduced to represent the auxiliary problem temperature distribution.

Equation 34. One-dimensional homogeneous auxiliary partial differential equation with boundary conditions

$$\frac{\partial^2 \psi}{\partial x^2} = \frac{1}{\alpha} * \frac{\partial \psi}{\partial t}$$

Boundary conditions (B.C.)

$$\text{(B.C. \#1)} \quad -\frac{\partial \psi}{\partial x} + \frac{h}{k} * \psi = 0 \quad @ \ x = 0$$

$$\text{(B.C. \#2)} \quad \frac{\partial \psi}{\partial x} + \frac{h}{k} * \psi = 0 \quad @ \ x = L$$

Initial condition (I.C)

$$\text{(I.C)} \quad \psi = f(x) - T_{amb} = f_2(x) \quad @ \ t=0$$

This auxiliary problem is solved with the traditional separation of variables technique. To do this, a solution is assumed to exist of the form given in Equation 35.

Equation 35. One-dimensional separation of variables assumed solution

$$\psi(x, t) = X(x) * \Gamma(t)$$

The next step is to substitute this assumed solution into auxiliary Equation 34 for $\psi(x, t)$. This can then re-arranged such that all the x dependent terms are separated from the time dependent terms as shown in Equation 36.

Equation 36. One-dimensional separation of variables re-arrangement

$$\frac{1}{X} \frac{d^2 X}{dx^2} = \frac{1}{\alpha * \Gamma} \frac{d\Gamma}{dt} = -\beta^2$$

Where:

$$-\beta^2 = \text{Separation constant}$$

Note that the partial derivatives can be converted to full derivatives because X is a function of x only, and Γ is a function of t only. Also, the equality given in Equation 36 can only be true if both sides of the equation are equal to the same constant, which is defined as $-\beta^2$. The constant is negative and squared because previous mathematicians observed that this is the cleanest and most time efficient way to represent this constant for diffusion problems.

Equation 36 can now be broken up and re-arranged into two independent ordinary differential equations. The x dependent ordinary differential equation is shown in Equation 37; and the time dependent ordinary differential equation is shown in Equation 38.

Equation 37. One-dimensional x dependent ordinary differential equation with conditions

$$\frac{d^2 X}{dx^2} + \beta^2 X = 0$$

Boundary conditions (B.C's)

$$\text{(B.C. \#1)} \quad -\frac{\partial X}{\partial x} + \frac{h}{k} * X = 0 \quad @ \ x = 0$$

$$\text{(B.C. \#2)} \quad \frac{\partial X}{\partial x} + \frac{h}{k} * X = 0 \quad @ \ x = L$$

Equation 38. Time dependent ordinary differential equation for one-dimensional model

$$\frac{d\Gamma}{dt} + \alpha\beta^2 T = 0$$

The solution to the time dependent ordinary differential equation is given in Equation 39.

Equation 39. Time dependent ordinary differential equation solution for one-dimensional model

$$\Gamma(t) = e^{-\alpha\beta^2 t}$$

The constants of integration will be ignored for now, but will be included together and evaluated by applying the non-homogeneous initial condition after the time dependent and x position dependent solutions have been combined.

The x ordinary differential equation is known as an eigenvalue problem (Haberman, 2004) because it has non-trivial solutions only for certain values of $\beta = \beta_m$ where $m = 1, 2, 3, \dots$. The values of β_m are a list of all the values of β which produce non-trivial solutions, and are called eigenvalues. The solution to the x ordinary differential equation $X(\beta_m, x)$ is known as an eigenfunction. This solution to this second-order linear differential equation is given in Equation 40.

Equation 40. X dependent ordinary differential equation solution for one-dimensional model

$$X(\beta_m, x) = B_m \cos(B_m x) + \frac{h}{k} \sin(B_m x)$$

Where the values of B_m are the positive roots of the expression given in Equation 41.

Equation 41. One-dimensional eigenvalue equation

$$\tan(B_m L) = \frac{B_m \left(\frac{2h}{k}\right)}{B_m^2 - \left(\frac{h}{k}\right)^2}$$

Note that this eigenvalue equation is a transcendental equation, meaning that it can't be solved directly by isolating the unknown variable. For this study the eigenvalues

were determined by first re-arranging Equation 41 as shown in Equation 42. The MATLAB function file applied to solve for the eigenvalues is available in Appendix B.

Equation 42. Re-arranged eigenvalue equation

$$\sin(\beta_m L) = \frac{\cos(\beta_m L) \beta_m \left(\frac{2h}{k}\right)}{B_m^2 - \left(\frac{h}{k}\right)^2}$$

The complete solution for $\psi(x, t)$ is determined by a linear superposition of the separated elementary solutions-- $X(\beta_m, x)$ and $\Gamma(t)$ --in the form given in Equation 43.

Equation 43. General solution of auxiliary one-dimensional problem

$$\psi(x, t) = \sum_{m=1}^{\infty} c_m X(\beta_m, x) e^{-\alpha \beta^2 t}$$

The constant, c_m , is evaluated by applying the non-homogeneous initial condition. In order to re-arrange this initial condition equation, the operator $\int_0^L X(\beta_{n,x}) dx$ is applied to both sides of the equation. Then, the orthogonality principal, which is shown in Equation 44 (Ozisk, 1993), can be applied to eliminate the summation. Next, Equation 43 is re-arranged, solving for the constant as shown in Equation 45.

Equation 44. Orthogonality principal

$$\int_0^L X(\beta_m, x) X(\beta_n, x) dx = \begin{cases} 0 & \text{when } m \neq n \\ N(\beta_m) & \text{when } m = n \end{cases}$$

Equation 45. One-dimensional constant

$$c_m = \frac{1}{N(\beta_m)} \int_0^L X(\beta_m, x') f_2(x') dx'$$

The prime (') character seen on x' in Equation 45 is inserted simply to distinguish between x variables inside the integral sign with x variables that will later appear outside

of the integral. The $N(\beta_m)$ term is referred to as the Norm. It arises when the operator $\int_0^L X(\beta_{n,x})dx$ was applied to Equation 43, and is defined in Equation 46.

Equation 46. Definition of the Norm

$$N(\beta_m) = \int_0^L [X(\beta_m, x)]^2 dx$$

The norm for this problem, given the solution to $X(\beta_m, x)$, is shown in Equation 47.

Equation 47. Norm solution for one-dimensional model

$$N(\beta_m) = 2 \left[\left(\beta_m^2 + \left(\frac{h}{k} \right)^2 \right) \left(L + \frac{\frac{h}{k}}{\beta_m^2 + \left(\frac{h}{k} \right)^2} \right) + \frac{h}{k} \right]$$

Therefore, the overall solution to the one-dimensional auxiliary problem becomes the expression given in Equation 48.

Equation 48. Solution to auxiliary problem

$$\psi(x, t) = \sum_{m=1}^{\infty} \frac{1}{N(\beta_m)} X(\beta_m, x) e^{-\alpha \beta^2 t} \int_0^L X(\beta_m, x') f_2(x') dx'$$

Where the values of $X(\beta_m, x)$ and $N(\beta_m)$ are given in Equation 40 and Equation 47, respectively.

Step 3. Determine Green's Function from the Auxiliary Solution:

In order to determine the overall transformed variable solution from the auxiliary solution, Green's function must be determined. For a one-dimensional case, Green's function can be evaluated by applying the relationship between the auxiliary solution and Green's function back in Equation 26. This application is shown in Equation 49.

Equation 49. Green's function expression for one-dimensional model

$$\begin{aligned}\psi(x, t) &= \int_0^L G(x, t|x', \tau)_{\tau=0} f_2(x) dx \\ &= \sum_{m=1}^{\infty} \frac{1}{N(\beta_m)} X(\beta_m, x) e^{-\alpha\beta^2 t} \int_0^L X(\beta_m, x') f_2(x') dx'\end{aligned}$$

From this equation, it can be seen that Green's function at $\tau = 0$ is the expression given in Equation 50.

Equation 50. Green's function at $\tau=0$ for the one-dimensional model

$$G(x, t|x', \tau)_{\tau=0} = \sum_{m=1}^{\infty} \frac{1}{N(\beta_m)} X(\beta_m, x) e^{-\alpha\beta_m^2 t} X(\beta_m, x')$$

The general form of Green's function can be obtained by replacing t with $t - \tau$ in Equation 50 to yield the final needed form of Green's function in Equation 51.

Equation 51. Green's function for one-dimensional model

$$G(x, t|x', \tau) = \sum_{m=1}^{\infty} \frac{1}{N(\beta_m)} X(\beta_m, x) e^{-\alpha\beta_m^2(t-\tau)} X(\beta_m, x')$$

Step 4: Determine Transformed Variable Solution:

Given Green's function, the solution to the one-dimensional problem with homogeneous boundary conditions can be determined from the relationship shown back in Equation 25.

For the special case in which the initial temperature distribution, $f(x)$, is equal to zero, the first term back in Equation 25 goes to zero. Also, for a point generation load at $x=a$ in the one-dimensional case, Equation 25 can be reduced to yield Equation 52.

Equation 52. Solution to transformed one-dimensional problem

$$\theta(x, t) = \frac{\alpha}{k} \int_{\tau=0}^t \int_0^L G(x, t|x', \tau) g_A^c \delta(x' - a) dx' d\tau$$

The integral with respect to position x can be applied (recall the integral property of the Dirac delta function given back in Equation 30) to determine a reduced form of the transformed one-dimensional solution as shown in Equation 53.

Equation 53. Reduced solution to transformed one-dimensional problem

$$\theta(x, t) = \frac{\alpha}{k} * \int_{\tau=0}^t G(x, t|a, \tau) g_A^c d\tau$$

Step 5. Determine Overall Solution:

Recall the transformation of variables performed back in step 1 in order to produce homogeneous boundary conditions at $x=0$ and $x=L$. The relationship defined from that step ($\theta(x, t) = T(x, t) - T_{amb}$) is applied to determine the final temperature distribution solution as shown in Equation 54.

Equation 54. Final temperature solution form for one-dimensional model

$$T(x, t) = \frac{\alpha}{k} \int_{\tau=0}^t G(x, t|a, \tau) g_A^c d\tau + T_{amb}$$

The last step is to substitute the expression for Green's function in Equation 51 into Equation 54 and integrate with respect to τ . Doing so will produce the temperature solution shown in Equation 55.

Equation 55. Final temperature solution for one-dimensional model

$$T(x, t) = \frac{\alpha g_A^c}{k} \sum_{m=1}^{\infty} \frac{X(\beta_m, x) X(\beta_m, a)}{N(\beta_m) \alpha \beta_m^2} (1 - e^{-\alpha \beta_m^2 t}) + T_{amb}$$

This is the overall analytical solution of the time and x position dependent temperature distribution for the one-dimensional model. The surface temperature for a given generation can be determined simply by setting $x=0$.

Recall that the value of Green's function, which appears as $G(x, t|a, \tau)$, is given back in Equation 51. Numerical solutions for several different generation amounts, generation depths, and specimen thicknesses were developed with the MATLAB input file shown in Appendix B. These results are given in Chapter 6.

Two-Dimensional Analytical Solution

Recall the two-dimensional heat transfer problem used to model vibrothermography from Equation 5 in Chapter 2 (shown again in Equation 56).

Equation 56. Two-dimensional mathematical model with boundary conditions

$$\frac{\partial^2 T}{\partial x^2} + \frac{\partial^2 T}{\partial y^2} + \frac{g(x, y, t)}{k} = \frac{1}{\alpha} * \frac{\partial T}{\partial t}$$

Boundary conditions (B.C.)

$$\text{(B.C. \#1)} \quad -\frac{\partial T}{\partial x} + \frac{h}{k} * T = T_{amb} \quad @ \ x = 0$$

$$\text{(B.C. \#2)} \quad \frac{\partial T}{\partial x} + \frac{h}{k} * T = T_{amb} \quad @ \ x = W$$

$$\text{(B.C. \#3)} \quad -\frac{\partial T}{\partial y} + \frac{h}{k} * T = T_{amb} \quad @ \ y = 0$$

$$\text{(B.C. \#4)} \quad \frac{\partial T}{\partial y} + \frac{h}{k} * T = T_{amb} \quad @ \ y = -H$$

Initial condition (I.C)

$$\text{(I.C)} \quad T = f(x, y) \quad @ \ t=0$$

The temperature distribution for this two-dimensional model was determined by following the steps outlined in the “Procedure for Determining Analytical Solution” section as follows:

Step 1. Perform Transformation of Variables:

First, a transformation of variables is performed to eliminate the non-homogeneous boundary conditions at $x=0$, $x=W$, $y=0$, $y=H$. This is done by defining a new variable, $\theta(x, y, t)$, with the relationship given in Equation 32.

Equation 57. Defined transformation variable

$$\theta(x, y, t) = T(x, y, t) - T_{amb}$$

The variable transformation is executed by re-arranging this defined relationship and substituting for $T(x, y, t)$ in the two-dimensional HDE from Equation 56. The transformed variable partial differential equation can now be written in terms of $\theta(x, y, t)$ as shown in Equation 58.

Equation 58. Two-dimensional transformed partial differential equation with boundary conditions

$$\frac{\partial^2 \theta}{\partial x^2} + \frac{\partial^2 \theta}{\partial y^2} + \frac{g(x, y, t)}{k} = \frac{1}{\alpha} * \frac{\partial \theta}{\partial t}$$

Boundary conditions (B.C.)

$$\text{(B.C. \#1)} \quad -\frac{\partial \theta}{\partial x} + \frac{h}{k} * \theta = 0 \quad @ \ x = 0$$

$$\text{(B.C. \#2)} \quad \frac{\partial \theta}{\partial x} + \frac{h}{k} * \theta = 0 \quad @ \ x = W$$

$$\text{(B.C. \#3)} \quad -\frac{\partial \theta}{\partial y} + \frac{h}{k} * \theta = 0 \quad @ \ y = 0$$

$$\text{(B.C. \#4)} \quad \frac{\partial \theta}{\partial y} + \frac{h}{k} * \theta = 0 \quad @ \ y = H$$

Initial condition (I.C)

$$(I.C) \quad \theta = f(x, y) - T_{amb} = f_2(x, y) \quad @ t=0$$

Note that by performing this transformation of variables, all the boundary condition become homogeneous.

Step 2. Solve Auxiliary Problem

Green's function can be determined by solving the auxiliary problem given in Equation 59.

Equation 59. Two-dimensional homogeneous auxiliary partial differential equation with boundary conditions

$$\frac{\partial^2 \psi}{\partial x^2} + \frac{\partial^2 \psi}{\partial y^2} = \frac{1}{\alpha} * \frac{\partial \psi}{\partial t}$$

Boundary conditions (B.C.)

$$(B.C. \#1) \quad -\frac{\partial \psi}{\partial x} + \frac{h}{k} * \psi = 0 \quad @ x = 0$$

$$(B.C. \#2) \quad \frac{\partial \psi}{\partial x} + \frac{h}{k} * \psi = 0 \quad @ x = W$$

$$(B.C. \#3) \quad -\frac{\partial \psi}{\partial y} + \frac{h}{k} * \psi = 0 \quad @ y = 0$$

$$(B.C. \#4) \quad \frac{\partial \psi}{\partial y} + \frac{h}{k} * \psi = 0 \quad @ y = H$$

Initial condition (I.C)

$$(I.C) \quad \psi = f(x, y) - T_{amb} = f_2(x, y) \quad @ t=0$$

The solution to this auxiliary problem can be obtained following the same Separation of Variables Technique procedure carried out in Step 2 of the “One-

dimensional Analytical Solution” section. The assumed solution is shown in Equation 60.

Equation 60. Two-dimensional separation of variables assumed solution

$$\psi(x, t) = X(x)Y(y)\Gamma(t)$$

This assumed solution is substituted into Equation 59, and re-arranged to produce the three ordinary differential equations given in Equation 61, Equation 62, and Equation 63, respectively.

Equation 61. X-direction ordinary differential equation for two-dimensional model

$$\frac{d^2X}{dx^2} + \beta^2X = 0$$

Boundary conditions (B.C's)

$$(B.C. \#1) \quad -\frac{\partial X}{\partial x} + \frac{h}{k} * X = 0 \quad @ \ x = 0$$

$$(B.C. \#2) \quad \frac{\partial X}{\partial x} + \frac{h}{k} * X = 0 \quad @ \ x = W$$

Equation 62. Y-direction ordinary differential equation for two-dimensional model

$$\frac{d^2Y}{dy^2} + \gamma^2Y = 0$$

Boundary conditions (B.C's)

$$(B.C. \#1) \quad -\frac{\partial Y}{\partial y} + \frac{h}{k} * Y = 0 \quad @ \ y = 0$$

$$(B.C. \#2) \quad \frac{\partial Y}{\partial y} + \frac{h}{k} * Y = 0 \quad @ \ y = H$$

Equation 63. Time dependent ordinary differential equation for two-dimensional model

$$\frac{d\Gamma}{dt} + \alpha(\beta^2 + \gamma^2)\Gamma = 0$$

Note that for the two-dimensional case, there now exists two eigenvalues, β and γ . The values of which produce non-trivial solutions will again be super positioned in terms of β_m and γ_n , where $m = 1, 2, 3, \dots$ and $n = 1, 2, 3, \dots$. The eigenfunction solutions to the ordinary differential equations are given in Equation 64, Equation 65, and Equation 66, respectively.

Equation 64. Time dependent ordinary differential equation solution for two-dimensional model

$$\Gamma(t) = e^{-\alpha(\beta^2 + \gamma^2)t}$$

Equation 65. X-dependent ordinary differential equation solution for two-dimensional model

$$X(\beta_m, x) = B_m \cos(B_m x) + \frac{h}{k} \sin(B_m x)$$

Equation 66. Y-dependent ordinary differential equation solution for two-dimensional model

$$Y(\gamma_n, y) = \gamma_n \cos(\gamma_n y) + \frac{h}{k} \sin(\gamma_n y)$$

Where the values of B_m and γ_n are the positive roots of the expressions given in Equation 67.

Equation 67. Eigenvalue expressions for two-dimensional model

$$\tan(\beta_m W) = \frac{\beta_m \left(\frac{2h}{k}\right)}{\beta_m^2 - \left(\frac{h}{k}\right)^2}$$

$$\tan(\gamma_n H) = \frac{\gamma_n \left(\frac{2h}{k}\right)}{\gamma_n^2 - \left(\frac{h}{k}\right)^2}$$

These solutions are combined and the constant is determined by applying the non-homogeneous initial condition and again taking advantage of the orthogonality principal.

The overall solution for the two-dimensional auxiliary problem is given in Equation 68, with the expression of the norms given in Equation 69.

Equation 68. Auxiliary solution for two-dimensional model

$$\begin{aligned} \psi(x, y, t) = & \sum_{m=1}^{\infty} \sum_{n=1}^{\infty} \frac{1}{N(\beta_m)N(\gamma_n)} X(\beta_m, x)Y(\gamma_n, y)e^{-\alpha\beta^2 t} \\ & * \int_{x'=0}^W \int_{y'=0}^H X(\beta_m, x')Y(\gamma_n, y')f_2(x')dx'dy' \end{aligned}$$

Equation 69. Norm solutions for the two-dimensional model

$$\begin{aligned} N(\beta_m) = & 2 \left[\left(\beta_m^2 + \left(\frac{h}{k} \right)^2 \right) \left(W + \frac{\frac{h}{k}}{\beta_m^2 + \left(\frac{h}{k} \right)^2} \right) + \frac{h}{k} \right] \\ N(\gamma_n) = & 2 \left[\left(\gamma_n^2 + \left(\frac{h}{k} \right)^2 \right) \left(H + \frac{\frac{h}{k}}{\gamma_n^2 + \left(\frac{h}{k} \right)^2} \right) + \frac{h}{k} \right] \end{aligned}$$

Step 3. Determine Green's Function from the Auxiliary Solution

For the two-dimensional model, Green's function can be evaluated by applying the relationship between the auxiliary solution and Green's function back in Equation 26.

This application is shown in Equation 70.

Equation 70. Green's function relationship for two-dimensional model

$$\begin{aligned} \psi(x, y, t) = & \int_{x'=0}^W \int_{y'=0}^H G(x, y, t|x', y', \tau)_{\tau=0} f_2(x, y)dx'dy' \\ = & \sum_{m=1}^{\infty} \sum_{n=1}^{\infty} \frac{1}{N(\beta_m)N(\gamma_n)} X(\beta_m, x)Y(\gamma_n, y)e^{-\alpha(\beta_m^2 + \gamma_n^2)t} \\ & * \int_{x'=0}^W \int_{y'=0}^H X(\beta_m, x')Y(\gamma_n, y')f_2(x', y')dx'dy' \end{aligned}$$

From this relationship, it can be observed that Green's function at $\tau = 0$ is the expression given in Equation 71.

Equation 71. Green's function at $\tau=0$ for the two-dimensional model

$$G(x, y, t | x', y', \tau)_{\tau=0} = \sum_{m=1}^{\infty} \sum_{n=1}^{\infty} \frac{1}{N(\beta_m)N(\gamma_n)} X(\beta_m, x) Y(\gamma_n, y) e^{-\alpha(\beta_m^2 + \gamma_n^2)t} * X(\beta_m, x') Y(\gamma_n, y')$$

The general form of Green's function can be obtained by replacing t with t- τ in Equation 71 to yield the final form of Green's function shown in Equation 72.

Equation 72. Green's function for the two-dimensional model

$$G(x, y, t | x', y', \tau) = \sum_{m=1}^{\infty} \sum_{n=1}^{\infty} \frac{1}{N(\beta_m)N(\gamma_n)} X(\beta_m, x) Y(\gamma_n, y) e^{-\alpha(\beta_m^2 + \gamma_n^2)(t-\tau)} X(\beta_m, x') Y(\gamma_n, y')$$

Step 4: Determine Transformed Variable Solution

Given Green's function, the solution to the two-dimensional transformed variable problem can be determined from the relationship shown back in Equation 25 in the "Overview of Green's Function" section.

For the special case in which the initial temperature distribution, $f_2(x, y)$, is equal to zero; and a point generation load located at (a,b) in a two-dimensional Cartesian coordinate system, Equation 25 can be reduced to yield Equation 73.

Equation 73. Solution to transformed two-dimensional problem

$$\theta(x, y, t) = \frac{\alpha}{k} \int_{\tau=0}^t \int_{x'=0}^W \int_{y'=0}^H G(x, y, t | x', y', \tau) g_L^c \delta(x' - a) \delta(y' - b) dx' dy' d\tau$$

Given the integral property given shown back in Equation 50, the integrals with respect to x' and y' can be executed, therefore reducing the transformed variable solution to the expression given in Equation 74.

Equation 74. Reduced solution to transformed two-dimensional problem

$$\theta(x, y, t) = \frac{\alpha}{k} * \int_{\tau=0}^t G(x, y, t|a, b, \tau) g_L^c d\tau$$

Step 5. Determine Overall Solution

The overall solution is obtained by looking back at the defined relationship of $\theta(x, y, t) = T(x, y, t) - T_{amb}$ from step 1. This relationship can be applied to Equation 74 to produce a solution in terms $T(x, y, t)$ as shown in Equation 75.

Equation 75. Final temperature solution form for the two-dimensional model

$$T(x, y, t) = \frac{\alpha}{k} \int_{\tau=0}^t G(x, y, t|a, b, \tau) g_L^c d\tau + T_{amb}$$

Next, Green's function (recall Equation 72) can be substituted into Equation 75, and the integral with respect to τ can be performed to yield the expression shown in Equation 76.

Equation 76. Final temperature solution for two-dimensional model

$$T(x, y, t) = \frac{\alpha g_L^c}{k} \sum_{m=1}^{\infty} \sum_{n=1}^{\infty} \frac{X(\beta_m, x)X(\beta_m, a)Y(\gamma_n, y)Y(\gamma_n, b)}{N(\beta_m)N(\gamma_n)\alpha(\beta_m^2 + \gamma_n^2)} (1 - e^{-\alpha(\beta_m^2 + \gamma_n^2)t}) + T_{amb}$$

This is the overall analytical solution of the time and location dependent temperature distribution for the two-dimensional model. The surface temperature of interested can be determined by simply setting $x=0$ or $y=0$.

Numerical solutions for several different generation amounts, generation locations, and specimen thicknesses were developed with the MATLAB input file shown in Appendix B. These results are given in Chapter 6.

Three-Dimensional Analytical Solution

Recall the three-dimensional heat transfer problem used to model vibrothermography from Equation 6in Chapter 2 (shown again in Equation 77).

Equation 77. Three-dimensional mathematical model with boundary conditions

$$\frac{\partial^2 T}{\partial x^2} + \frac{\partial^2 T}{\partial y^2} + \frac{\partial^2 T}{\partial z^2} + \frac{g(x, y, z, t)}{k} = \frac{1}{\alpha} * \frac{\partial T}{\partial t}$$

Boundary conditions (B.C.)

$$\text{(B.C. \#1)} \quad -\frac{\partial T}{\partial x} + \frac{h}{k} * T = T_{amb} \quad @ \ x = 0$$

$$\text{(B.C. \#2)} \quad \frac{\partial T}{\partial x} + \frac{h}{k} * T = T_{amb} \quad @ \ x = W$$

$$\text{(B.C. \#3)} \quad -\frac{\partial T}{\partial y} + \frac{h}{k} * T = T_{amb} \quad @ \ y = 0$$

$$\text{(B.C. \#4)} \quad \frac{\partial T}{\partial y} + \frac{h}{k} * T = T_{amb} \quad @ \ y = H$$

$$\text{(B.C. \#5)} \quad -\frac{\partial T}{\partial z} + \frac{h}{k} * T = T_{amb} \quad @ \ z = 0$$

$$\text{(B.C. \#6)} \quad \frac{\partial T}{\partial z} + \frac{h}{k} * T = T_{amb} \quad @ \ z = L$$

Initial condition (I.C)

$$\text{(I.C)} \quad T = f(x, y, z) \quad @ \ t=0$$

The temperature distribution for this three-dimensional model was determined by following the steps outlined in the “Procedure for Determining Analytical Solution” section as follows:

Step 1. Perform Transformation of Variables

First, a transformation of variables is performed to eliminate the non-homogeneous boundary conditions at $x=0$, $x=W$, $y=0$, $y=H$, $z=0$, and $z=L$. This is done by defining a new variable, $\theta(x, y, z, t)$, with the relationship given in Equation 78.

Equation 78. Defined transformation variable

$$\theta(x, y, z, t) = T(x, y, z, t) - T_{amb}$$

The variable transformation is executed by re-arranging this defined relationship and substituting for $T(x, y, z, t)$ in the three-dimensional HDE from Equation 77. The transformed variable partial differential equation can now be written in terms of $\theta(x, y, z, t)$ as shown in Equation 79.

Equation 79. Three-dimensional transformed partial differential equation with boundary conditions

$$\frac{\partial^2 \theta}{\partial x^2} + \frac{\partial^2 \theta}{\partial y^2} + \frac{\partial^2 \theta}{\partial z^2} + \frac{g(x, y, z, t)}{k} = \frac{1}{\alpha} * \frac{\partial \theta}{\partial t}$$

Boundary conditions (B.C.)

$$\text{(B.C. \#1)} \quad -\frac{\partial \theta}{\partial x} + \frac{h}{k} * \theta = 0 \quad @ \ x = 0$$

$$\text{(B.C. \#2)} \quad \frac{\partial \theta}{\partial x} + \frac{h}{k} * \theta = 0 \quad @ \ x = W$$

$$\text{(B.C. \#3)} \quad -\frac{\partial \theta}{\partial y} + \frac{h}{k} * \theta = 0 \quad @ \ y = 0$$

$$\text{(B.C. \#4)} \quad \frac{\partial \theta}{\partial y} + \frac{h}{k} * \theta = 0 \quad @ \ y = H$$

$$\text{(B.C. \#5)} \quad -\frac{\partial \theta}{\partial z} + \frac{h}{k} * \theta = 0 \quad @ z = 0$$

$$\text{(B.C. \#6)} \quad \frac{\partial \theta}{\partial z} + \frac{h}{k} * \theta = 0 \quad @ z = L$$

Initial condition (I.C)

$$\text{(I.C)} \quad \theta = f(x, y, z) - T_{amb} = f_2(x, y, z) \quad @ t=0$$

Note that by performing this transformation of variables, all the boundary condition become homogeneous.

Step 2. Solve Auxiliary Problem

Green's function can be determined by solving the auxiliary problem given in Equation 80.

Equation 80. Three-dimensional homogeneous auxiliary partial differential equation with boundary conditions

$$\frac{\partial^2 \psi}{\partial x^2} + \frac{\partial^2 \psi}{\partial y^2} + \frac{\partial^2 \psi}{\partial z^2} = \frac{1}{\alpha} * \frac{\partial \psi}{\partial t}$$

Boundary conditions (B.C.)

$$\text{(B.C. \#1)} \quad -\frac{\partial \psi}{\partial x} + \frac{h}{k} * \psi = 0 \quad @ x = 0$$

$$\text{(B.C. \#2)} \quad \frac{\partial \psi}{\partial x} + \frac{h}{k} * \psi = 0 \quad @ x = W$$

$$\text{(B.C. \#3)} \quad -\frac{\partial \psi}{\partial y} + \frac{h}{k} * \psi = 0 \quad @ y = 0$$

$$\text{(B.C. \#4)} \quad \frac{\partial \psi}{\partial y} + \frac{h}{k} * \psi = 0 \quad @ y = H$$

$$\text{(B.C. \#5)} \quad -\frac{\partial \psi}{\partial z} + \frac{h}{k} * \psi = 0 \quad @ z = 0$$

$$\text{(B.C. \#6)} \quad \frac{\partial \psi}{\partial z} + \frac{h}{k} * \psi = 0 \quad @ z = L$$

Initial condition (I.C)

$$(I.C) \quad \psi = f(x, y, z) - T_{amb} = f_2(x, y, z) \quad @ t=0$$

The solution to this auxiliary problem can be obtained following the same Separation of Variables Technique procedure carried out in Step 2 of the “One-dimensional Analytical Solution” section. The assumed solution is shown in Equation 81.

Equation 81. Three-dimensional separation of variables assumed solution

$$\psi(x, t) = X(x)Y(y)Z(z)\Gamma(t)$$

This assumed solution is substituted into Equation 80, and re-arranged to produce the four ordinary differential equations given in Equation 82, Equation 83, Equation 84, and Equation 85.

Equation 82. X-direction ordinary differential equation for three-dimensional model

$$\frac{d^2X}{dx^2} + \beta^2X = 0$$

Boundary conditions (B.C's)

$$(B.C. \#1) \quad -\frac{\partial X}{\partial x} + \frac{h}{k} * X = 0 \quad @ x = 0$$

$$(B.C. \#2) \quad \frac{\partial X}{\partial x} + \frac{h}{k} * X = 0 \quad @ x = W$$

Equation 83. Y-direction ordinary differential equation for three-dimensional model

$$\frac{d^2Y}{dy^2} + \gamma^2Y = 0$$

Boundary conditions (B.C's)

$$(B.C. \#1) \quad -\frac{\partial Y}{\partial y} + \frac{h}{k} * Y = 0 \quad @ y = 0$$

$$(B.C. \#2) \quad \frac{\partial Y}{\partial y} + \frac{h}{k} * Y = 0 \quad @ y = H$$

Equation 84. Z-direction ordinary differential equation for three-dimensional model

$$\frac{d^2 Z}{dz^2} + \eta^2 Z = 0$$

Boundary conditions (B.C's)

$$\text{(B.C. \#1)} \quad -\frac{\partial Z}{\partial z} + \frac{h}{k} * Z = 0 \quad @ \ z = 0$$

$$\text{(B.C. \#2)} \quad \frac{\partial Z}{\partial z} + \frac{h}{k} * Z = 0 \quad @ \ z = L$$

Equation 85. Time dependent ordinary differential equation for three-dimensional model

$$\frac{d\Gamma}{dt} + \alpha(\beta^2 + \gamma^2 + \eta^2)\Gamma = 0$$

Note that for the three-dimensional case, there now exists three eigenvalues, $\beta, \gamma,$ and η . The values of which produce non-trivial solutions will again be super positioned in terms of $\beta_m, \gamma_n,$ and η_p where $m = 1, 2, 3, \dots, n = 1, 2, 3, \dots,$ and $p = 1, 2, 3, \dots$. The eigenfunction solutions to the ordinary differential equations are given in Equations 86-89.

Equation 86. Time dependent ordinary differential equation solution for three-dimensional model

$$\Gamma(t) = e^{-\alpha(\beta^2 + \gamma^2 + \eta^2)t}$$

Equation 87. x dependent ordinary differential equation solution for three-dimensional model

$$X(\beta_m, x) = B_m \cos(\beta_m x) + \frac{h}{k} \sin(\beta_m x)$$

Equation 88. y dependent ordinary differential equation solution for three-dimensional model

$$Y(\gamma_n, y) = \gamma_n \cos(\gamma_n y) + \frac{h}{k} \sin(\gamma_n y)$$

Equation 89. z dependent ordinary differential equation solution for three-dimensional model

$$Z(\eta_p, z) = \eta_p \cos(\eta_p z) + \frac{h}{k} \sin(\eta_p z)$$

Where the eigenvalues of B_m, γ_n , and η_p are the positive roots of the expressions shown in Equation 90.

Equation 90. Eigenvalue expressions for the three-dimensional model

$$\tan(\beta_m W) = \frac{\beta_m \left(\frac{2h}{k}\right)}{\beta_m^2 - \left(\frac{h}{k}\right)^2}$$

$$\tan(\gamma_n H) = \frac{\gamma_n \left(\frac{2h}{k}\right)}{\gamma_n^2 - \left(\frac{h}{k}\right)^2}$$

$$\tan(\eta_p Z) = \frac{\eta_p \left(\frac{2h}{k}\right)}{\eta_p^2 - \left(\frac{h}{k}\right)^2}$$

These ODE solutions are combined and the constant is determined by applying the non-homogeneous initial condition and again taking advantage of the orthogonality principal. The overall solution for the three-dimensional auxiliary problem is given in Equation 91, with the expression of the norms given in Equation 92.

Equation 91. Auxiliary solution for three-dimensional model

$$\begin{aligned} \psi(x, y, z, t) = & \sum_{m=1}^{\infty} \sum_{n=1}^{\infty} \sum_{p=1}^{\infty} \frac{1}{N(\beta_m)N(\gamma_n)N(\eta_p)} X(\beta_m, x)Y(\gamma_n, y)Z(\eta_p, z)e^{-\alpha\beta^2 t} \\ & * \int_{x'=0}^W \int_{y'=0}^H \int_{z'=0}^L X(\beta_m, x')Y(\gamma_n, y')Z(\eta_p, z')f_2(x', y', z') dx' dy' dz' \end{aligned}$$

Equation 92. Norm solutions for three-dimensional model

$$N(\beta_m) = 2 \left[\left(\beta_m^2 + \left(\frac{h}{k} \right)^2 \right) \left(W + \frac{\frac{h}{k}}{\beta_m^2 + \left(\frac{h}{k} \right)^2} \right) + \frac{h}{k} \right]$$

$$N(\gamma_n) = 2 \left[\left(\gamma_n^2 + \left(\frac{h}{k} \right)^2 \right) \left(H + \frac{\frac{h}{k}}{\gamma_n^2 + \left(\frac{h}{k} \right)^2} \right) + \frac{h}{k} \right]$$

$$N(\eta_p) = 2 \left[\left(\eta_p^2 + \left(\frac{h}{k} \right)^2 \right) \left(L + \frac{\frac{h}{k}}{\eta_p^2 + \left(\frac{h}{k} \right)^2} \right) + \frac{h}{k} \right]$$

Step 3. Determine Green's Function from Auxiliary Solution

For the two-dimensional model, Green's function can be evaluated by applying the relationship between the auxiliary solution and Green's function back in Equation 26. This application is shown in Equation 93.

Equation 93. Green's function relationship for three-dimensional model

$$\begin{aligned} \psi(x, y, z, t) &= \int_{x'=0}^{\infty} \int_{y'=0}^{\infty} \int_{z'=0}^{\infty} G(x, y, z, t | x', y', z', \tau)_{\tau=0} f_2(x, y, z,) dx' dy' dz' \\ &= \sum_{m=1}^{\infty} \sum_{n=1}^{\infty} \sum_{p=1}^{\infty} \frac{X(\beta_m, x) Y(\gamma_n, y) Z(\eta_p, z)}{N(\beta_m) N(\gamma_n) N(\eta_p)} \\ &\quad * \int_{x'=0}^W \int_{y'=0}^H \int_{z'=0}^L X(\beta_m, x') Y(\gamma_n, y') Z(\eta_p, z') f_2(x', y', z') dx' dy' dz' \end{aligned}$$

From this relationship, it can be observed that Green's function at $\tau = 0$ is the expression given in Equation 94.

Equation 94. Green's function at $\tau=0$ for the three-dimensional model

$$G(x, y, z, t | x', y', z', \tau)_{\tau=0} = \sum_{m=1}^{\infty} \sum_{n=1}^{\infty} \sum_{p=1}^{\infty} \frac{X(\beta_m, x)Y(\gamma_n, y)Z(\eta_p, z)}{N(\beta_m)N(\gamma_n)N(\eta_p)} e^{-\alpha(\beta_m^2 + \gamma_n^2 + \eta_p^2)t} X(\beta_m, x')Y(\gamma_n, y')Z(\eta_p, z')$$

The general form of Green's function can be obtained by replacing t with $t - \tau$ in Equation 94 to yield the final form of Green's function shown in Equation 95.

Equation 95. Green's function for the three-dimensional model

$$G(x, y, z, t | x', y', z', \tau) = \sum_{m=1}^{\infty} \sum_{n=1}^{\infty} \sum_{p=1}^{\infty} \frac{X(\beta_m, x)Y(\gamma_n, y)Z(\eta_p, z)}{N(\beta_m)N(\gamma_n)N(\eta_p)} e^{-\alpha(\beta_m^2 + \gamma_n^2 + \eta_p^2)(t-\tau)} X(\beta_m, x')Y(\gamma_n, y')Z(\eta_p, z')$$

Step 4. Determine Transformed Variable Solution

Given Green's function, the solution to the three-dimensional transformed variable problem can be determined from the relationship shown back in Equation 25 in the "Overview of Green's Function" section.

For the special case in which the initial temperature distribution, $f_2(x, y, z)$, is equal to zero; and a point generation load located at (a, b, c) in a Cartesian coordinate system, Equation 25 can be reduced to yield Equation 96.

Equation 96. Solution to transformed three-dimensional model

$$\begin{aligned} \theta(x, y, z, t) &= \frac{\alpha}{k} \int_{\tau=0}^t \int_{x'=0}^W \int_{y'=0}^H \int_{z'=0}^L G(x, y, z, t | x', y', z', \tau) g_L^c \\ &\quad * \delta(x' - a)\delta(y' - b)\delta(y' - c) dx' dy' d\tau \end{aligned}$$

Given the integral property given shown back in Equation 50, the integrals with respect to x' and y' can be executed, therefore reducing the transformed variable solution to the expression given in Equation 97.

Equation 97. Reduced solution to transformed three-dimensional model

$$\theta(x, y, z, t) = \frac{\alpha}{k} \int_{\tau=0}^t G(x, y, z, t|a, b, c, \tau) g_p^c d\tau$$

Step 5. Determine Overall Solution

The overall solution is obtained by looking back at the defined relationship of $\theta(x, y, z, t) = T(x, y, z, t) - T_{amb}$ from step 1. This relationship can be applied to Equation 97 to produce a solution in terms $T(x, y, z, t)$ as shown in Equation 98.

Equation 98. Final temperature solution form for the three-dimensional model

$$T(x, y, z, t) = \frac{\alpha}{k} \int_{\tau=0}^t G(x, y, z, t|a, b, c, \tau) g_p^c d\tau + T_{amb}$$

Next, Green's function (recall Equation 95) can be substituted into Equation 98, and the integral with respect to τ can be performed to yield the expression shown in Equation 99.

Equation 99. Final temperature solution for three-dimensional model

$$T(x, y, z, t) = \frac{\alpha g_p^c}{k} \sum_{m=1}^{\infty} \sum_{n=1}^{\infty} \sum_{p=1}^{\infty} \frac{X(\beta_m, x)X(\beta_m, a)Y(\gamma_n, y)Y(\gamma_n, b)Z(\eta_p, z)Z(\eta_p, c)}{N(\beta_m)N(\gamma_n)N(\eta_p)} \\ * (1 - e^{-\alpha(\beta_m^2 + \gamma_n^2 + \eta_p^2)t}) + T_{amb}$$

This is the overall analytical solution of the time and location dependent temperature distribution for the three-dimensional model. The surface temperature of interested can be determined by simply setting $x=0$, $y=0$, or $z=0$.

Numerical solutions for several different generation amounts, generation locations, and specimen thicknesses were developed with the MATLAB input file shown in Appendix B. These results are given in Chapter 6.

CHAPTER 6 – MODEL RESULTS

One-Dimensional Model Results

This section gives an overview of the solutions obtained from the one-dimensional vibrothermography model shown in Figure 5 and Equation 4 back in Chapter 2. A heat-generating flaw was modeled as a heat flux point source which generated heat for a period of 5 minutes (to simulate a vibrothermography test which lasted five minutes). After the five minute period expires, the heat generation at the flaw is set to zero, but the model continues to simulate the heat transfer occurring within the specimen until thermal equilibrium is achieved. Each of the simulations observed the surface temperature as a function of generation amount, flaw depth, and specimen thickness.

The temperature solutions for the one-dimensional model were determined with the finite difference, finite element, and analytical solution methods. These results include a time-dependent study; and a parametric study of the parameters shown in Table 1.

Table 1. Test plan for one-dimensional model

Generation Amount	Specimen Thickness	Flaw Depth
1 W/m ²	0.1 - 2 in. (0.254 – 5.08 cm)	10% - 90% specimen thickness

Time Dependent Solutions for the One-Dimensional Model

The finite difference, finite element, and analytical transient surface temperature solutions for various flaw depths are shown in Figure 19. During these simulations, the specimen thickness was set to 1 inch and the generation amount was $1 \frac{W}{m^2}$.

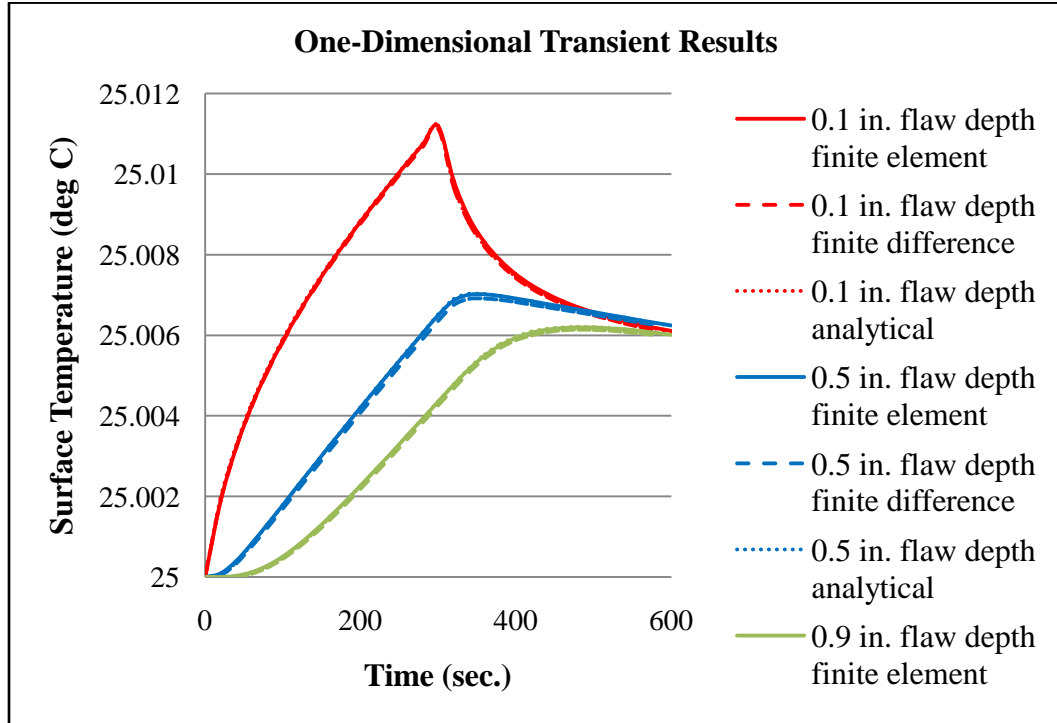


Figure 19. Transient surface temperature results for the one-dimensional model

In Figure 19, the 0.1 inch (0.254 cm) flaw depth results are represented as red lines, the 0.5 inch (1.27 cm) flaw depth is represented as blue lines, and the 0.9 inch (2.286 cm) flaw depth is represented as green lines. The solid lines represent the solutions obtained by the finite element method; the dashed lines represent the solutions obtained by the finite difference method; and the dotted lines represent the solutions obtained by the analytical method.

Note that the time delay during the beginning of the test (amount of time that passes before a noticeable surface temperature change) and end of the test (amount of time that passes after generation stops and a maximum surface temperature is observed) increase as a function of flaw depth. This is useful because, once models have been calibrated to the thickness of the specimen under observation; the depth of the flaw can

be estimated directly by measuring these time delays. A relationship between the time delay at the end of test and flaw depth is shown in Figure 20.

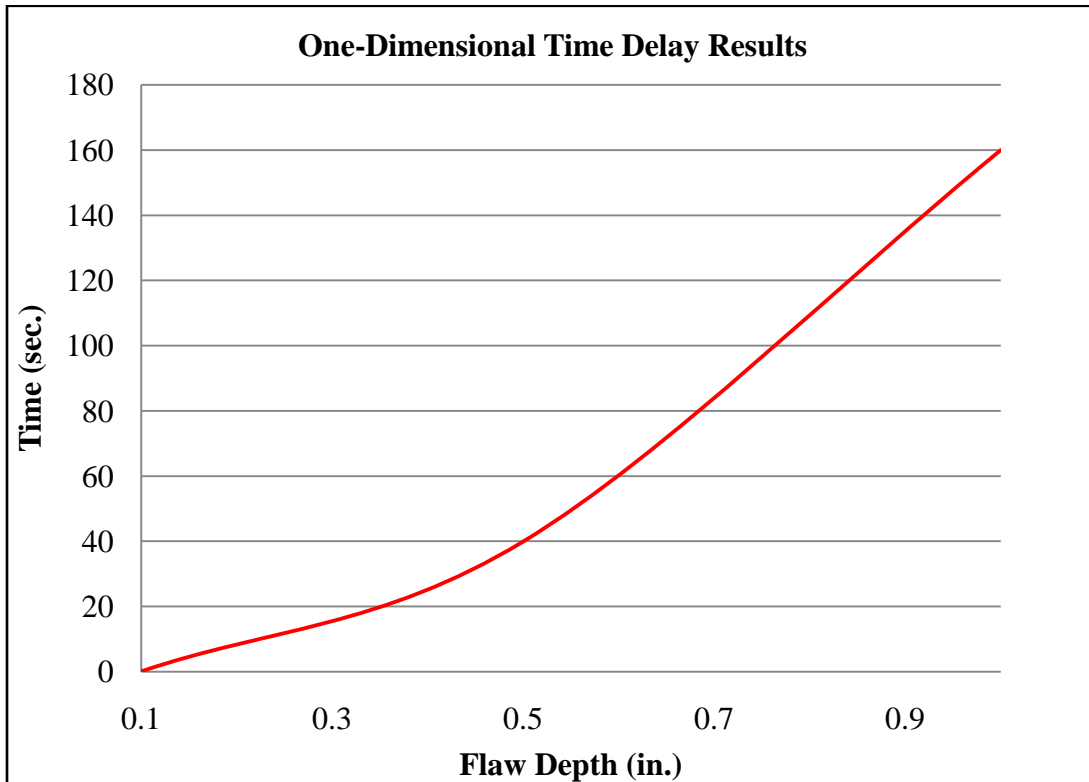


Figure 20. Time delay between generation stopping and maximum recorded surface temperature in the one-dimensional model

Generation Amount Dependent Solutions for the One-Dimensional Model

The second investigation performed investigated the effect flaw generation amount has on the maximum recorded surface temperature. This study was performed with a specimen thickness of 1 inch (2.54 cm), flaw depths at 0.1 inches (0.254 cm), 0.5 inches (1.27 cm), and 0.9 inches (2.286 cm), and generation amounts varying from 100 $\frac{W}{m^2}$ to 500 $\frac{W}{m^2}$. These results are shown in Figure 21.

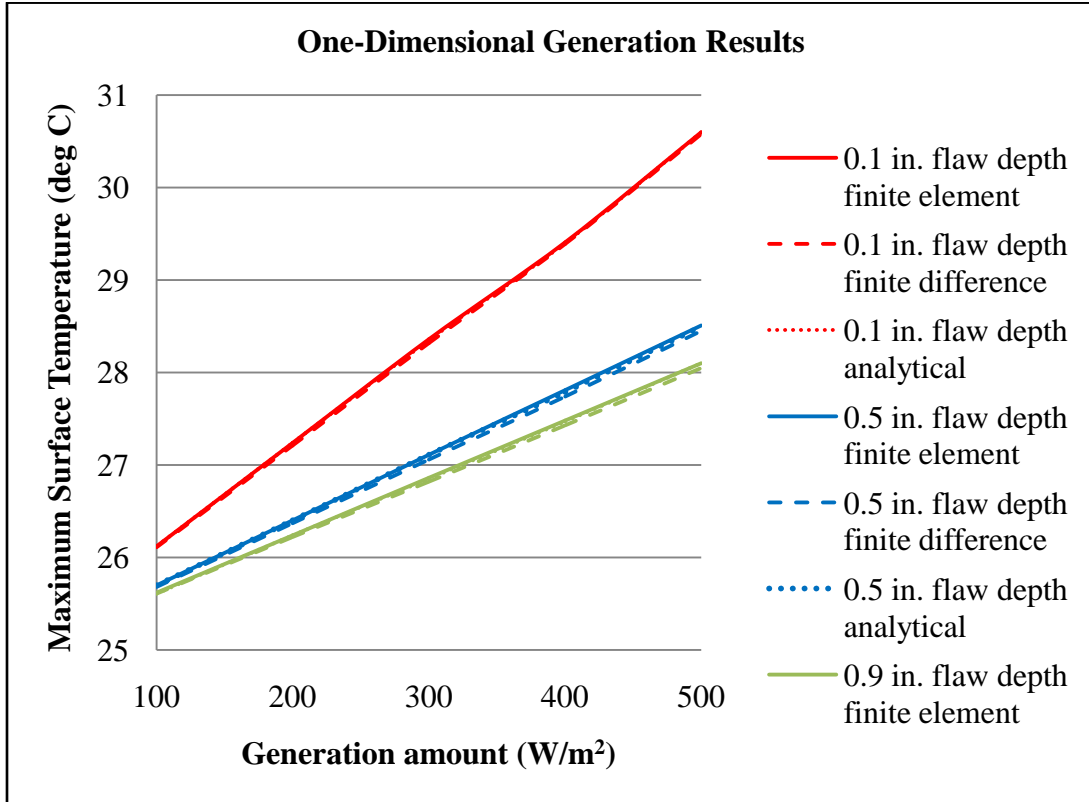


Figure 21. Maximum surface temperature results as a function of generation amount in the one-dimensional model

Specimen Thickness Dependent Solutions for the One-Dimensional Model

The third and final parameter investigated with the one-dimensional model was the effect of specimen thickness on the maximum recorded surface temperature. This study was performed with a generation amount of $1 \frac{W}{m^2}$, flaw depths of 10%, 50%, and 90% of the specimen thickness, and a specimen thickness varying from 0.1 inches (0.254 cm) to 2 inches (5.08 cm). These results are shown in Figure 22.

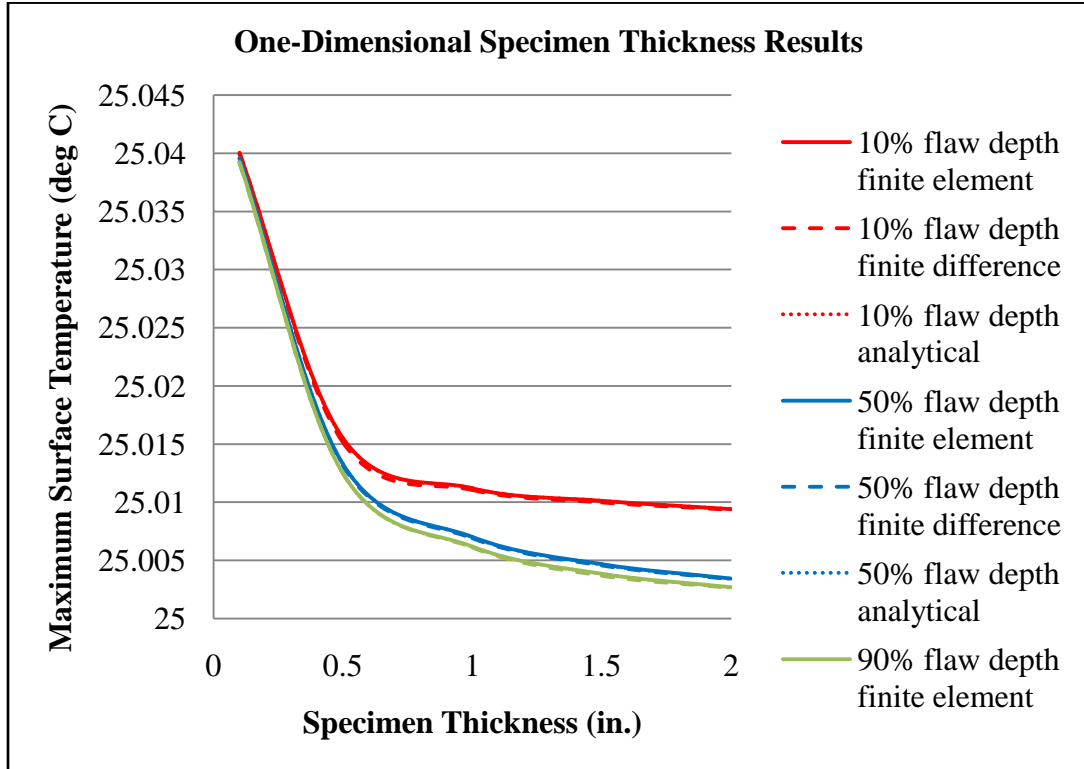


Figure 22. Maximum surface temperature results as a function of specimen thickness for the one-dimensional model

Discussion of One-Dimensional Model Results

The one-dimensional model simulations provide some insight into quantifying the effects of time delay, flaw depth, generation amount, and specimen thickness can have on the observed maximum surface temperature. The primary objective of the one-dimensional model, however, was to compare the finite element, finite difference, and analytical methods. The maximum percent difference between each of the methods was 0.55% (see APPENDIX D for actual data sets). These small percent errors were well within the numerical and round-off errors associated with each of the methods. To demonstrate this, slight fluctuations in the finite element mesh density and mesh size, fluctuations in the finite difference node density and node spacing, and the number of and

precision of the eigenvalues calculated with the analytical method would all fluctuate the results up to 0.8%.

As for application to physical problems, only vibrothermography instances in which a flaw is evenly distributed through the entire cross-section--which is extremely rare--could a one-dimensional model accurately predict the heat transfer effects. Therefore, two-dimensional and three-dimensional models are needed to simulate test parameters that more accurately resemble real-life situations.

Two-Dimensional Model Results

This section gives an overview of the solutions obtained from the two-dimensional vibro-thermography model shown in Figure 6 and Equation 5 back in Chapter 2. The heat-generating flaw was modeled either as a line source or a point source (the analytical method used only a point source while the finite element method could apply either a line source or a point source). The flaw once again was modeled to produce heat for a period of 5 minutes. For all of the solutions determined in these simulations, the specimen was assumed to be 5 inches (12.7 cm) wide. The parameters investigated with the two-dimensional model were:

- Generation amount
- Flaw depth
- Specimen thickness
- Flaw size
- Flaw orientation

The temperature solutions for the two-dimensional model were determined with the finite element and the analytical solution methods. These results include a time-dependent study; and a parametric study of the parameters shown in Table 2.

Table 2. Test plan for two-dimensional model

Generation amount	Flaw Depth	Specimen Thickness	Flaw size	Flaw orientation
1 W/m	10% - 90% specimen thickness	0.1 - 2 inches (0.254 – 5.08 cm)	0.1 - 1 inch (0.254 – 2.54 cm)	0° - 90°

Time Dependent Solutions for the Two-Dimensional Model

The finite element and analytical transient surface temperature solutions for various flaw depths are shown in Figure 23. During these simulations, the specimen thickness was set to 1 inch and the generation amount was $1 \frac{W}{m}$. The heat generating flaw was modeled as a point source in order to insure consistency between the analytical and finite element results.

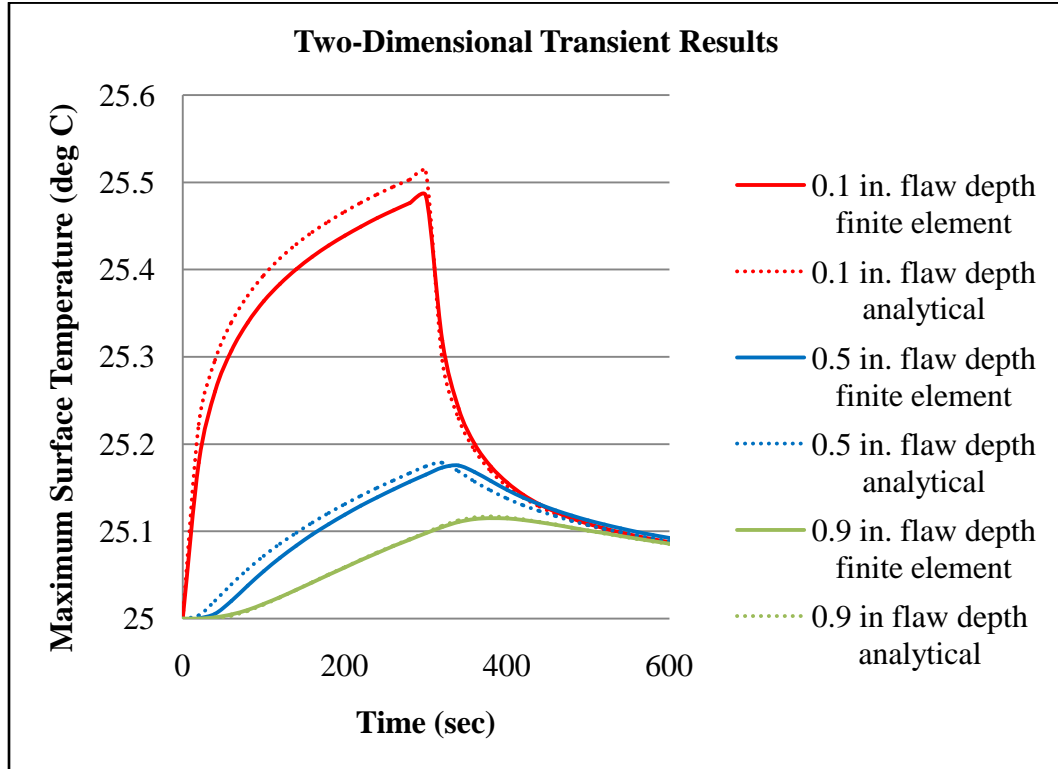


Figure 23. Transient surface temperature results for the two-dimensional model

The time delay between the generation stopping and the maximum surface temperature being attained is shown in Figure 24.

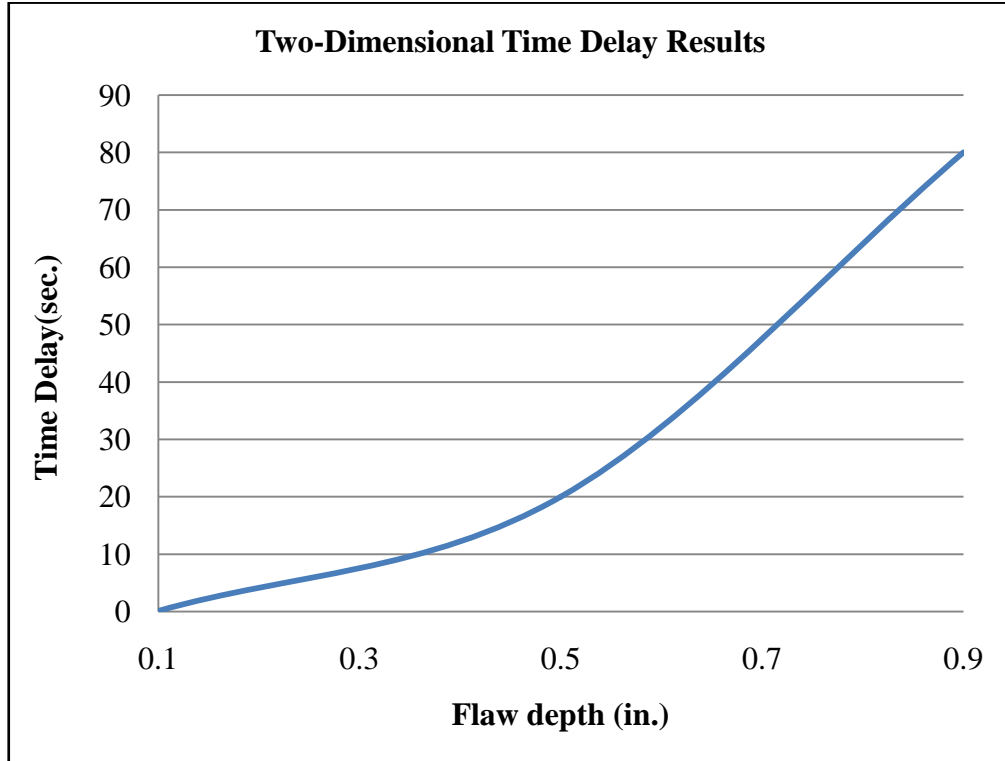


Figure 24. Time delay between generation stopping and maximum recorded surface temperature in the two-dimensional model

Generation Amount Dependent Solutions for the Two-Dimensional Model

The second investigation performed investigated the effect the flaw generation amount has on the maximum recorded surface temperature. This study was performed with a specimen thickness of 1 inch, a specimen width of 5 inches (12.7 cm), flaw depths at 0.1 inches (0.254 cm), 0.5 inches (1.27 cm), and 0.9 inches (2.286 cm), and generation amounts varying from $10\frac{W}{m}$ to $50\frac{W}{m}$ with a point load heat source. These results are shown in Figure 25.

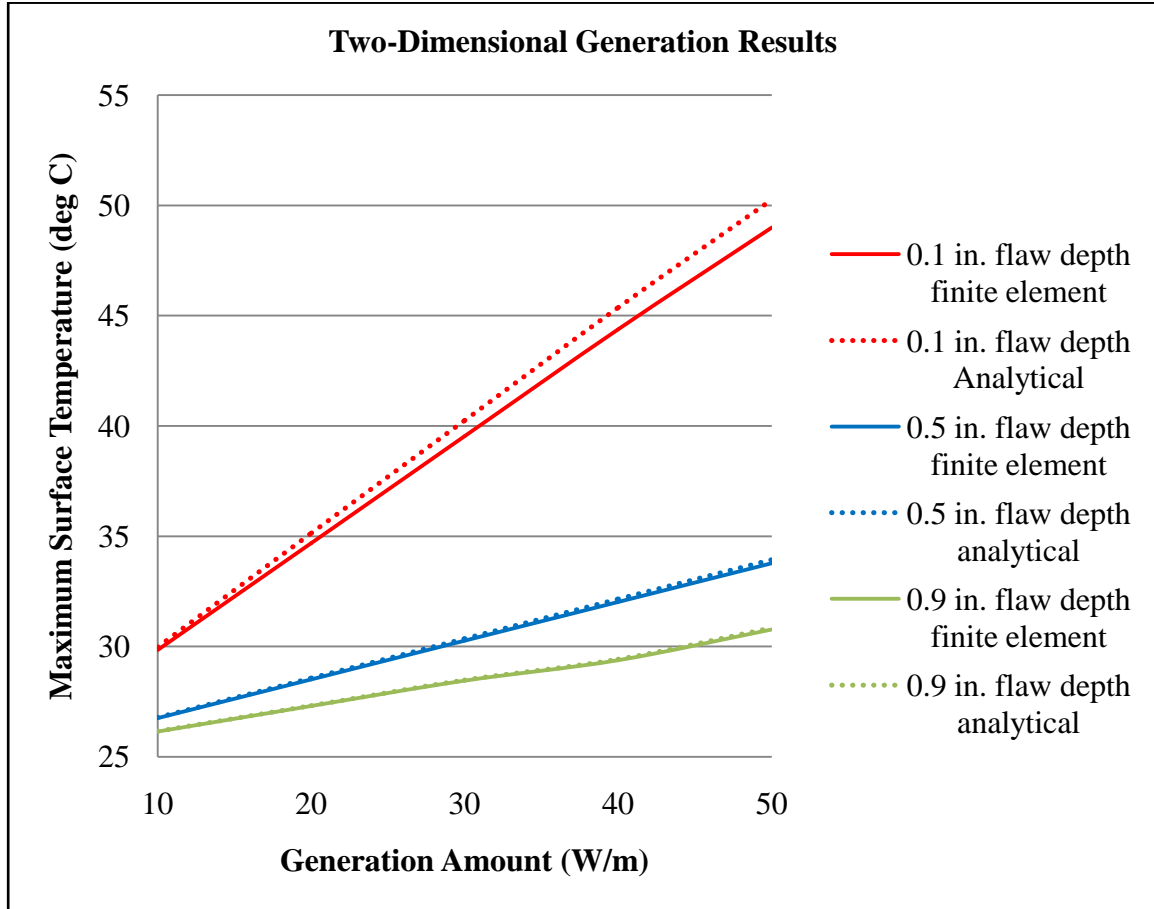


Figure 25. Maximum surface temperature results as a function of generation amount in the two-dimensional model

Specimen Thickness Dependent Solutions for the Two-Dimensional Model

The third parameter investigated with the two-dimensional model was the effect of specimen thickness. This study was performed with a generation amount of $1 \frac{W}{m}$, flaw depths of 10%, 50%, and 90% of the specimen thickness, and a specimen thickness varying from 0.1 inches (0.254 cm) to 2 inches (5.08 cm). These results are shown in Figure 26.

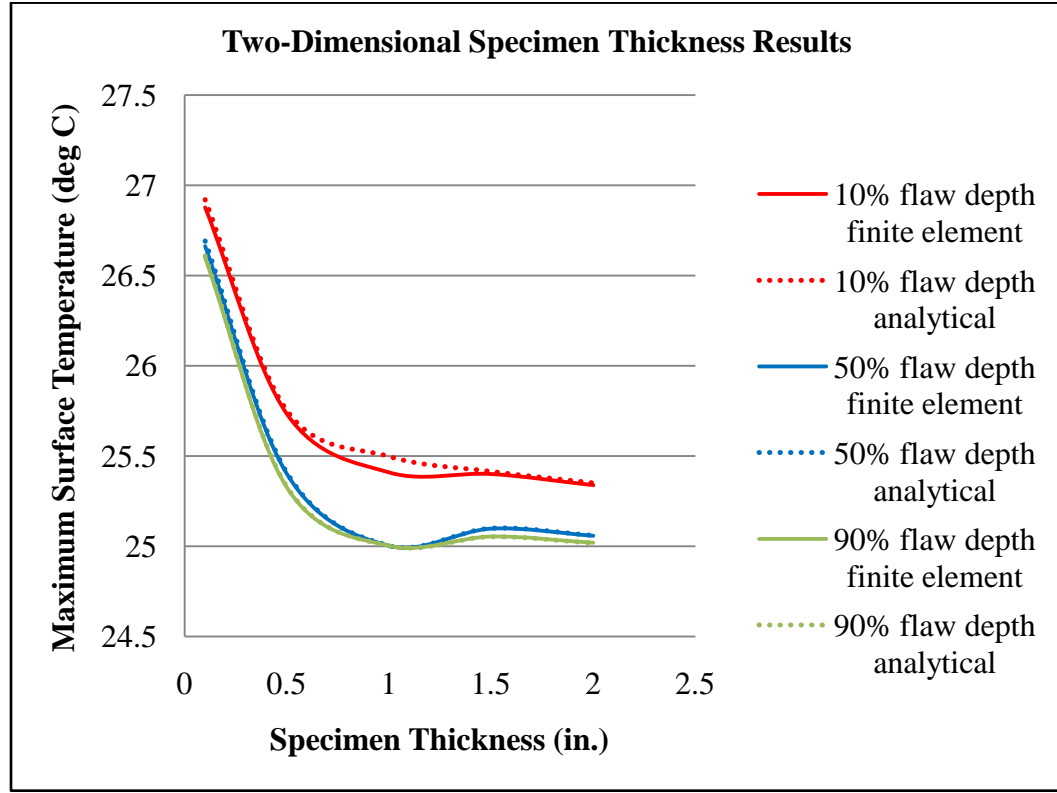


Figure 26. Maximum surface temperature results as a function of specimen thickness for the two-dimensional model

Flaw Orientation Dependent Solutions for the Two-Dimensional Model

The fourth parameter investigated with the two-dimensional model is effect of flaw orientation. For this study, the specimen thickness was 1 inch (2.54 cm), the flaw was a 0.5 inch (1.27 cm) line heat source, the flaw depth was 0.1 inches (0.254 cm), 0.5 inches (1.27 cm), and 0.9 inches (2.286 cm), and the generation was $1 \frac{W}{m^2}$. The flaw orientation results are shown in Figure 27.

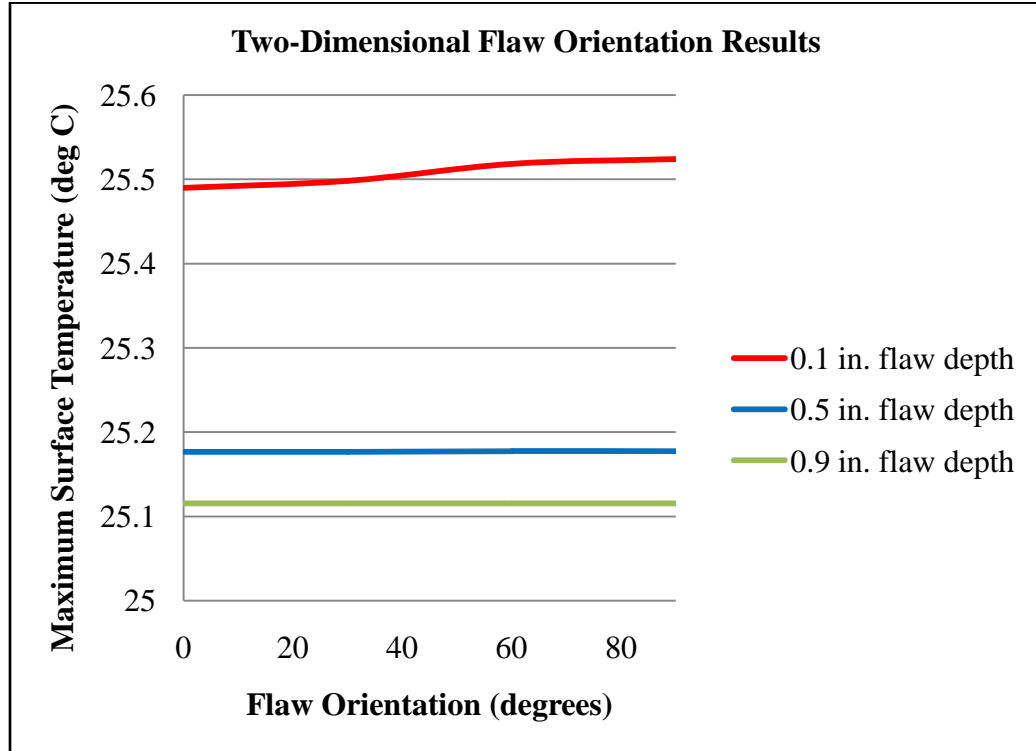


Figure 27. Maximum surface temperature results as a function of flaw orientation in the two-dimensional model

Flaw Size Dependent Solution for the Two-Dimensional Model

The fifth and final parameter investigated with the two-dimensional model was the flaw size. For this study, the specimen thickness was 1 inch, the flaw was a horizontal line heat source, the flaw depth was 0.1 inches (0.254 cm), 0.5 inches (1.27 cm), and 0.9 inches (2.286 cm), and the generation was $1 \frac{W}{m^2}$. These flaw size results are shown in Figure 28.

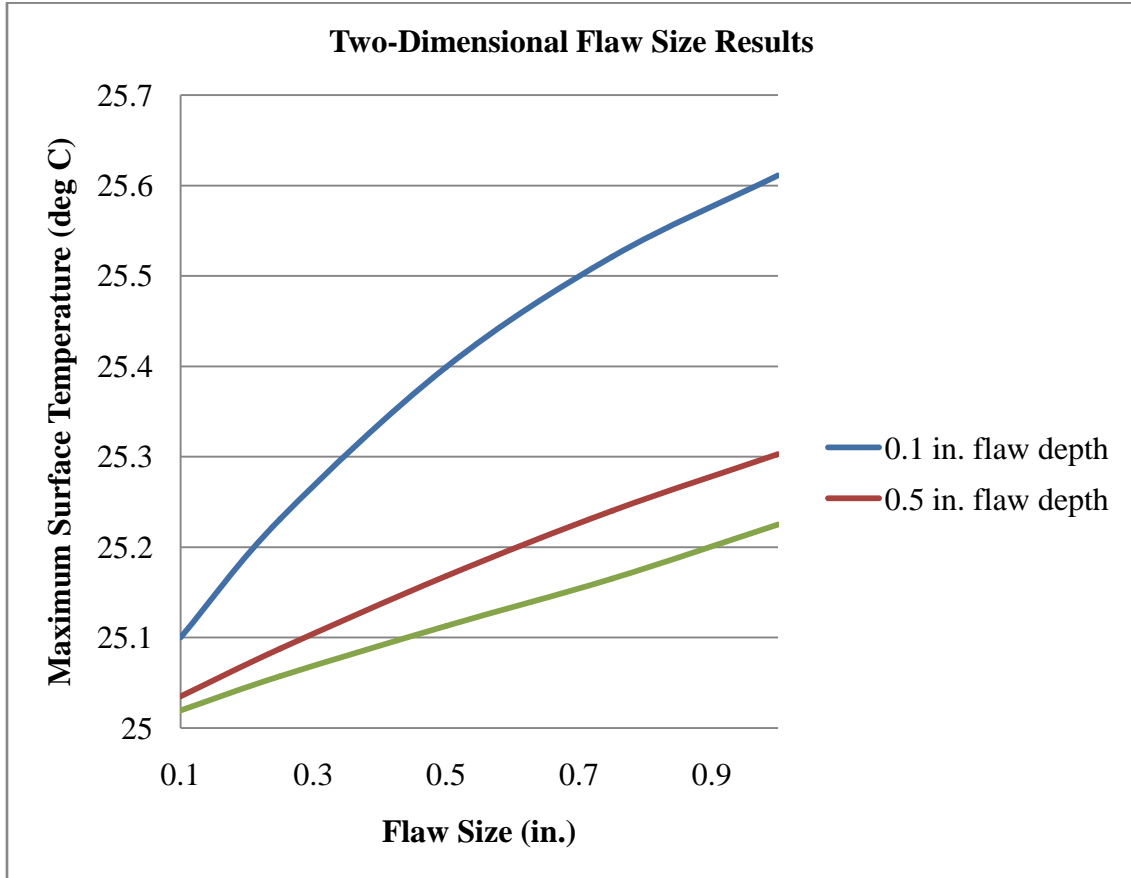


Figure 28. Maximum surface temperature results as a function of flaw orientation in the two-dimensional model

Discussion of Two-Dimensional Model Results

The two-dimensional model gave more detailed and practical insight to the effects that flaw depth, generation amount, specimen thickness, flaw size, and flaw orientation can have on the observed surface temperature. The two-dimensional model represents a model that is one unit long (in the z direction) with the flaw expanding that entire length. Although, this does not occur frequently, some types of delaminations and flaws could very easily be accurately represented by this model.

The time delay results given in Figure 24 can be easily obtained from the model for a specimen of any width and height, and the results for flaw depth can be directly interpolated. The relationships between each of the other individual parameters and the observed maximum surface temperature shown in Figures 20-23 show the effect each of the flaw's thermal parameters, and can be applied to predict the influence changing any individual parameter will have on the vibrothermography test.

The maximum percent difference between the analytical and finite element two-dimensional model solutions was 5.5% (See APPENDIX D for a complete list for individual simulation results and their corresponding percent differences). The percent differences were larger in the two-dimensional model than in the one-dimensional model. Greater error is expected in the two-dimensional finite element model because more elements are needed in order to model both directions, resulting in greater round off errors. In the analytical method, the initial error that exists in the x and y dependent ordinary differential equation solutions is increased because the two solutions are multiplied by each other (therefore multiplying their errors as well). This causes a reduction in the number of significant digits and a precision in the two-dimensional solution when compared to the one-dimensional solution.

Three-Dimensional Model Results

This section gives an overview of the solutions obtained from the three-dimensional vibrothermography model shown in Figure 7 and Equation 6 back in Chapter 2. The heat-generating flaw was modeled either as an area source or a point source. The flaw once again was modeled to produce heat for a period of 5 minutes. For all of the

solutions determined with the three-dimensional model, the specimen was assumed to be 5 inches wide (in the x-direction) and 5 inches long (in the z direction). The parameters investigated with the three-dimensional model were:

- Generation amount
- Flaw depth
- Specimen thickness
- Flaw size
- Flaw orientation

The temperature solutions for the three-dimensional model were determined with the finite element and the analytical solution methods. These results include a time-dependent study; and a parametric study of the parameters shown in Table 3.

Table 3. Test plan for three-dimensional model

Generation amount	Flaw Depth	Specimen Thickness	Flaw size	Flaw orientation
0.2 – 1 W	10% - 90% specimen thickness	0.1 - 2 inches (0.254 – 5.08 cm)	0.1 - 1 inches ² (0.65 – 6.5 cm ²)	0° - 90°

Time Dependent Solutions for the Three-Dimensional Model

The finite element and analytical transient surface temperature solutions for various flaw depths are shown in Figure 29. During these simulations, the specimen thickness was set to 1 inch (2.54 cm) and the generation amount was 1 W located at depths of 0.1 inches (0.254 cm), 0.5 inches (1.27 cm), and 0.9 inches (2.286 cm) (in the y-direction) from the top surface. The heat generating flaw was modeled as a point source in order to insure consistency between the analytical and finite element results.

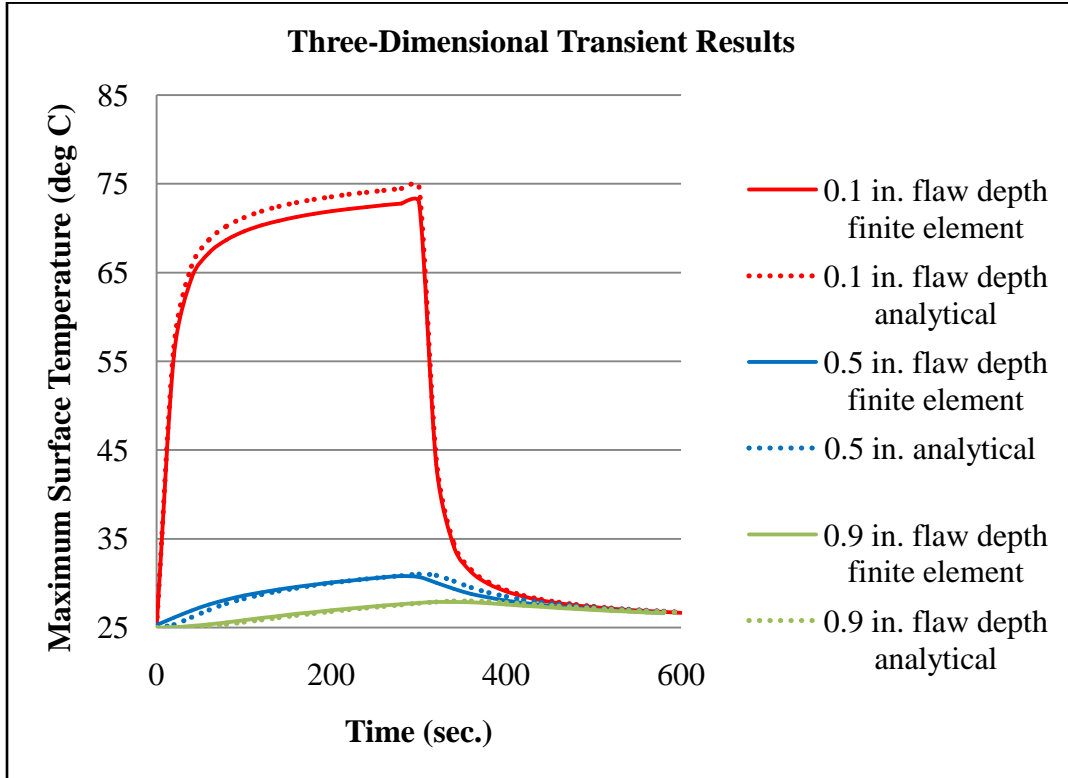


Figure 29. Transient surface temperature results for the three-dimensional model

The time delay between the generation stopping and the maximum surface temperature being attained is shown in Figure 30.

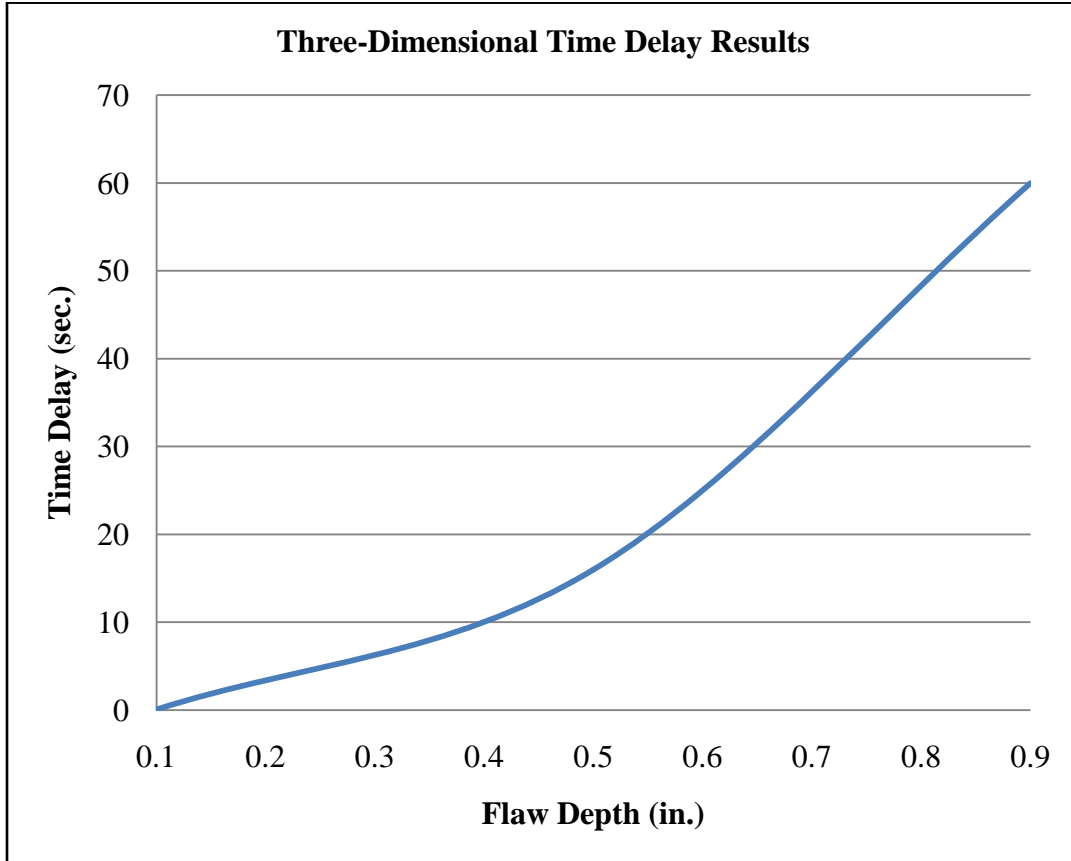


Figure 30. Time delay between generation stopping and maximum recorded surface temperature in the three-dimensional model

Generation Amount Dependent Solutions for the Three-Dimensional Model

The second investigation investigated the effect flaw generation amount has on the maximum recorded surface temperature. This study was performed with a specimen thickness of 1 inch (2.54 cm), a specimen width of 5 inches (12.7 cm), flaw depths at 0.1 inches (0.254 cm), 0.5 inches (1.27 cm), and 0.9 inches (2.286 cm), and the generation amounts varying from 0.2 W to 1 W with a point load heat source. These results are shown in Figure 31.

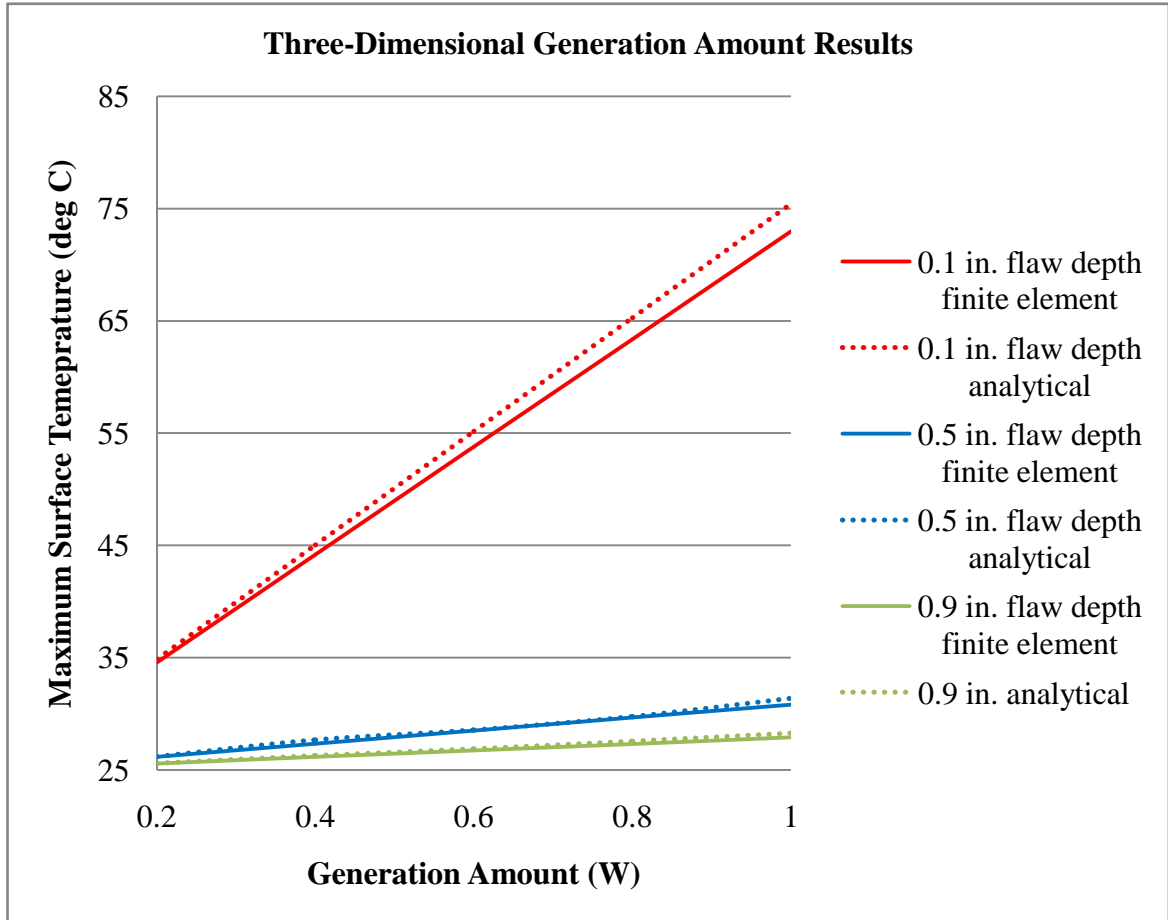


Figure 31. Maximum surface temperature results as a function of generation amount in the three-dimensional model

Specimen Thickness Dependent Solutions for the Three-Dimensional Model

The third parameter investigated with the three-dimensional model was the effect of specimen thickness on the maximum recorded surface temperature. This study was performed with a generation amount of 1 W, flaw depths of 10%, 50%, and 90% of the specimen thickness, and a specimen thickness varying from 0.1 inches (0.254 cm) to 2 inches (5.08 cm). These results are shown in Figure 32.

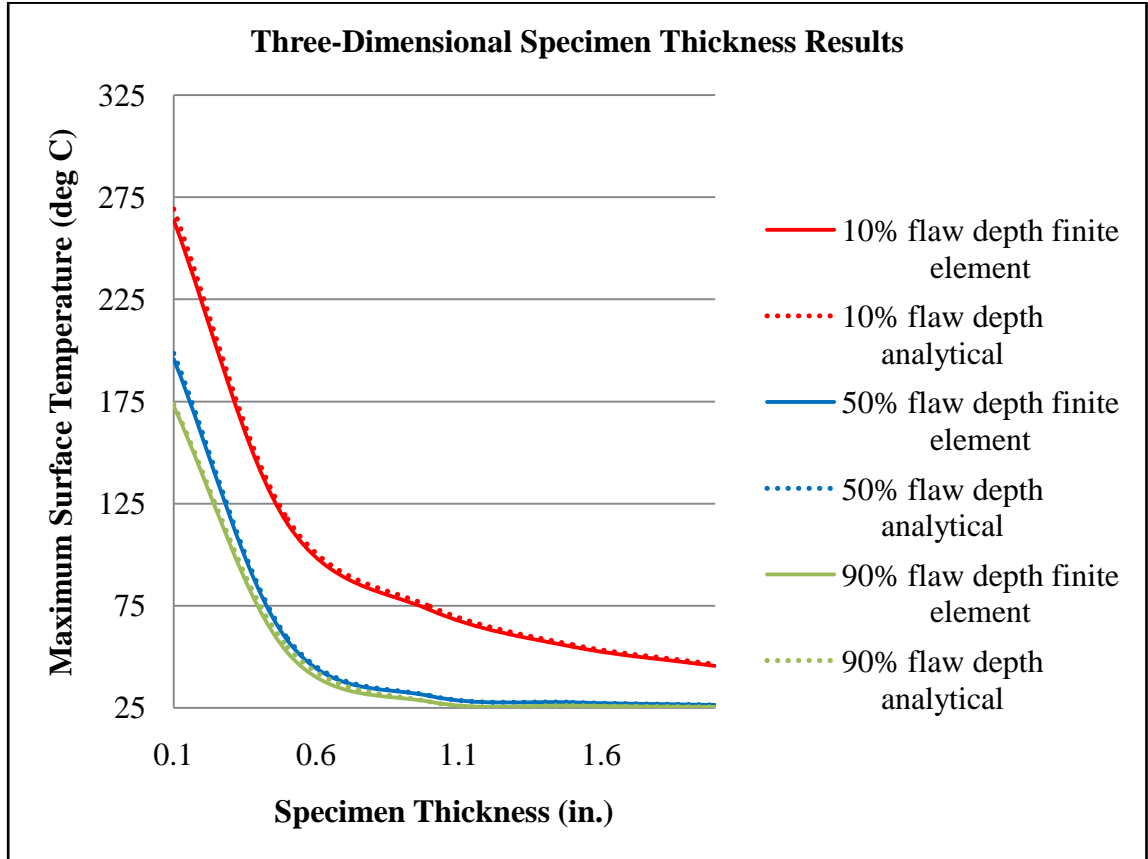


Figure 32. Maximum surface temperature results as a function of specimen thickness for the two-dimensional model

Flaw Orientation Dependent Solutions for the Three-Dimensional Model

The fourth parameter investigated with the three-dimensional model is effect of flaw orientation on the maximum recorded surface temperature. For this study, the specimen thickness was 1 inch (2.54 cm), the flaw was a 0.5 inch (1.27 cm) line heat source, the flaw depth was 0.1 inches (0.254 cm), 0.5 inches (1.27 cm), and 0.9 inches (2.286 cm), and the generation was 0.2 W. The flaw was modeled as a rectangular area which was rotated between 0 to 90 deg with respect to the z-axis. The flaw orientation results are shown in Figure 33.

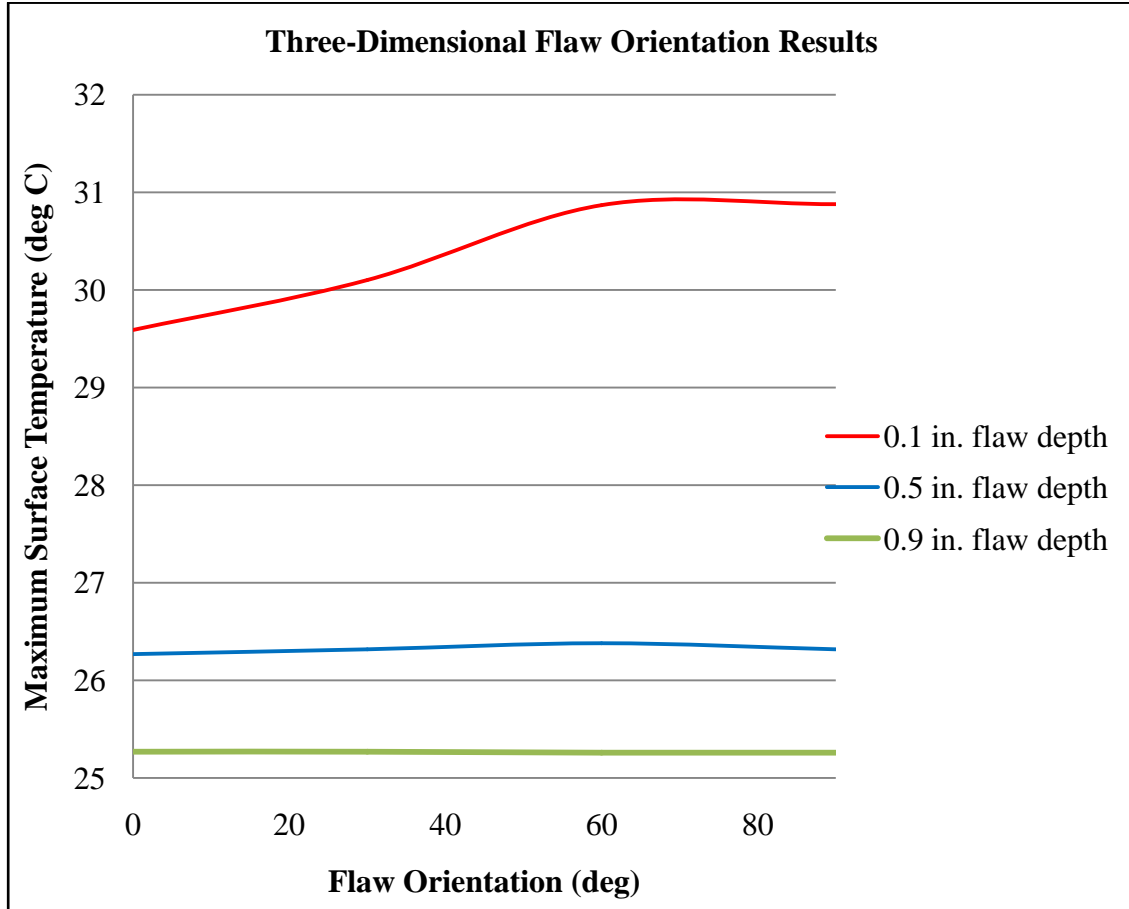


Figure 33. Maximum surface temperature results as a function of flaw orientation in the three-dimensional model

Flaw Size Dependent Solution for the Three-Dimensional Model

The fifth and final parameter investigated with the two-dimensional model was the flaw size. For this study, the specimen thickness was 1 inch, the flaw was a horizontal area heat source, the flaw depth was 0.1 inches (0.254 cm), 0.5 inches (1.27 cm), and 0.9 inches (2.286 cm), and the generation was 1 W. These flaw size results are shown in Figure 34.

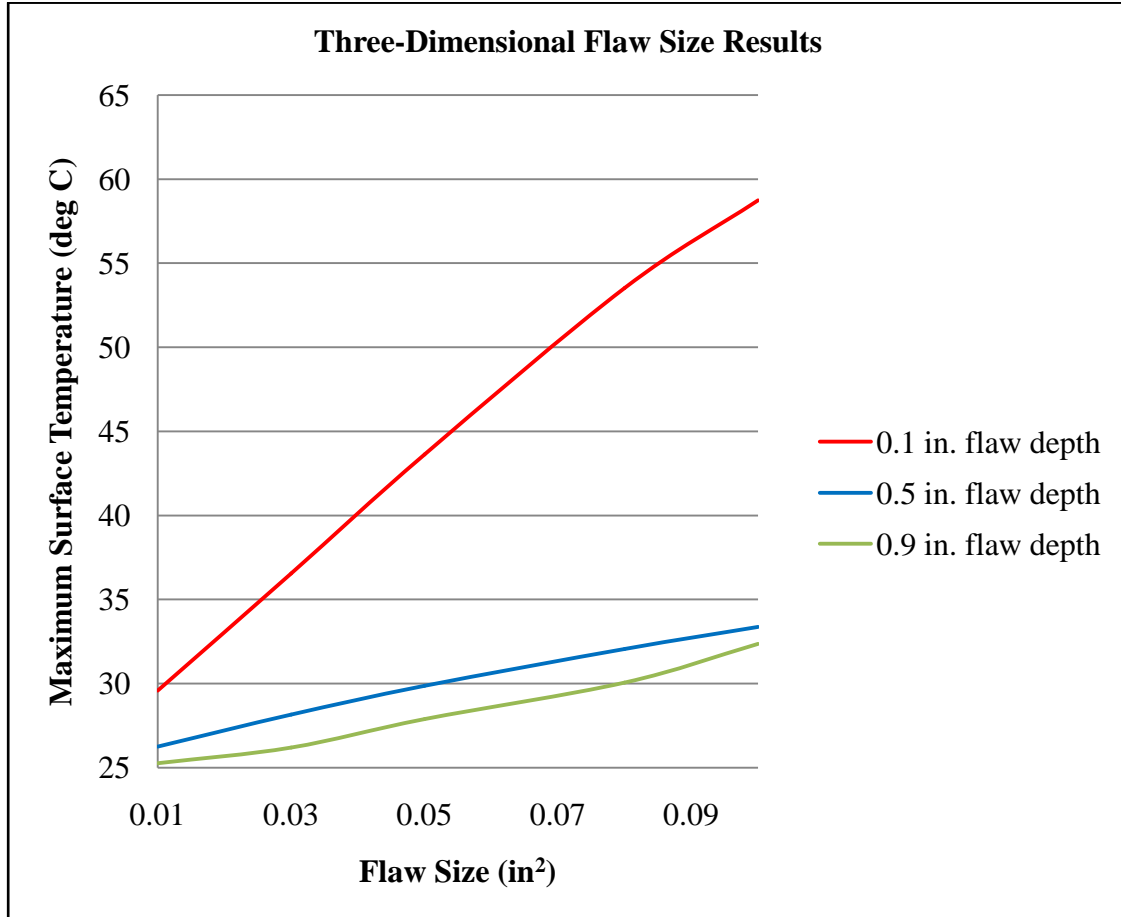


Figure 34. Maximum surface temperature results as a function of flaw orientation in the two-dimensional model

Discussion of Three-Dimensional Model Results

The three-dimensional model gave the most detailed and practical insight to the effects that flaw depth, generation amount, specimen thickness, flaw size, and flaw orientation can have on the observed surface temperature. The flaw can modeled as a point, line, or area source which allows for enough versatility to accurately model a wide variety of flaw sizes and types commonly seen in composites.

The time delay results given in Figure 30 can be easily obtained from the model for a specimen of any width and height, and the results for flaw depth can be directly interpolated.

The relationships between each of the other individual parameters and the observed maximum surface temperature shown in Figures 25-29 show the effect each of the flaw's thermal parameters, and can be applied to predict the influence changing any individual parameter will have on the vibrothermography test.

The maximum percent difference between the analytical and finite element three-dimensional model solutions was 12.3 % with an average percent difference of 4.4% (see APPENDIX D for a complete list for individual simulation results and their corresponding percent differences). These larger percent differences can again be attributed to the numerical errors which exist in each of the methods being multiplied and accumulating. Also, the analytical solution method required as many as 100 eigenvalues (actual number of eigenvalues required for solution convergence appeared to increase as a function of the specimen thickness), which contributed to larger analytical round off errors and increased computational times. The longest simulation with the three-dimensional analytical method took 34 minutes, compared to 8 minutes for the finite element method and less than 5 minutes for all of the two-dimensional and one-dimensional model simulations.

Two-Dimensional Combined Analysis

The two-dimensional combined analysis was performed to fully simulate an actual vibrothermography test. For this study, the other group's two-dimensional

mechanical model was applied in order to simulate the amount of heat generated in a given flaw. Next, this heat generation was input into the two-dimensional finite element model described in this study to determine the surface temperature results.

Two-Dimensional Combined Analysis Parameters:

The two-dimensional test was performed with the following parameters:

- Specimen width = 5 in. (12.7 cm)
- Specimen thickness = 1 in. (2.54 cm)
- Crack length = 0.5 in. (1.27 cm)
- Crack orientation = 0° with respect to horizontal
- Crack center location in x direction = 2.5 in. (6.35 cm) from left edge (half of the width)
- Crack center location in y direction = 0.5 in. (1.27 cm) from top edge (half of the thickness)
- Transducer location = on top surface, and 4.5 in. (11.43 cm) from left edge--2 in. (5.08 cm) offset from center
- Transducer frequency = 2000 Hz
- Transducer Amplitude = 1 mm

Two-Dimensional Combined Analysis Results

The mechanical model results, shown in Figure 35, show the heat generation amount as a function of time.

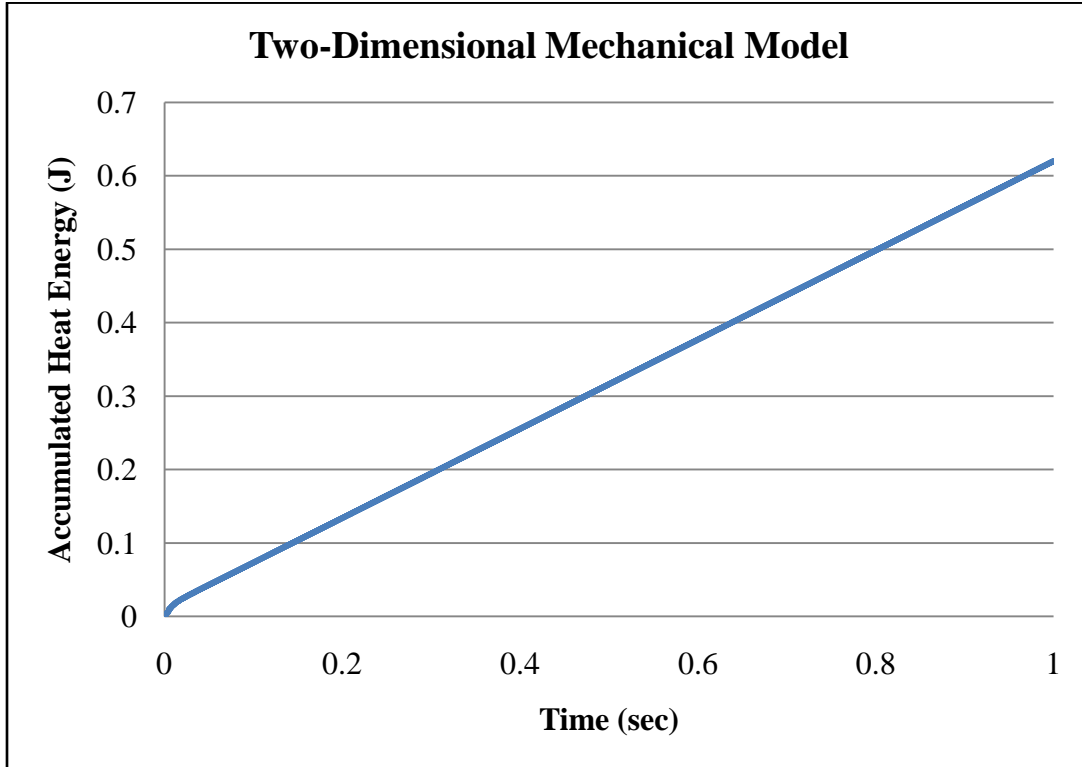


Figure 35. Heat generation results for the two-dimensional mechanical model

The average heat generation amount, which was determined by taking a numerical derivative of the accumulated joules given in Figure 35, was determined to be $63 \frac{W}{m}$. This value was then input into the two-dimensional finite element model.

A screenshot and surface temperature results for the two-dimensional model are given in Figure 36 and Figure 37 respectively.

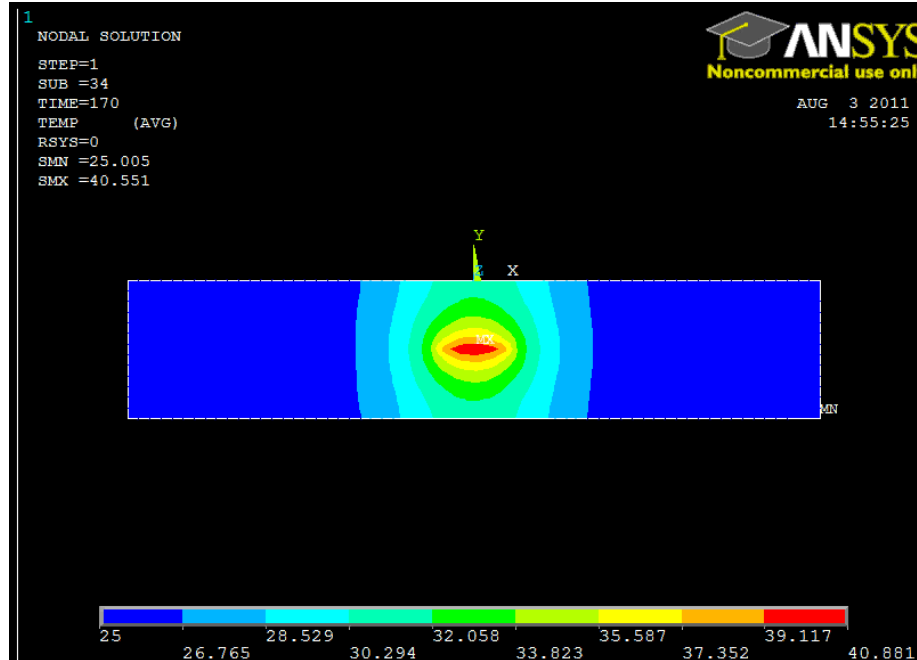


Figure 36. Screenshot of two-dimensional combined analysis

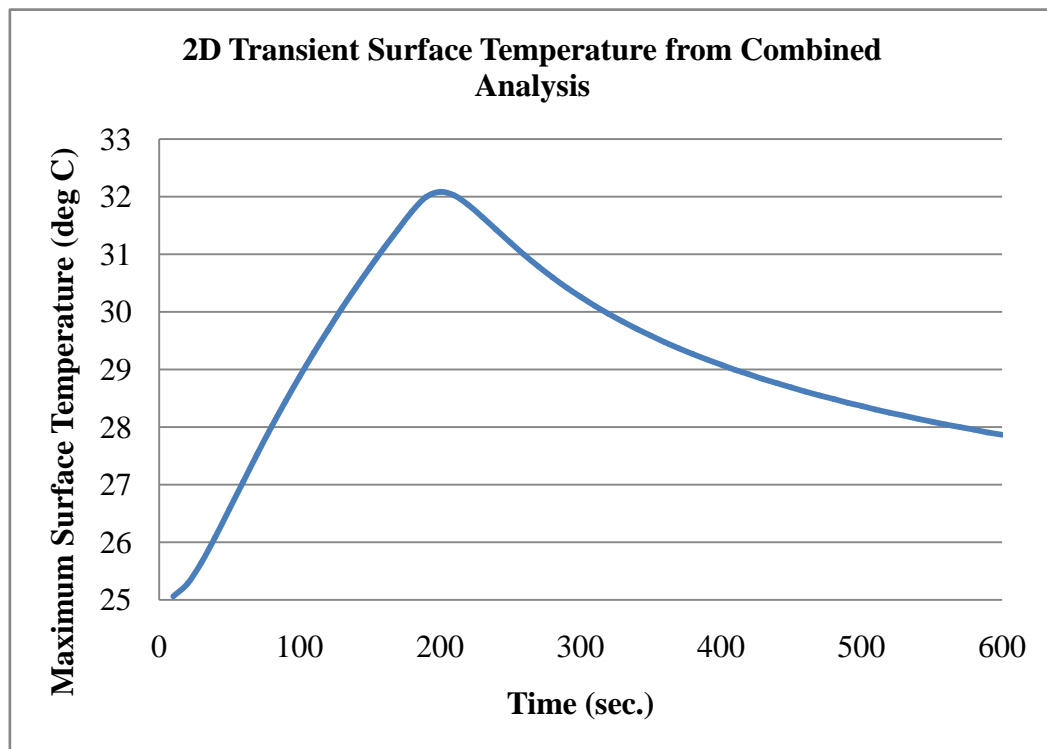


Figure 37. Two-dimensional combined analysis surface temperature result

Discussion of Two-Dimensional Model Results:

The results produced by the two-dimensional models appear to give reasonable maximum surface temperature results at 32.23 deg C. Resodyn is currently performing experiments on a similarly shaped specimen, and seem to get temperature results within the same order of magnitude (the maximum surface temperature in their experiments range from 27 deg C to 36 deg C depending on the experimental parameters). This same order of magnitude does show promise that the models at least appear to be able to show potential in predicting the vibrothermography phenomenon. The actual precision and accuracy of these combined models remains unknown until more experimental and modeling to work can be completed.

One important note during the two-dimensional analysis is that all of the heat generation data as well as input energy data were given in units of $\frac{W}{m}$. Therefore, in order to have accurate representation of the input energy, the actual energy being input energy, which can be calculated in terms of W, had to be scaled by an assumed material thickness in order to get the correct units, $\frac{W}{m}$.

Three-Dimensional Combined Analysis

Three-Dimensional Combined Analysis Parameters

The combined analysis was then repeated by applying the three-dimensional models with the following parameters:

- Specimen width = 5 in. (12.7 cm)
- Specimen length = 5 in. (12.7 cm)

- Specimen thickness = 1 in. (2.54 cm)
- Crack size = 0.25 sq. in. (1.6 sq. cm)
- Crack geometry = 0.5 in. (1.27 cm) x. 0.5 in. square
- Crack orientation = planar with respect to the x-z plane
- Crack center location in x direction = 2.5 in. (6.35 cm) with respect to left face
- Crack center location in y direction = 0.5 in. (1.27 cm) with respect to top face
- Crack center location in z direction = 2.5 in. (6.35 cm) with respect to front face
- Transducer location = On top surface, 4.5 in. (11.43 cm) from left face, 2.5 in. (6.35 cm) from front face
- Transducer frequency = 2000 Hz
- Transducer amplitude = 1 mm

Three-Dimensional Combined Analysis Results

The other group's mechanical model produced the heat generation results given in Figure 38.

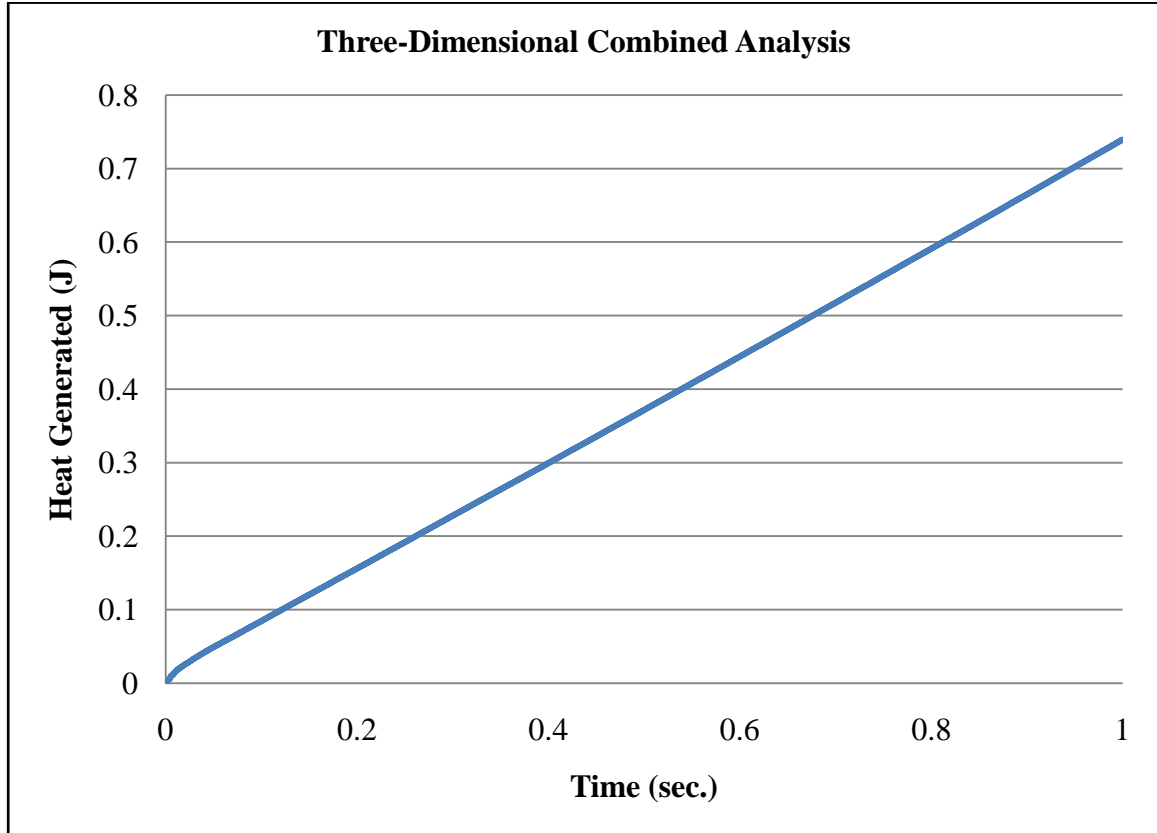


Figure 38. Heat generation results for the three-dimensional mechanical model

The numerical derivative was taken on the results in Figure 38 to produce an estimated heat generation of 0.73 W. This heat generation value was input into the three-dimensional finite element thermal model as shown in the screenshot in Figure 39 to give the surface temperature result shown in Figure 40.

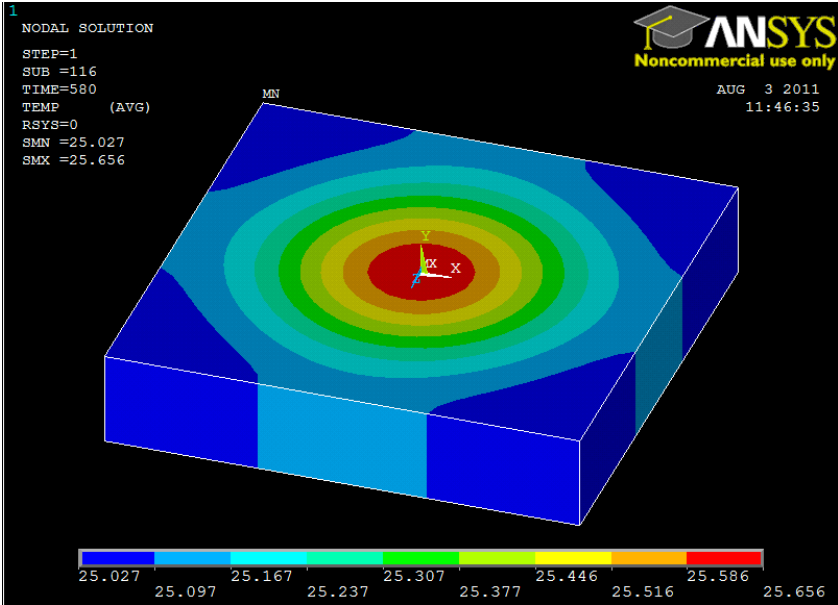


Figure 39. Screenshot of three-dimensional combined analysis

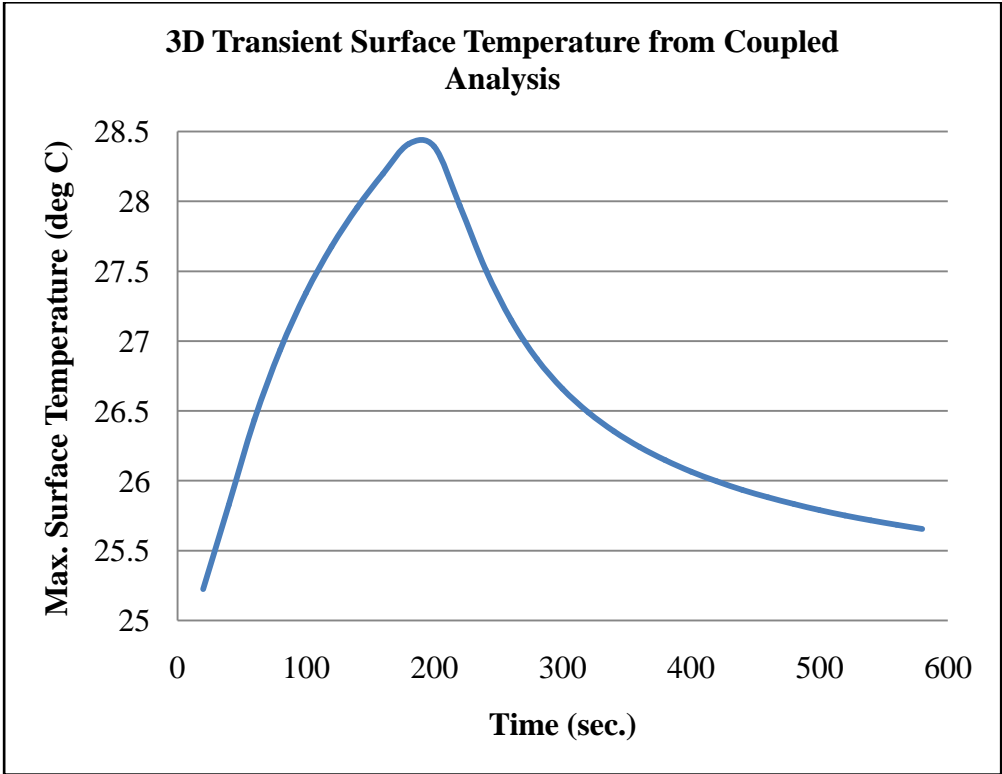


Figure 40. Three-dimensional combined analysis surface temperature result

Discussion of Three-Dimensional Model Results:

Once again the three-dimensional model produced reasonable surface temperature results, but more experimental and modeling joint work is again required to fully quantify the accuracy and precision of the combined three-dimensional vibrothermography simulation. Also, there is some error expected to be associated with the modeling as many parameters, such the coefficient of friction on a crack surface, still remain unknown. These tests merely provide a starting point for future work to be done in developing full vibrothermography simulations.

CHAPTER 7 – CONCLUSION

Results Summary

The finite element, finite difference, and analytical solution methods all produced consistent and very similar surface temperature results for all of the parameters investigated. Of the methods, it is believed that the analytical method will probably be the most accurate because it has the fewest induced numerical errors. However, the analytical method can only represent the flaw as a point heat source, and therefore is unable to take into account flaw size and orientation effects. Lastly, the analytical solution often requires many eigenvalues (actual number of eigenvalues required is a function of specimen thermal conductivity, specimen size, and desired precision), which is more computationally intensive than the finite element or finite difference models. The finite element and finite difference methods yielded nearly identical surface temperature results. However, because of available finite element software, the finite element models were much easier to develop and test. Also, one of the biggest advantages of the finite element method is the ability to simulate problems with multiple types of loads and boundary conditions, and will be the easiest method to use in order to produce coupled structural-thermal models to simulate the vibrothermography experiments completely as opposed to investigating only the heat transfer.

The parametric study performed quantifies the predicted affect of many thermal parameters which may influence the temperature results of a vibrothermography. The thermal affects of specimen thickness, flaw size, flaw generation, flaw depth, and flaw orientation have been thoroughly simulated and presented in Chapter 6. These results are

believed to be the only quantified parametric study currently available associated with the thermal effects in vibrothermography. The study shows that the generation amount, flaw size, and flaw depth all substantially affect surface temperature solutions, causing raises in surface temperature greater than 10 degrees C in some cases. The flaw orientation has almost no effect on the surface temperature solution, and the specimen thickness has very little effect on surface temperature results as long as the flaw depth is held constant.

Also, the other group at Montana State has begun developing mechanical finite element models designed to simulate the amount of heat produced as a function of flaw type, size, location, and excitation force, frequency, and location. Early results taken from trial runs of this group's mechanical models have been applied to the finite element thermal models developed in this study. These combined analyses simulations produce surface temperatures that appear reasonable when compared to typical vibrothermography experimental results. However, more modeling and experimentation is required in order to fully quantify the precision and accuracy of the joint models.

Future Work

The following list is a summary of the work that must continue in order to develop vibrothermography as a NDE technique for composite materials:

1. Continue to combine structural finite element models with the thermal models produced in this study to allow for simulations capable of predicating surface temperatures as a function of flaw geometry, specimen geometry, and excitation parameters during a vibrothermography test

2. Complete a series of vibrothermography tests to determine surface temperature results for a specimen with known material flaw sizes, types, locations, and orientations
3. Validate the structural and thermal models by simulating the vibrothermography tests from step 3 and comparing surface temperature results
4. Perform a parametric study to determine the expected effect of flaw size, flaw location, specimen size, and excitation parameters
5. Use models in vibrothermography testing as an aid to help determine optimal excitation parameters and interpret surface temperature results.

One important area of interest not covered in this study is the effect of orthotropic thermal conductivities. Composite materials often have very different thermal conductivities in the transverse and longitudinal directions (some fiberglass composites have a longitudinal thermal conductivity that is ten times as great as the transverse thermal conductivity). It will be important to determine whether or not these different conductivities will be destructive in interpreting results, or, if in some cases it is actually helpful in having more information to determine such parameters as flaw orientation.

The other group's recently completed structural models can be combined with the thermal models developed in this study to simulate the effects of a vibrothermography test in its entirety. These simulations will soon be able to be compared with experimental results at Resodyn. The comparisons will be extremely valuable as they will help aid in determining a few unknown model parameters (the main unknown being the coefficient

of friction between crack surfaces) as well as quantifying the precision and accuracy of the combined models. If the models do indeed prove to be able to accurately and consistently predict vibrothermography results, the models could then be applied to aid in the development of optimal vibrothermography testing procedures as well as a correlation between temperature results and flaws that exist within the specimen.

REFERENCES

- Huge Gas Tank Collapses. (1898, December 14). *New York Times*.
- Anderson, W. (1969). An engineer views brittle fracture history. *Boieng Report*.
- Broek, D. (1986). *Elementary Engineering Fracture Mechanics, 4th revised edition*. Boston: Kluwer Academic Publishers.
- Chapra, S. C. (2008). *Applied Numerical Methods with MATLAB, 2nd Edition*. New York: McGraw-Hill Companies, Inc.
- Cook, R. D., Malkus, D. S., Plesha, M. E., & Witt, R. J. (2002). *Concepts and Applications of Finite Element Analysis 4th edition*. John Wiley and Sons Inc.
- Cortz, L. (1995). *Nondestructive Testing*. Milwaukee: ASM International.
- Favro, L. D., Han, X., Ouyang, Z., Sun, G., Sui, H., & Thomas, R. L. (2000). Infrared imaging of defects heated by a sonic pulse. *Rev. of Sci. Inst.*, 2418-2421.
- Griffith, A. A. (1920). The phenomena of rupture and flow in solids. *Philosophical Transactions of the Royal Society of London*.
- Haberman, R. (2004). *Applied Partial Differential Equations with Fourier Series and Boundary Value Problems 4th edition*. New Jersey: Pearson Education Inc.
- Henneke II, E. G., Reifsnider, K. L., & Stinchcomb, W. W. (1979). Thermography - An NDI Method for Damage Detection. *Metals*, 11-15.
- Huang, Y. (1982). Shearography: A new optical method for strain measurement and non-destructive testing. *Optical Engineering*, 391-395.
- Hung, Y. Y. (1996). Shearography for non-destructive evaluation of composite structures. *Optics and lasers in engineering*, 161-182.
- Mabrouki, F., Thomas, M., Genest, M., & Fahr, A. (2010). Numerical modeling of vibrothermography based on plastic deformation. *NDT&E International*, 476-483.
- Mian, A., Newaz, G., Han, X., Mahmood, T., & Saha, C. (2004). Response of sub-surface fatigue damage under sonic load - a computational study. *Composite Science and Technology*, 1115-1122.
- Ozisik, M. N. (1993). *Heat Conduction, 2nd Edition*. New York: John Wiley and Sons, Inc.

APPENDICES

APPENDIX A

FINITE DIFFERENCE METHOD MATLAB FILES

File name: finitedifference.m

```

% Tony Trudnowski
%
% Date created: 1/4/2011
% Date revised: 1/10/2011
%
%% Problem Statement:
% Determine the heat conduction through a one dimensional
specimen with % a user input thickness (ranging from 0.1 in
to 2.0 in thick), and a
% user-defined flaw location and generation amount

%
%% List of Variables:
% k      = thermal conductivity of the specimen
% row    = density of the specimen (kg/m^3)
% C      = specific heat of the specimen
% alpha  = emissivity of the specimen
% time   = time variable
% t      = thickness of the specimen
% depth  = depth of flaw
% gen    = heat generated at the flaw
% T      = temperature matrix of the specimen
%
%           Note: Temp(i,j) refers to the temperature
of the specimen
%           at depth x(i) and time time(j).
% A      = coefficient matrix
% d      = solution vector
% h      = convective heat transfer coefficient
% gen    = heat flux generated at the flaw

%%%%%%%%%%%%%%%%%%%%%%%%%%%%%%%%%%%%%%%%%%%%%%%%%%%%%%%%%%%%%%%%%%%%%%%%
%%%%%%%%%%%%%%%%%%%%%%%%%%%%%%%%%%%%%%%%%%%%%%%%%%%%%%%%%%%%%%%%%%%%%%%%
% Clear any currently saved variables and displays
clear all;
close all;
clc;

%% Givens
% Material properties and convection properties
k = 1.34; % thermal conductivity
(W/m*C)
C = 800; % specific heat
(J/kg*C)

```

```

T_amb = 25; % ambient air
temperature (deg C)
row = 1850; % density of specimen
(kg/m^3)
h = 10; % convective heat
transfer coefficient (W/m^2*K)
gen = 500; % W
alpha = k/(row*C);
gentime = 5*60;

thick = 1*2.54/100;
depth = 0.5;

timeend = 10*60;
timediv = 50000;
delttime = timeend/(timediv-1);

%% Create node spacing
xdiv = 101;
gennode = round(xdiv*depth)+1;

T = zeros(xdiv,timediv);
delx = thick/(xdiv-1);
r = alpha*delttime/(delx^2)

%% Apply initial condition
time = zeros(timediv,1);
fori = 2:timediv
    time(i) = time(i-1)+delttime;
end
T(:,1) = 25;

SurfaceTemp=zeros(timediv,1);
SurfaceTemp(1)=25;
for j = 2:timediv
    [A,d] =
crank_nicolson(alpha,delttime,delx,k,h,T,gen,gennode,time(j)
,gentime,xdiv,j,T_amb);
    T(:,j) = A\d;
    SurfaceTemp(j)=T(1,j);
end

plot(time,SurfaceTemp)

```

```
Answer = max(SurfaceTemp)

check = 1;
for i = 1:length(time)
    if time(i) >= 20*check
        time2(check)=time(i);
        Tsurf2(check) = SurfaceTemp(i);
        check = check +1;
    end
end

time2 = time2';
Tsurf2 = Tsurf2';
```

APPENDIX B

ANALYTICAL METHOD MATLAB FILES

One-Dimensional Model

File name: Analytical1D.m

```

% Tony Trudnowski
%
% One-Dimensional analytical top surface temperature vs
time
%
% Determines surface temperature for a one-dimensional
model with user
% input thickness, generation amount, and generation
location

%% Re-set
clear all; close all; clc;

%% Givens

% Material parameters
L = 1*2.54/100;           % units of m
a = 0.9*L;               % Crack depth in units of m
gen = 500;               % units of W
gentime = 5*60;         % amount of time heat is generated

% Problem parameters
row = 1850;              % kg/m^3
C = 800;                 % J/kg*K
t = 0:20:60*10;         % array of time values
h = 10;                  % Convective heat transfer
coefficient (W/m^2K)
k = 1.34;                % Conduction coefficient (W/mK)
H = h/k;
alpha = k/(row*C);      % thermal diffusivity
%
%
%%%%%%%%%%%%%%%%%%%%%%%%%%%%%%%%%%%%%%%%%%%%%%%%%%%%%%%%%%%%%%%%%%%%%%%%
%%%%%%%%%%%%%%%%%%%%%%%%%%%%%%%%%%%%%%%%%%%%%%%%%%%%%%%%%%%%%%%%%%%%%%%%
%

%% Step 1: Determine first four eigenvalues
B(1),B(2),B(3),B(4)
% From equation:  $\tan(BL) = (2*H*L^2)/(BL^2 - (HL)^2)$ 
% Determine graphically, MATLAB finds intersections

```

```

B = eigenfinder2(L,h,k);

%% Step 2 Determine the values of each norm

% Run created function Norm (for details see the norm
function .m file also
% attached)
Norm = normCalc(B,h,k,L);

%% Step 3 PLUG IN VALUES AND SOLVE
SurfaceTemp = zeros(1,length(t));

for j = 1:length(t)
    Theta = 0;
    if t(j) <= gentime
        for i = 1:length(B)
            X1 = XSolve(B(i),0,h,k);
            X2 = XSolve(B(i),a,h,k);
            Theta1 = X1*X2*gen*(1-exp(-alpha*B(i)^2*t(j)))
/ (k*Norm(i)*B(i)^2);
            Theta = Theta + Theta1;
        end
    else
        t2 = t(j) - gentime;
        for i = 1:length(B)
            X1 = XSolve(B(i),0,h,k);
            X2 = XSolve(B(i),a,h,k);
            Theta1 = gen/(Norm(i)*k*B(i)^2)*X1*X2*exp(-
alpha*B(i)^2*t2)*(1-exp(-alpha*B(i)^2*gentime));
            Theta = Theta + Theta1;
        end
    end
    SurfaceTemp(j) = Theta + 25;
end
figure
plot(t,SurfaceTemp)
Answer = max(SurfaceTemp)

SurfaceTemp = SurfaceTemp';
t = t'

```

Two-Dimensional Model

File name: Analytical2D.m

```

% Tony Trudnowski
%
% Two-Dimensional analytical top surface temperature vs
time

%% Re-set
clear all; close all;

%% Givens
% Material parameters
Wth = 5*2.54/100;           % width in units of m (x-
direction)
Ht = 1*2.54/100;          % height in units of m (y-
direction)
a = 0.5*Wth;               % Crack x coordinate location
b = 0.5*Ht;                % Crack y coordinate location
gen = 50;                  % point generation amount in W
gentime = 5*60;           % generation time in sec

%% Problem parameters
row = 1850;                % kg/m^3
C = 800;                   % J/kg*K
t = 0:5:60*10;             % array of time values
h = 10;                    % Convective heat transfer
coefficient (W/m^2K)
k = 1.34;                  % Conduction coefficient (W/mK)
H = h/k;
alpha = k/(row*C);        % thermal diffusivity

%% STEP 1: DETERMINE EIGENVALUES
Beta = eigenfinder2(Wth,h,k);
Gamma = eigenfinder2(Ht,h,k);

%% STEP 2: DETERMINE NORMS
NormX = normCalc(Beta,h,k,Wth);
NormY = normCalc(Gamma,h,k,Ht);

%% STEP 3: SOLVE TEMPERATURE AT SURFACE NODE
TopSurfaceTemp = zeros(1,length(t));

```

```

for j = 1:length(t)
    Theta = 0;
    if t(j) <= gentime
    for m = 1:length(Beta)
    for n = 1:length(Gamma)
        X1 = Xsolve(Beta(m), a, h, k);
        X2 = Xsolve(Beta(m), a, h, k);
        Y1 = Xsolve(Gamma(n), 0, h, k);
        Y2 = Xsolve(Gamma(n), b, h, k);
    eigen = Beta(m)^2 + Gamma(n)^2;
        Thetal =
    (1/(k*eigen*NormX(m)*NormY(n)))*gen*X1*X2*Y1*Y2*(1-exp(-
alpha*eigen*t(j)));
        Theta = Thetal + Theta;
    end
    end
    else
        t2 = t(j) - gentime;
    for m = 1:length(Beta)
    for n = 1:length(Gamma)
        X1 = Xsolve(Beta(m), a, h, k);
        X2 = Xsolve(Beta(m), a, h, k);
        Y1 = Xsolve(Gamma(n), 0, h, k);
        Y2 = Xsolve(Gamma(n), b, h, k);
    eigen = Beta(m)^2 + Gamma(n)^2;
        Thetal = exp(-
alpha*eigen*t2)*X1*Y1*gen*X2*Y2*(1-exp(-
alpha*eigen*gentime))/(k*eigen*NormX(m)*NormY(n));
        Theta = Theta + Thetal;
    end
    end
    end

TopSurfaceTemp(j) = Theta + 25;
end
figure
plot(t, TopSurfaceTemp)

t = t';
TopSurfaceTemp = TopSurfaceTemp';

Answer = max(TopSurfaceTemp)

```

Three-Dimensional Model

File name: Analytical3D.m

```

% Tony Trudnowski
%
% Three-Dimensional analytical top surface temperature vs
time

%% clear previous work
clear all; close all; clc;
tstart = tic;
%% Givens
% Material parameters
Wth = 5*2.54/100;           % width in units of m (x-
direction)
Ht = 1*2.54/100;          % height in units of m (y-
direction)
Lth = 1*2.54/100;         % length in units of m (z-
direction)
a = 0.5*Wth;              % Crack x coordinate location
b = 0.5*Ht;               % Crack y coordinate location
c = 0.5*Lth;              % Crack z coordinate location
x = a;                    % x loc of temperature output
y = 0;                    % y loc of temperature output
z = b;                    % z loc of temperature output
gen = 1;                  % point generation amount in W
gentime = 60*60;         % generation time in sec

%% Problem parameters
row = 1850;               % kg/m^3
C = 800;                  % J/kg*K
t = 0:5:60*5;            % array of time values
h = 10;                   % Convective heat transfer
coefficient (W/m^2K)
k = 1.34;                 % Conduction coefficient (W/mK)
H = h/k;
alpha = k/(row*C);        % thermal diffusivity

%% STEP 1: Determine eigenvalues
Beta = eigenfinder2(Wth,h,k);
Gamma = eigenfinder2(Ht,h,k);
Eta = eigenfinder2(Lth,h,k);
%% STEP 2: Determine Norms

```

```

NormX = normCalc(Beta,h,k,Wth);
NormY = normCalc(Gamma,h,k,Ht);
NormZ = normCalc(Eta,h,k,Lth);

%% STEP 3: Solve temperature at top surface
SurfaceTemp = zeros(1,length(t));
check = zeros(1,length(t));
for j = 1:length(t)
    Theta = 0;
    for m = 1:length(Beta)
    for n = 1:length(Gamma)
    for p = 1:length(Eta)
        X1 = Xsolve(Beta(m),0.5*Wth,h,k);    % node
of interest x loc
        X2 = Xsolve(Beta(m),a,h,k);        % crack
x loc
        Y1 = Xsolve(Gamma(n),0,h,k);    % node of
interest y loc
        Y2 = Xsolve(Gamma(n),b,h,k);    % crack
y loc
        Z1 = Xsolve(Eta(p),0.5*Lth,h,k);    % node
of interest z loc
        Z2 = Xsolve(Eta(p),c,h,k);    % crack z
loc
        eigen = Beta(m)^2 + Gamma(n)^2 + Eta(p)^2;
        check(j) = check(j) + eigen*alpha*t(j);

%Theta1 = (gen/(k*eigen))*X1*X2*Y1*Y2*Z1*Z2*NormInvX(m)^-
1*NormInvY(n)^-1*NormInvZ(p)^-1*(1-exp(-alpha*eigen*t(j)));
%Theta1 =
gen*X1*X2*Y1*Y2*Z1*Z2/k/eigen/NormX(m)/NormY(n)/NormZ(p)*(1
-exp(-alpha*eigen*t(j)));
        Theta1 = (1-exp(-
alpha*eigen*t(j)))*gen*X1*X2*Y1*Y2*Z1*Z2/k/eigen/NormX(m)/N
ormY(n)/NormZ(p);
        Theta = Theta + Theta1;
    end
    end
    end
    SurfaceTemp(j) = Theta + 25;
end

%% STEP 4: Display solution
figure

```

```
plot(t, SurfaceTemp)
telapsed = toc(tstart)/60
```

APPENDIX C

FINITE ELEMENT METHOD ANSYS INPUT FILES

One-Dimensional Model

File name: 1d_heat_transfer

```
FINISH
/CLEAR
/FILNAME, 1DHEATGEN
/TITLE, 1D HEAT TRANSFER WITH GENERATION AT A CRACK
/UNITS,MKS
```

```
! DATE CREATED: JANUARY 3, 2011
! DATE REVISED: MARCH 2, 2011
```

```
/COM, TONY TRUDNOWSKI
```

```
/COM,***PREPROCESSOR***
/PREP7
```

```
/COM,***DEFINE USER INPUT PARAMETERS***
THICK = 1*2.54/100                ! thickness of the material
DEPTH_RATIO = 0.5                ! depth of the crack as a percentage of the
total thickness
TIME_END = 20*60                 ! how long to evaluate the thermal effect (sec)
TIME_INCR = 5                    ! time between load substeps (i.e. display
temp distribution every TIME_INR time value)
T_AMB = 25                       ! ambient temperature in deg C
gen = 500
```

```
/COM,***MATERIAL PARAMETERS***
H = 10                           ! convective heat transfer coefficient
DEPTH = DEPTH_RATIO*THICK        ! depth of the crack
XDIV = 200                       ! number of desired divisions for the model
DELX = THICK/(XDIV-1)
```

```
/COM,***CREATE TABLE OF HEAT GENERATION VS. TIME***
*DIM,HEATGEN,TABLE,9,1,1,TIME,
HEATGEN(1) = 0, gen, gen, gen, gen, gen, 0, 0, 0
HEATGEN(1,0) = 1E-6, 1E-5*60, 2*60, 3*60, 4*60, 5*60, 5.1*60, 7*60, 8*60
! This is used to create a table of heat gen vs. time values for time-dependent heat
generation cases
```

```
/COM,***DEFINE ELEMENT TYPE***
```

```
ET,1,LINK34          ! convection element
R,1,1
ET,2,LINK32          ! conduction element
```

```
/COM,***MATERIAL PROPERTIES***
```

```
MP,KXX,1,1.34
MP,DENS,1,1850
MP,C,1,800
MP,HF,1,H
```

```
/COM,***BUILD GEOMETRY***
```

```
K,1,0,0
K,2,0,-DEPTH
K,3,0,-THICK
L,1,2
L,2,3
```

```
/COM,***MESH GEOMETRY***
```

```
LESIZE,1,DELX
LESIZE,2,DELX
TYPE,2
LMESH,ALL
```

```
/COM,***CREATE CONVECTION ELEMENTS AT THE END***
```

```
NKPT,XDIV+3,1
NKPT,XDIV+4,3
TYPE,1
E,XDIV+3,1
E,XDIV+4,XDIV
```

```
/COM,***SOLUTION***
```

```
FINISH
/SOLU
/COM,***DEFINE ANALYSIS TYPE***
ANTYPE,TRANSIENT,NEW
TIME,TIME_END
DELTIM,TIME_INCR
OUTRES,,4
```

```
/COM,***INITIAL CONDITIONS***
```

```
TUNIF,25
TREF,25
TIME,TIME_END
```

```
/COM,***BOUDARY CONDITIONS***  
D,XDIV+3,TEMP,T_AMB  
D,XDIV+4,TEMP,T_AMB  
  
/COM,***APPLY GENERATION TERM***  
F,2,HEAT,%HEATGEN%,,  
!F,2,HEAT,gen,,  
  
/COM,***SOLVE***  
ALLSEL  
SOLVE  
FINISH  
  
/COM,***POST-PROCESSOR***  
/POST26  
NSOL,2,1,TEMP,,TOPSURFACETEMP  
PLVAR,2  
PRVAR,2
```

Two-Dimensional Models

File name: 2D_heat_transfer

This model was used for cases in which heat generation was modeled as a point source

```
FINISH  
/CLEAR  
/FILENAME, 1DHEATGEN  
/TITLE, 2D HEAT TRANSFER WITH GENERATION AT A CRACK  
/UNITS,MKS  
  
! DATE CREATED: JANUARY 13, 2011  
! DATE REVISED: JANUARY 24, 2011  
  
/COM, TONY TRUDNOWSKI  
  
/COM,***PREPROCESSOR***  
/PREP7
```

/COM,***PARAMETERS***

WIDTH = 5*2.54/100

! these lines of code if total heat generation is given

GENERATION = 50

THICK = 2*2.54/100

DEPTH = 0.9

! crack depth: range from 1% - 90% of
thickness

CRACKDEPTH = DEPTH*THICK

CRACKXLOC = 0

H = 10

TIMEEND = 15*60

! time to end transient analysis

TIMEINCR = 5

! time increment between load steps

/COM,***DEFINE ELEMENT TYPE***

ET,1,PLANE55

! 4-node quad element

/COM,***MATERIAL PROPERTIES***

MP,KXX,1,1.34

! thermal conductivity

MP,DENS,1,1850

! density

MP,C,1,800

! specific heat capacity

MP,HF,1,H

! convective heat transfer coefficient

/COM,***BUILD GEOMETRY***

/COM,***KEYPOINTS***

K,1,CRACKXLOC,-CRACKDEPTH

K,2,-WIDTH/2,0

K,3,CRACKXLOC,0

K,4, WIDTH/2,0

K,5,-WIDTH/2,-CRACKDEPTH

K,6,WIDTH/2,-CRACKDEPTH

K,7,-WIDTH/2,-THICK

K,8,CRACKXLOC,-THICK

K,9,WIDTH/2,-THICK

/COM,***LINES***

L,2,3

L,3,4

L,2,5

L,3,1

L,4,6

L,5,1

L,1,6

L,5,7

L,1,8

L,6,9

L,7,8

L,8,9

/COM,***AREAS***

AL,1,4,6,3

AL,2,5,7,4

AL,6,9,11,8

AL,7,10,12,9

/COM,***MESH AREAS***

SIZEFACTOR = 50

FACTORX = WIDTH/(CRACKXLOC+(WIDTH/2))

LESIZE,6,WIDTH/SIZEFACTOR,,0.1

LESIZE,7,WIDTH/SIZEFACTOR,,10

FACTORY = DEPTH/THICK

LESIZE,4,WIDTH/SIZEFACTOR,,0.5

LESIZE,9,WIDTH/SIZEFACTOR,,2

ESIZE,WIDTH/SIZEFACTOR

AMESH,ALL

/COM,***SOLUTION***

/SOLU

/COM,***ANALYSIS SETTINGS***

ANTYPE,TRANSIENT,NEW

TIME,TIMEEND

DELTIM,TIMEINCR

OUTRES,,4

/COM,***INITIAL CONDITIONS***

TUNIF,25

TREF,25

/COM,***BOUNDARY CONDITIONS

NSEL,S,LOC,Y,0

NSEL,A,LOC,Y,-THICK

NSEL,A,LOC,X,-WIDTH/2

NSEL,A,LOC,X,WIDTH/2

SF,ALL,CONV,H,25

/COM,***CREATE HEAT GENERATION TABLE***

*DIM,HEATGEN,TABLE,10,1,1,TIME,

```

HEATGEN(1) = 0,
GENERATION,GENERATION,GENERATION,GENERATION,GENERATION,GEN
ERATION,0, 0, 0
HEATGEN(1,0) = 1E-6,1E-5, 1*60, 2*60, 3*60, 4*60, 5*60, 5.1*60,
7*60, 8*60

```

```

/COM,***APPLY HEAT GENERATION AT THE CRACK POINT**
KSEL,S,,1
NSLK,S
F,ALL,HEAT,%HEATGEN%

```

```

/COM,***SOLVE***
ALLSEL
SOLVE
KSEL,S,,3
NSLK,S
NLIST

```

```

/COM,***POST-PROCESSOR***
ALLSEL
/POST26
NSOL,2,2,TEMP,,TOPSURFACETEMP
PRVAR,2
PLVAR,2

```

File name: 2D_heat_transfer_linegeneration

This file was applied when the generation was modeled as a line source

```

FINISH
/CLEAR
/FILNAME, 1DHEATGEN
/TITLE, 1D HEAT TRANSFER WITH GENERATION AT A CRACK
/UNITS,MKS
! DATE CREATED: JANUARY 13, 2011
! DATE REVISED: JANUARY 24, 2011
/COM, TONY TRUDNOWSKI

/COM,***PREPROCESSOR***
/REP7

```

```

/COM,***PARAMETERS***
LENGTH = 5*2.54/100                                ! specimen thickness can
range from 0.1 in to 2.0 in
THICK = 1*2.54/100
DEPTH = 0.9                                         ! crack depth: range from 1% - 90% of
thickness
CRACKDEPTH = DEPTH*THICK
CRACKXLOC = 0
CRACKLENGTH = 1*2.54/100
CRACKANGLE = 0*3.14159/180
CRACKSTARTX = CRACKXLOC - ((CRACKLENGTH/2)*COS(CRACKANGLE))
CRACKSTARTY = -CRACKDEPTH - ((CRACKLENGTH/2)*SIN(CRACKANGLE))
CRACKENDX = CRACKXLOC + ((CRACKLENGTH/2)*COS(CRACKANGLE))
CRACKENDY = -CRACKDEPTH + ((CRACKLENGTH/2)*SIN(CRACKANGLE))
GENERATION = 100                                    ! total watts produced
H = 10
TIMEEND = 10*60                                    ! time to end transient analysis
TIMEINCR = 5                                        ! time increment between load steps

/COM,***DEFINE ELEMENT TYPE***
ET,1,PLANE55                                        ! 4-node quad element

/COM,***MATERIAL PROPERTIES***
MP,KXX,1,1.34                                       ! thermal conductivity
MP,DENS,1,1850                                       ! density
MP,C,1,800                                           ! specific heat capacity
MP,HF,1,H                                           ! convective heat transfer coefficient

/COM,***BUILD GEOMETRY***
K, 1, -LENGTH/2, 0                                    ! keypoints around outer perimeter
K, 2, -LENGTH/2, -THICK
K, 3, LENGTH/2, -THICK
K, 4, LENGTH/2, 0
K, 5, CRACKSTARTX, CRACKSTARTY                       ! keypoints at crack tips
K, 6, CRACKENDX, CRACKENDY
K, 7, CRACKSTARTX-(CRACKLENGTH/2), 0                 ! keypoints for a better mesh
around crack tip
K, 8, CRACKENDX+(CRACKLENGTH/2), 0
K, 9, CRACKSTARTX-(CRACKLENGTH/2), -THICK
K,10, CRACKENDX+(CRACKLENGTH/2), -THICK
K,11, CRACKSTARTX-(CRACKLENGTH/2), -CRACKDEPTH -
(CRACKLENGTH*SIN(CRACKANGLE))
K,12, CRACKENDX+(CRACKLENGTH/2), -CRACKDEPTH +
(CRACKLENGTH*SIN(CRACKANGLE))

```

```

L,5,6
L,11,5
L,6,12
L,1,7
L,7,8
L,8,4
L,2,9
L,9,10
L,10,3
L,1,2
L,4,3
L,7,11
L,11,9
L,8,12
L,12,10
AL,10,4,12,13,7
AL,5,14,3,1,2,12
AL,2,1,3,15,8,13
AL,14,6,11,9,15

! lines connecting all of the keypoints

! areas generated form lines

/COM,***MESH AREAS***
FACTOR=25
ESIZE,2*THICK/FACTOR
LESIZE,1,THICK/FACTOR
AMESH,ALL
FINISH
/COM,***SOLUTION***
/SOLU

/COM,***ANALYSIS SETTINGS***
ANTYPE,TRANSIENT,NEW
TIME,TIMEEND
DELTIM,TIMEINCR
OUTRES,,2

/COM,***INITIAL CONDITIONS***
TUNIF,25
TREF,25

/COM,***BOUNDARY CONDITIONS
NSEL,S,LOC,Y,0
NSEL,A,LOC,Y,-THICK
NSEL,A,LOC,X,-LENGTH/2
NSEL,A,LOC,X,LENGTH/2

```

```

SF,ALL,CONV,H,25
LSEL,S,,1
NSLL,S,1
*GET,NODES,NODE,,COUNT

/COM,***CREATE HEAT GENERATION TABLE***
*DIM,HEATGEN,TABLE,10,1,1,TIME,
HEATGEN(1) = 0,
GENERATION/NODES,GENERATION/NODES,GENERATION/NODES,GENERATI
ON/NODES,GENERATION/NODES,GENERATION/NODES, 0, 0, 0
HEATGEN(1,0) = 1E-6, 1E-5, 4.73E-02*60, 4.74E-02*60, 3*60,
4*60, 5*60, 5.1*60,7*60, 8*60

/COM,***APPLY HEAT GENERATION AT THE CRACK
F,ALL,HEAT,%HEATGEN%

/COM,***SOLVE***
ALLSEL
SOLVE

/COM,***POST-PROCESSOR***
/POST1
nsl,s,loc,x,0
nsl,r,loc,y,0
nlist
allse
/POST26
allsel
NSOL,2,344,TEMP,,TOPSURFACE
PRVAR,2
PLVAR,2

```

Three-Dimensional Models

File name: 3d_heat_transfer

This file was applied when the generation was modeled as a point source

```

FINISH
/CLEAR
/FILNAME, 3DHEATGEN
/TITLE, 3D HEAT TRANSFER WITH GENERATION AT A CRACK
/UNITS,MKS

```

```

! DATE CREATED: FEBRUARY 17, 2011
! DATE REVISED: FEBRUARY 17, 2011
/COM,***PREPROCESSOR***
/PREP7

/COM,***DEFINE PARAMETERS***
  /COM,***PROPERTY PARAMETERS***
    H = 10
    GEN = 1

  /COM,*** GEOMETRY PARAMETERS***
    WIDTH = 5*2.54/100      ! specimen width in m (2.54/100 term converts from
in. to m) in x direction
    THICK = 1*2.54/100     ! specimen thickness in Z direction
    LENGTH = 5*2.54/100   ! specimen length in Y direction
    DEPTRATIO = 0.1
    DEPTH = DEPTRATIO*THICK

  /COM,***CRACK LOCATION***
    CRACKXLOC = 0
    CRACKYLOC = -DEPTH
    CRACKZLOC = 0

/COM,***BUILD THE MODEL***
/COM,***DEFINE ELEMENT TYPE***
ET,1,SOLID70
ET,2,PLANE55

/COM,***DEFINE MATERIAL PROPERTIES***
MP,KXX,1,1.34              ! thermal conductivity
MP,DENS,1,1850            ! density
MP,C,1,800                ! specific heat capacity
MP,HF,1,H                 ! convective heat transfer coefficient

/COM,***DEFINE MODEL GEOMETRY***
  /COM,***DEFINE KEYPOINTS***
  /COM,***CRACK LOCATION KEYPOINT***
  K, 1, CRACKXLOC, CRACKYLOC, CRACKZLOC
  /COM,***TOP SURFACE KEYPOINTS***
  K, 2,-WIDTH/2, 0, LENGTH/2
  K, 3, WIDTH/2, 0, LENGTH/2
  K, 4, WIDTH/2, 0,-LENGTH/2
  K, 5,-WIDTH/2, 0,-LENGTH/2
  K, 6, CRACKXLOC,0, CRACKZLOC

```

K, 7, -WIDTH/2, 0, CRACKZLOC
 K, 8, CRACKXLOC,0,-LENGTH/2
 K, 9, CRACKXLOC,0, LENGTH/2
 K,10, WIDTH/2, 0, CRACKZLOC

/COM,***BOTTOM SURFACE KEYPOINTS***

K,11,-WIDTH/2, -THICK,-LENGTH/2
 K,12, WIDTH/2, -THICK,-LENGTH/2
 K,13, WIDTH/2, -THICK, LENGTH/2
 K,14,-WIDTH/2, -THICK, LENGTH/2
 K,15, CRACKXLOC,-THICK, CRACKZLOC
 K,16, CRACKXLOC,-THICK,-LENGTH/2
 K,17, WIDTH/2, -THICK, CRACKZLOC
 K,18, CRACKXLOC,-THICK, LENGTH/2
 K,19,-WIDTH/2, -THICK, CRACKZLOC

/COM,***LEFT SURFACE KEYPOINTS***

K,20,-WIDTH/2,CRACKYLOC,-LENGTH/2
 K,21,-WIDTH/2,CRACKYLOC,CRACKZLOC
 K,22,-WIDTH/2,CRACKYLOC,LENGTH/2

/COM,***RIGHT SURFACE KEYPOINTS***

K,23,WIDTH/2,CRACKYLOC,-LENGTH/2
 K,24,WIDTH/2,CRACKYLOC,CRACKZLOC
 K,25,WIDTH/2,CRACKYLOC,LENGTH/2

/COM,***FRONT SURFACE KEYPOINTS***

K,26,CRACKXLOC,CRACKYLOC,-LENGTH/2

/COM,***BACK SURFACE KEYPOINTS***

K,27,CRACKXLOC,CRACKYLOC,LENGTH/2

/COM,***CREATE VOLUMES***

V,5,8,6,7,20,26,1,21
 V,7,6,9,2,21,1,27,22
 V,20,26,16,11,21,1,15,19
 V,21,1,15,19,22,27,18,14

V,8,4,23,26,6,10,24,1
 V,6,10,24,1,9,3,25,27
 V,26,23,12,16,1,24,17,15
 V,1,24,17,15,27,25,13,1

```

/COM,*** MESH AREA MODELS ***
  FACTOR = 200
  DESIZE,,,,,,,,,WIDTH/FACTOR,,
  VMESH,ALL

/COM,***SOLUTION AND TIME STEP SETTINGS***
  FINISH
  /SOLU

  /COM,***ANALYSIS PARAMETERS***
  TIMEEND = 15*60
  TIMEINCR = 5

  /COM,***ANALYSIS SETTINGS***
  ANTYPE,TRANSIENT,NEW
  TIME,TIMEEND
  DELTIM,TIMEINCR
  OUTRES,,4

/COM,***BOUNDARY AND INITIAL CONDITIONS***
/COM,***INITIAL CONDITIONS***
  TUNIF,25
  TREF,25

  /COM,***BOUNDARY CONDITIONS***
  NSEL,S,LOC,X,-WIDTH/2
  NSEL,A,LOC,X,WIDTH/2
  NSEL,A,LOC,Y,-LENGTH/2
  NSEL,A,LOC,Y,LENGTH/2
  NSEL,A,LOC,Z,0
  NSEL,A,LOC,Z,-THICK
  SF,ALL,CONV,H,25

/COM,***APPLIED HEAT GENERATION LOAD***
/COM,*** CREATE HEAT GEN VS. TIME TABLE***
  *DIM,HEATGEN,TABLE,10,1,1,TIME,
  HEATGEN(1) = 0,  GEN, GEN, GEN,  GEN,  GEN,  GEN, 0, 0, 0
  HEATGEN(1,0) = 1E-6,1E-5, 1*60, 2*60, 3*60, 4*60, 5*60, 5.1*60, 7*60,
8*60

  /COM,***APPLY HEAT GEN AT CRACK AREA***
  KSEL,S,,1
  NSLK,S
  F,ALL,HEAT,%HEATGEN%

```

```
!F,ALL,HEAT,GEN
```

```
/COM,***SOLVE***
```

```
ALLSEL
SOLVE
```

```
/COM,***POST-PROCESSING***
```

```
/POST26
KSEL,S,,6
NSLK,S
NLIST
```

```
ALLSEL
NSOL,2,17,TEMP,,TOPSURFACETEMP
PRVAR,2
PLVAR,2
```

File name: 3d_heat_transfer_linegeneration

This file was applied when the generation was applied as a line source

```
FINISH
```

```
/CLEAR
```

```
/FILNAME, 3DHEATGEN
```

```
/TITLE, 3D HEAT TRANSFER WITH GENERATION AT A CRACK
```

```
/UNITS,MKS
```

```
! DATE CREATED: FEBRUARY 17, 2011
```

```
! DATE REVISED: FEBRUARY 17, 2011
```

```
/COM,***PREPROCESSOR***
```

```
/PREP7
```

```
/COM,***DEFINE PARAMETERS***
```

```
/COM,***PROPERTY PARAMETERS***
```

```
H = 10
```

```
GEN = 1
```

```
! Watts per meter
```

```
/COM,*** GEOMETRY PARAMETERS***
```

```
WIDTH = 5*2.54/100
```

```
! specimen width in m (2.54/100 term
```

```
converts from in. to m) in x direction
```

```
THICK = 1*2.54/100
```

```
! specimen thickness in Z direction
```

```
LENGTH = 1*2.54/100
```

```
! specimen length in Y direction
```

```
DEPTH RATIO = 0.5
```

DEPTH = DEPTRATIO*THICK

```
/COM,***CRACK LINE LOCATION***
CRACKXSTART = -0.25*2.54/100
CRACKXEND = 0.25*2.54/100
CRACKYSTART = -DEPTH
CRACKYEND = -DEPTH
CRACKZSTART = 0
CRACKZEND = 0
```

```
/COM,***BUILD THE MODEL***
/COM,***DEFINE ELEMENT TYPE***
ET,1,SOLID70
ET,2,PLANE55
```

```
/COM,***DEFINE MATERIAL PROPERTIES***
MP,KXX,1,1.34           ! thermal conductivity
MP,DENS,1,1850         ! density
MP,C,1,800             ! specific heat capacity
MP,HF,1,H              ! convective heat transfer coefficient
```

```
/COM,***DEFINE MODEL GEOMETRY***
/COM,***DEFINE KEYPOINTS***
/COM,***CRACK LOCATION KEYPOINT***
k,1,CRACKXSTART,CRACKYSTART,CRACKZSTART
k,2,CRACKXEND,CRACKYEND,CRACKZEND
```

```
/com,***top surface***
K,3,-WIDTH/2,0,-LENGTH/2
K,4,-WIDTH/2,0,CRACKZSTART
K,5,-WIDTH/2,0,LENGTH/2
K,6,CRACKXSTART,0,-LENGTH/2
K,7,CRACKXSTART,0,CRACKZSTART
K,8,CRACKXSTART,0,LENGTH/2
K,9,CRACKXEND,0,-LENGTH/2
K,10,CRACKXEND,0,CRACKZEND
K,11,CRACKXEND,0,LENGTH/2
K,12,WIDTH/2,0,-LENGTH/2
K,13,WIDTH/2,0,CRACKZEND
K,14,WIDTH/2,0,LENGTH/2
```

```
/COM,***BOTTOM SURFACE***
K,15,-WIDTH/2,-THICK,-LENGTH/2
```

K,16,-WIDTH/2,-THICK,CRACKZSTART
 K,17,-WIDTH/2,-THICK,LENGTH/2
 K,18,CRACKXSTART,-THICK,-LENGTH/2
 K,19,CRACKXSTART,-THICK,CRACKZSTART
 K,20,CRACKXSTART,-THICK,LENGTH/2
 K,21,CRACKXEND,-THICK,-LENGTH/2
 K,22,CRACKXEND,-THICK,CRACKZEND
 K,23,CRACKXEND,-THICK,LENGTH/2
 K,24,WIDTH/2,-THICK,-LENGTH/2
 K,25,WIDTH/2,-THICK,CRACKZEND
 K,26,WIDTH/2,-THICK,LENGTH/2

/COM,***REAR SURFACE***

K,27,-WIDTH/2,CRACKYSTART,LENGTH/2
 K,28,CRACKXSTART,CRACKYSTART,LENGTH/2
 K,29,CRACKXEND,CRACKYEND,LENGTH/2
 K,30,WIDTH/2,CRACKYEND,LENGTH/2

/COM,***FRONT SURFACE***

K,31,-WIDTH/2,CRACKYSTART,-LENGTH/2
 K,32,CRACKXSTART,CRACKYSTART,-LENGTH/2
 K,33,CRACKXEND,CRACKYEND,-LENGTH/2
 K,34,WIDTH/2,CRACKYEND,-LENGTH/2

/COM,***LEFT SURFACE***

K,35,-WIDTH/2,CRACKYSTART,CRACKZSTART

/COM,***RIGHT SURFACE

K,36,WIDTH/2,CRACKYEND,CRACKZEND

/COM,***CREATE VOLUMES***

/COM,***CENTER VOLUMES***

V,1,2,29,28,7,10,11,8
 V,1,2,33,32,7,10,9,6
 V,1,2,29,28,19,22,23,20
 V,1,2,33,32,19,22,21,18

/COM,***LEFT VOLUMES***

V,4,5,27,35,7,8,28,1
 V,3,4,35,31,6,7,1,32
 V,15,16,35,31,18,19,1,32
 V,35,27,17,16,1,28,20,19

/COM,***RIGHT VOLUMES***

V,13,14,30,36,10,11,29,2
 V,9,10,2,33,12,13,36,34
 V,33,2,22,21,34,36,25,24
 V,36,30,26,25,2,29,23,22

/COM,*** MESH AREA MODELS ***
 FACTOR = 75
 DESIZE,,,,,,,,,WIDTH/FACTOR,,
 NUMELEMENTS=9
 VMESH,ALL

/COM,***SOLUTION AND TIME STEP SETTINGS***
 FINISH
 /SOLU
 /COM,***ANALYSIS PARAMETERS***
 TIMEEND = 10*60
 TIMEINCR = 15
 /COM,***ANALYSIS SETTINGS***
 ANTYPE,TRANSIENT,NEW
 TIME,TIMEEND
 DELTIM,TIMEINCR
 OUTRES,,2

/COM,***BOUNDARY AND INITIAL CONDITIONS***
 /COM,***INITIAL CONDITIONS***
 TUNIF,25
 TREF,25
 /COM,***BOUNDARY CONDITIONS***
 NSEL,S,LOC,X,-WIDTH/2
 NSEL,A,LOC,X,WIDTH/2
 NSEL,A,LOC,Z,-LENGTH/2
 NSEL,A,LOC,Z,LENGTH/2
 NSEL,A,LOC,Y,0
 NSEL,A,LOC,Y,-THICK
 SF,ALL,CONV,H,25

/COM,***APPLIED HEAT GENERATION LOAD***
 /COM,*** CREATE HEAT GEN VS. TIME TABLE***
 *DIM,HEATGEN,TABLE,10,1,1,TIME,
 HEATGEN(1) = 0, GEN/NUMELEMENTS, GEN/NUMELEMENTS,
 GEN/NUMELEMENTS, GEN/NUMELEMENTS, GEN/NUMELEMENTS,
 GEN/NUMELEMENTS, 0, 0, 0
 HEATGEN(1,0) = 1E-6,1E-5, 1*60, 2*60, 3*60, 4*60, 5*60, 6*60, 7*60,
 8*60

```

/COM,***APPLY HEAT GEN AT CRACK AREA***
LSEL,S,,1
NSLL,S,1
NLIST
F,ALL,HEAT,%HEATGEN%

```

```

/COM,***SOLVE***

```

```

ALLSEL
SOLVE

```

```

/COM,***POST-PROCESSING***

```

```

/POST26
KSEL,S,,6
NSLK,S
NLIST
ALLSEL
NSOL,2,17,TEMP,,TOPSURFACETEMP
PRVAR,2
PLVAR,2

```

File name: 3d_heat_transfer_areagen

This file was applied when the generation was modeled as an area heat source

```

FINISH

```

```

/CLEAR

```

```

/FILNAME, 3DHEATGEN

```

```

/TITLE, 3D HEAT TRANSFER WITH GENERATION AT A CRACK

```

```

/UNITS,MKS

```

```

! DATE CREATED: FEBRUARY 17, 2011

```

```

! DATE REVISED: FEBRUARY 17, 2011

```

```

/COM,***PREPROCESSOR***

```

```

/PREP7

```

```

/COM,***DEFINE PARAMETERS***

```

```

/COM,***PROPERTY PARAMETERS***

```

```

H = 15

```

```

GEN = 5000

```

```

/COM,*** GEOMETRY PARAMETERS***

```

```

WIDTH = 5*2.54/100      ! specimen width in m (2.54/100 term converts from
in. to m) in x direction

```

```

THICK = 1*2.54/100     ! specimen thickness in Z direction

```

LENGTH = 1*2.54/100 ! specimen length in Y direction

/COM,*** CRACK LOCATION PARAMETERS ***

XONE = -0.5*2.54/100

YONE = -0.25*2.54/100

ZONE = -0.5*THICK

XTWO = 0.5*2.54/100

YTWO = -0.25*2.54/100

ZTWO = -0.5*THICK

XTHREE = 0.5*2.54/100

YTHREE = 0.25*2.54/100

ZTHREE = -0.5*THICK

XFOUR = -0.5*2.54/100

YFOUR = 0.25*2.54/100

ZFOUR = -0.5*THICK

/COM,***DEFINE ELEMENT TYPE***

ET,1,SOLID70

ET,2,PLANE55

/COM,***DEFINE MATERIAL PROPERTIES***

MP,KXX,1,1.34 ! thermal conductivity

MP,DENS,1,1850 ! density

MP,C,1,800 ! specific heat capacity

MP,HF,1,H ! convective heat transfer coefficient

/COM,***DEFINE MODEL GEOMETRY***

/COM,***DEFINE KEYPOINTS***

/COM,***SURFACE AREA OF CRACK KEYPOINTS***

K, 1,XONE, YONE, ZONE

K, 2,XTWO, YTWO, ZTWO

K, 3,XTHREE,YTHREE,ZTHREE

K, 4,XFOUR, YFOUR, ZFOUR

K, 5,-WIDTH/2,-LENGTH/2,ZONE

K, 6,WIDTH/2,-LENGTH/2,ZTWO

K, 7,WIDTH/2,LENGTH/2,ZTHREE

K, 8,-WIDTH/2,LENGTH/2,ZFOUR

K, 9,XONE,-LENGTH/2,ZONE

K,10,XTWO,-LENGTH/2,ZTWO

K,11,WIDTH/2,YTWO,ZTWO
 K,12,WIDTH/2,YTHREE,ZTHREE
 K,13,XTHREE,LENGTH/2,ZTHREE
 K,14,XFOUR,LENGTH/2,ZFOUR
 K,15,-WIDTH/2,YFOUR,ZFOUR
 K,16,-WIDTH/2,YONE,ZONE

/COM,***CREATE AREAS***

A,1,2,3,4
 A,16,1,9,5
 A,9,10,2,1
 A,2,11,6,10
 A,2,11,12,3
 A,3,12,7,13
 A,14,13,3,4
 A,15,4,14,8
 A,15,4,1,16

/COM,*** MESH AREA MODELS ***

FACTOR = 20
 LESIZE,1,THICK/FACTOR
 LESIZE,2,THICK/FACTOR
 LESIZE,3,THICK/FACTOR
 LESIZE,4,THICK/FACTOR
 TYPE,2
 ESIZE,THICK/FACTOR
 AMESH,1
 LESIZE,21,2*THICK/FACTOR,,,1/3
 LESIZE,5,2*THICK/FACTOR,,,1/3
 LESIZE,15,2*THICK/FACTOR,,,1/3
 LESIZE,11,2*THICK/FACTOR,,,3
 TYPE,2
 ESIZE,2*THICK/FACTOR
 AMESH,8
 AMESH,6
 AMESH,2
 AMESH,4
 AMESH,7
 AMESH,3
 AMESH,9
 AMESH,5

/COM,*** EXTRUDE MODEL ***

```

TYPE,1
ESIZE,,FACTOR/2
VEXT,1,9,1,0,0,-0.5*THICK
VEXT,1,9,1,0,0,0.5*THICK

```

```

/COM,***SOLUTION AND TIME STEP SETTINGS***

```

```

    FINISH
    /SOLU
    /COM,***ANALYSIS PARAMETERS***
    TIMEEND = 10*60
    TIMEINCR = 5
    /COM,***ANALYSIS SETTINGS***
    ANTYPE,TRANSIENT,NEW
    TIME,TIMEEND
    DELTIM,TIMEINCR
    OUTRES,,2

```

```

/COM,***BOUNDARY AND INITIAL CONDITIONS***

```

```

    /COM,***INITIAL CONDITIONS***
    TUNIF,25
    TREF,25

```

```

    /COM,***BOUNDARY CONDITIONS***

```

```

    NSEL,S,LOC,X,-WIDTH/2
    NSEL,A,LOC,X,WIDTH/2
    NSEL,A,LOC,Y,-LENGTH/2
    NSEL,A,LOC,Y,LENGTH/2
    NSEL,A,LOC,Z,0
    NSEL,A,LOC,Z,-THICK
    SF,ALL,CONV,H,25

```

```

/COM,***APPLIED HEAT GENERATION LOAD***

```

```

    ELEMENTSIZE = THICK*THICK/(FACTOR*FACTOR)
    /COM,*** CREATE HEAT GEN VS. TIME TABLE***
    *DIM,HEATGEN,TABLE,9,1,1,TIME,
    HEATGEN(1) = GEN*ELEMENTSIZE, GEN*ELEMENTSIZE,
    GEN*ELEMENTSIZE, GEN*ELEMENTSIZE, GEN*ELEMENTSIZE,
    GEN*ELEMENTSIZE, 0, 0, 0
    HEATGEN(1,0) = 1E-6, 1*60, 2*60, 3*60, 4*60, 5*60, 6*60, 7*60, 8*60
    /COM,***APPLY HEAT GEN AT CRACK AREA***
    ASEL,S,,1
    NSLA,S,1
    NLIST

```

```
F,ALL,HEAT,%HEATGEN%  
/COM,***SOLVE***  
ALLSEL  
SOLVE
```

```
/COM,***POST-PROCESSING***  
/POST26  
NSEL,S,LOC,X,0  
NSEL,R,LOC,Y,0  
NSEL,R,LOC,Z,0  
NLIST  
ALLSEL  
!NSOL,2,6096,TEMP,,TOPSURFACETEMP  
!PRVAR,2  
!PLVAR,2
```

APPENDIX D

SIMULATION DATA

One-Dimensional Time-Dependent Results

Gen 1 W/m²
 Depth 10% % of thickness
 Thickness 1 in.

Finite Element Method		Finite Difference Method		Analytical Method	
Time (sec)	Surface Temp (deg C)	Time (sec)	Surface Temp (deg C)	Time (sec)	Surface Temp (deg C)
0.00	25.00	0.00	25.00	0.00	25.00
20.00	25.00	20.00	25.00	20.00	25.00
40.00	25.00	40.01	25.00	40.00	25.00
60.00	25.00	60.00	25.00	60.00	25.00
80.00	25.01	80.01	25.01	80.00	25.01
100.00	25.01	100.01	25.01	100.00	25.01
120.00	25.01	120.00	25.01	120.00	25.01
140.00	25.01	140.01	25.01	140.00	25.01
160.00	25.01	160.01	25.01	160.00	25.01
180.00	25.01	180.00	25.01	180.00	25.01
200.00	25.01	200.01	25.01	200.00	25.01
220.00	25.01	220.00	25.01	220.00	25.01
240.00	25.01	240.00	25.01	240.00	25.01
260.00	25.01	260.01	25.01	260.00	25.01
280.00	25.01	280.00	25.01	280.00	25.01
300.00	25.01	300.01	25.01	300.00	25.01
320.00	25.01	320.01	25.01	320.00	25.01
340.00	25.01	340.00	25.01	340.00	25.01
360.00	25.01	360.01	25.01	360.00	25.01
380.00	25.01	380.01	25.01	380.00	25.01
400.00	25.01	400.00	25.01	400.00	25.01
420.00	25.01	420.01	25.01	420.00	25.01
440.00	25.01	440.00	25.01	440.00	25.01
460.00	25.01	460.01	25.01	460.00	25.01
480.00	25.01	480.01	25.01	480.00	25.01
500.00	25.01	500.00	25.01	500.00	25.01
520.00	25.01	520.01	25.01	520.00	25.01
540.00	25.01	540.01	25.01	540.00	25.01
560.00	25.01	560.00	25.01	560.00	25.01

580.00	25.01	580.01	25.01	580.00	25.01
--------	-------	--------	-------	--------	-------

Gen 1 W/m²
 Depth 50% % of thickness
 Thickness 1 in.

Finite Element Method		Finite Difference Method		Analytical Method	
Time (sec)	Surface Temp (deg C)	Time (sec)	Surface Temp (deg C)	Time (sec)	Surface Temp (deg C)
0.00	25.00	0.00	25.00	0.00	25.00
20.00	25.00	20.00	25.00	20.00	25.00
40.00	25.00	40.01	25.00	40.00	25.00
60.00	25.00	60.00	25.00	60.00	25.00
80.00	25.00	80.01	25.00	80.00	25.00
100.00	25.00	100.01	25.00	100.00	25.00
120.00	25.00	120.00	25.00	120.00	25.00
140.00	25.00	140.01	25.00	140.00	25.00
160.00	25.00	160.01	25.00	160.00	25.00
180.00	25.00	180.00	25.00	180.00	25.00
200.00	25.00	200.01	25.00	200.00	25.00
220.00	25.00	220.00	25.00	220.00	25.00
240.00	25.01	240.00	25.01	240.00	25.01
260.00	25.01	260.01	25.01	260.00	25.01
280.00	25.01	280.00	25.01	280.00	25.01
300.00	25.01	300.01	25.01	300.00	25.01
320.00	25.01	320.01	25.01	320.00	25.01
340.00	25.01	340.00	25.01	340.00	25.01
360.00	25.01	360.01	25.01	360.00	25.01
380.00	25.01	380.01	25.01	380.00	25.01
400.00	25.01	400.00	25.01	400.00	25.01
420.00	25.01	420.01	25.01	420.00	25.01
440.00	25.01	440.00	25.01	440.00	25.01
460.00	25.01	460.01	25.01	460.00	25.01
480.00	25.01	480.01	25.01	480.00	25.01
500.00	25.01	500.00	25.01	500.00	25.01
520.00	25.01	520.01	25.01	520.00	25.01
540.00	25.01	540.01	25.01	540.00	25.01

560.00	25.01	560.00	25.01	560.00	25.01
580.00	25.01	580.01	25.01	580.00	25.01

Gen 1 W/m²
Depth 90% % of thickness
Thickness 1 in.

Finite Element Method		Finite Difference Method		Analytical Method	
Time (sec)	Surface Temp (deg C)	Time (sec)	Surface Temp (deg C)	Time (sec)	Surface Temp (deg C)
0.00	25.00	0.00	25.00	0.00	25.00
20.00	25.00	20.00	25.00	20.00	25.00
40.00	25.00	40.01	25.00	40.00	25.00
60.00	25.00	60.00	25.00	60.00	25.00
80.00	25.00	80.01	25.00	80.00	25.00
100.00	25.00	100.01	25.00	100.00	25.00
120.00	25.00	120.00	25.00	120.00	25.00
140.00	25.00	140.01	25.00	140.00	25.00
160.00	25.00	160.01	25.00	160.00	25.00
180.00	25.00	180.00	25.00	180.00	25.00
200.00	25.00	200.01	25.00	200.00	25.00
220.00	25.00	220.00	25.00	220.00	25.00
240.00	25.00	240.00	25.00	240.00	25.00
260.00	25.00	260.01	25.00	260.00	25.00
280.00	25.00	280.00	25.00	280.00	25.00
300.00	25.00	300.01	25.00	300.00	25.00
320.00	25.00	320.01	25.00	320.00	25.00
340.00	25.01	340.00	25.01	340.00	25.01
360.00	25.01	360.01	25.01	360.00	25.01
380.00	25.01	380.01	25.01	380.00	25.01
400.00	25.01	400.00	25.01	400.00	25.01
420.00	25.01	420.01	25.01	420.00	25.01
440.00	25.01	440.00	25.01	440.00	25.01
460.00	25.01	460.01	25.01	460.00	25.01
480.00	25.01	480.01	25.01	480.00	25.01

500.00	25.01	500.00	25.01	500.00	25.01
520.00	25.01	520.01	25.01	520.00	25.01
540.00	25.01	540.01	25.01	540.00	25.01
560.00	25.01	560.00	25.01	560.00	25.01
580.00	25.01	580.01	25.01	580.00	25.01

One-Dimensional Parametric Study Results

Flaw Depth (% of thickness)	Specimen Thickness (in.)	Max Surface Temp (deg C)		
		Finite Difference	Finite element	Analytical
0.10	1.00	25.01	25.01	25.01
0.10	1.00	25.01	25.01	25.01
0.10	1.00	25.01	25.01	25.01
0.10	1.00	25.01	25.01	25.01
0.10	1.00	25.01	25.01	25.01
0.50	1.00	25.01	25.01	25.01
0.50	1.00	25.01	25.01	25.01
0.50	1.00	25.01	25.01	25.01
0.50	1.00	25.01	25.01	25.01
0.50	1.00	25.01	25.01	25.01
0.90	1.00	25.01	25.01	25.01
0.90	1.00	25.01	25.01	25.01
0.90	1.00	25.01	25.01	25.01
0.90	1.00	25.01	25.01	25.01
0.90	1.00	25.01	25.01	25.01
0.10	0.10	25.04	25.04	25.04
0.10	0.50	25.02	25.02	25.02
0.10	1.00	25.01	25.01	25.01
0.10	1.50	25.01	25.01	25.01
0.10	2.00	25.01	25.01	25.01
0.50	0.10	25.04	25.04	25.04
0.50	0.50	25.01	25.01	25.01
0.50	1.00	25.01	25.01	25.01
0.50	1.50	25.00	25.00	25.00
0.50	2.00	25.00	25.00	25.00

0.90	0.10	25.04	25.04	25.04
0.90	0.50	25.01	25.01	25.01
0.90	1.00	25.01	25.01	25.01
0.90	1.50	25.00	25.00	25.00
0.90	2.00	25.00	25.00	25.00

Two-Dimensional Time-Dependent Results

Gen 1 W/m
Depth 10% % of thickness
Thickness 1 in.

Finite Element Method		Analytical	
Time (sec)	Surface Temp (deg C)	Time (sec)	Surface Temp (deg C)
0.00	25.00	0.00	25.00
20.00	25.18	20.00	25.22
40.00	25.26	40.00	25.30
60.00	25.31	60.00	25.34
80.00	25.34	80.00	25.37
100.00	25.36	100.00	25.39
120.00	25.38	120.00	25.41
140.00	25.40	140.00	25.43
160.00	25.41	160.00	25.44
180.00	25.43	180.00	25.46
200.00	25.44	200.00	25.47
220.00	25.45	220.00	25.48
240.00	25.46	240.00	25.49
260.00	25.47	260.00	25.50
280.00	25.48	280.00	25.50
300.00	25.48	300.00	25.51
320.00	25.32	320.00	25.30
340.00	25.24	340.00	25.23
360.00	25.20	360.00	25.19
380.00	25.17	380.00	25.17

400.00	25.16	400.00	25.15
420.00	25.14	420.00	25.14
440.00	25.13	440.00	25.13
460.00	25.12	460.00	25.12
480.00	25.11	480.00	25.11
500.00	25.11	500.00	25.11
520.00	25.10	520.00	25.10
540.00	25.10	540.00	25.10
560.00	25.09	560.00	25.09
580.00	25.09	580.00	25.09
600.00	25.09	600.00	25.09

Gen 1 W/m²
Depth 50% % of thickness
Thickness 1 in.

Finite Element Method		Analytical	
Time (sec)	Surface Temp (deg C)	Time (sec)	Surface Temp (deg C)
0.00	25.00	0.00	25.00
20.00	25.01	20.00	25.00
40.00	25.02	40.00	25.02
60.00	25.04	60.00	25.04
80.00	25.05	80.00	25.06
100.00	25.07	100.00	25.07
120.00	25.08	120.00	25.09
140.00	25.10	140.00	25.10
160.00	25.11	160.00	25.11
180.00	25.12	180.00	25.12
200.00	25.13	200.00	25.13
220.00	25.14	220.00	25.14
240.00	25.15	240.00	25.15
260.00	25.16	260.00	25.16
280.00	25.17	280.00	25.17
300.00	25.17	300.00	25.17
320.00	25.18	320.00	25.18

340.00	25.17	340.00	25.17
360.00	25.16	360.00	25.16
380.00	25.15	380.00	25.15
400.00	25.14	400.00	25.14
420.00	25.13	420.00	25.13
440.00	25.12	440.00	25.12
460.00	25.12	460.00	25.12
480.00	25.11	480.00	25.11
500.00	25.11	500.00	25.11
520.00	25.10	520.00	25.10
540.00	25.10	540.00	25.10
560.00	25.10	560.00	25.10
580.00	25.09	580.00	25.09
600.00	25.09	600.00	25.09

Gen 50 W/m²
Depth 90% % of thickness
Thickness 1 in.

Finite Element Method		Analytical	
Time (sec)	Surface Temp (deg C)	Time (sec)	Surface Temp (deg C)
0.00	25.00	0.00	25.00
20.00	25.00	20.00	25.00
40.00	25.00	40.00	25.00
60.00	25.00	60.00	25.00
80.00	25.01	80.00	25.01
100.00	25.02	100.00	25.02
120.00	25.02	120.00	25.02
140.00	25.03	140.00	25.03
160.00	25.04	160.00	25.04
180.00	25.05	180.00	25.05
200.00	25.06	200.00	25.06
220.00	25.07	220.00	25.07

240.00	25.08	240.00	25.08
260.00	25.08	260.00	25.08
280.00	25.09	280.00	25.09
300.00	25.10	300.00	25.10
320.00	25.11	320.00	25.11
340.00	25.11	340.00	25.11
360.00	25.11	360.00	25.12
380.00	25.12	380.00	25.12
400.00	25.11	400.00	25.12
420.00	25.11	420.00	25.11
440.00	25.11	440.00	25.11
460.00	25.11	460.00	25.11
480.00	25.10	480.00	25.10
500.00	25.10	500.00	25.10
520.00	25.10	520.00	25.10
540.00	25.09	540.00	25.09
560.00	25.09	560.00	25.09
580.00	25.09	580.00	25.09
600.00	25.09	600.00	25.09

Two-Dimensional Parametric Data

Flaw Depth (% of thickness)	Specimen Thickness (in.)	Max Surface Temp (deg C)	
		Finite element	Analytical
0.10	1.00	25.48	25.50
0.10	1.00	25.48	25.51
0.10	1.00	25.48	25.51
0.10	1.00	25.48	25.51
0.10	1.00	25.48	25.51
0.50	1.00	25.18	25.18
0.50	1.00	25.18	25.18
0.50	1.00	25.18	25.18
0.50	1.00	25.18	25.18
0.50	1.00	25.18	25.18
0.90	1.00	25.12	25.12
0.90	1.00	25.12	25.12

0.90	1.00	25.12	25.12
0.90	1.00	25.11	25.11
0.90	1.00	25.12	25.12

Three-Dimensional Time-Dependant Results

Gen 1 W
Depth 10% % of thickness
Thickness 1 in.

Finite Element Method		Analytical	
Time (sec)	Surface Temp (deg C)	Time (sec)	Surface Temp (deg C)
0	25	0	25
20	55.6076	20	56.678866
40	64.3497	40	65.7269395
60	67.2154	60	68.692939
80	68.6884	80	70.217494
100	69.6373	100	71.1996055
120	70.3196	120	71.905786
140	70.8432	140	72.447712
160	71.2637	160	72.8829295
180	71.6131	180	73.2445585
200	71.911	200	73.552885
220	72.1705	220	73.8214675
240	72.4005	240	74.0595175
260	72.6071	260	74.2733485
280	72.795	280	74.467825
300	72.9673	300	74.6461555
320	43.3522	320	43.994527
340	34.1343	340	34.4540005
360	31.2853	360	31.5052855
380	29.9068	380	30.078538
400	29.0652	400	29.207482
420	28.491	420	28.613185

440	28.0731	440	28.1806585
460	27.755	460	27.851425
480	27.5045	480	27.5921575
500	27.3018	500	27.382363
520	27.134	520	27.20869
540	26.9925	540	27.0622375
560	26.8713	560	26.9367955
580	26.766	580	26.82781
600	26.6735	600	26.7320725

Gen 1 W
Depth 50% % of thickness
Thickness 1 in.

Finite Element Method		Analytical	
Time (sec)	Surface Temp (deg C)	Time (sec)	Surface Temp (deg C)
0	25	0	25
20	25.3024	20	25.312984
40	26.107	40	26.145745
60	26.9254	60	26.992789
80	27.6012	80	27.692242
100	28.147	100	28.257145
120	28.5962	120	28.722067
140	28.9752	140	29.114332
160	29.302	160	29.45257
180	29.5888	180	29.749408
200	29.8444	200	30.013954
220	30.0747	220	30.2523145
240	30.2844	240	30.469354
260	30.4767	260	30.6683845
280	30.6545	280	30.8524075
300	30.8197	300	31.0233895
320	30.6949	320	30.8942215
340	30.0478	340	30.224473
360	29.3615	360	29.5141525

380	28.8084	380	28.941694
400	28.3798	400	28.498093
420	28.0429	420	28.1494015
440	27.7719	440	27.8689165
460	27.5487	460	27.6379045
480	27.3613	480	27.4439455
500	27.2014	500	27.278449
520	27.0631	520	27.1353085
540	26.9421	540	27.0100735
560	26.8353	560	26.8995355
580	26.7401	580	26.8010035
600	26.6548	600	26.712718

Gen 1 W
Depth 90% % of thickness
Thickness 1 in.

Finite Element Method		Analytical	
Time (sec)	Surface Temp (deg C)	Time (sec)	Surface Temp (deg C)
0	25	0	25
20	25.0054	20	25.005589
40	25.0544	40	25.056304
60	25.1794	60	25.185679
80	25.3686	80	25.381501
100	25.5947	100	25.6155145
120	25.8356	120	25.864846
140	26.0776	140	26.115316
160	26.313	160	26.358955
180	26.5382	180	26.592037
200	26.7516	200	26.812906
220	26.9529	220	27.0212515
240	27.1422	240	27.217177
260	27.3204	260	27.401614
280	27.488	280	27.57508
300	27.646	300	27.73861

320	27.7903	320	27.8879605
340	27.8849	340	27.9858715
360	27.8967	360	27.9980845
380	27.8367	380	27.9359845
400	27.7323	400	27.8279305
420	27.6068	420	27.698038
440	27.4745	440	27.5611075
460	27.3437	460	27.4257295
480	27.2186	480	27.296251
500	27.1012	500	27.174742
520	26.9923	520	27.0620305
540	26.8918	540	26.958013
560	26.7993	560	26.8622755
580	26.7143	580	26.7743005
600	26.6362	600	26.693467

Three-Dimensional Model Parametric Data

Point source generation data:

Generation amount (W)	Flaw Depth (% of thickness)	Specimen Thickness (in.)	Max Surface Temp (deg C)		% difference
			Finite element	Analytical	
0.2	0.1	1	34.59	34.86	2.8%
0.4	0.1	1	44.17	45.04	4.4%
0.6	0.1	1	53.78	55.17	4.7%
0.8	0.1	1	63.38	65.29	4.9%
1	0.1	1	72.97	75.42	5.0%
0.2	0.5	1	26.16	26.19	2.6%
0.4	0.5	1	27.33	27.67	13.6%
0.6	0.5	1	28.49	28.56	2.0%
0.8	0.5	1	29.66	29.75	1.9%
1	0.5	1	30.82	31.38	9.2%
0.2	0.9	1	25.58	25.59	1.7%
0.4	0.9	1	26.16	26.27	9.1%
0.6	0.9	1	26.74	26.89	8.3%
0.8	0.9	1	27.32	27.57	10.2%

1	0.9	1	27.9	28.28	12.3%
1	0.1	0.1	263.83	269.21	2.2%
1	0.1	0.5	115.16	117.46	2.5%
1	0.1	1	72.97	74.68	3.5%
1	0.1	1.5	54.86	55.87	3.3%
1	0.1	2	45.52	46.23	3.4%
1	0.5	0.1	195.76	198.61	1.7%
1	0.5	0.5	57.86	59.01	3.4%
1	0.5	1	30.82	30.93	1.9%
1	0.5	1.5	27.67	27.71	1.5%
1	0.5	2	26.41	26.44	2.1%
1	0.9	0.1	172.68	173.64	0.6%
1	0.9	0.5	51.9	54.7	9.9%
1	0.9	1	27.9	27.94	1.4%
1	0.9	1.5	26.03	26.04	1.0%
1	0.9	2	25.45	25.46	2.2%

Area source generation data:

Flaw size (in. ²)	Flaw Orientation (deg)	Generation amount (W/m ²)	Generation amount (W)	Flaw Depth (% of thickness)	Specimen Thickness (in.)	Max Surface Temp (deg C)
0.01	0	31000	0.20	10%	1	29.59
0.01	30	31000	0.20	10%	1	30.1
0.01	60	31000	0.20	10%	1	30.87
0.01	90	31000	0.20	10%	1	30.88
0.01	0	31000	0.20	50%	1	26.27
0.01	30	31000	0.20	50%	1	26.32
0.01	60	31000	0.20	50%	1	26.38
0.01	90	31000	0.20	50%	1	26.32
0.01	0	31000	0.20	90%	1	25.27
0.01	30	31000	0.20	90%	1	25.27
0.01	60	31000	0.20	90%	1	25.26
0.01	90	31000	0.20	90%	1	25.26
0.01	0	31000	0.20	10%	1	29.59
0.03	0	31000	0.60	10%	1	36.55

0.05	0	31000	1.00	10%	1	43.64
0.08	0	31000	1.60	10%	1	53.53
0.1	0	31000	2.00	10%	1	58.74
0.01	0	31000	0.20	50%	1	26.27
0.03	0	31000	0.60	50%	1	28.17
0.05	0	31000	1.00	50%	1	29.87
0.08	0	31000	1.60	50%	1	32.07
0.1	0	31000	2.00	50%	1	33.37
0.01	0	31000	0.20	90%	1	25.27
0.03	0	31000	0.60	90%	1	26.2
0.05	0	31000	1.00	90%	1	27.9
0.08	0	31000	1.60	90%	1	30.07
0.1	0	31000	2.00	90%	1	32.37